

In addition to many advantages, composite materials have been increased applications in industries such as aerospace, naval and automobile. However, this technology imposes a new level of difficulties to manufacturers, since small variabilities in the manufacturing of composite components have a high influence on the effective properties of the product. The objective of this work consists of a methodology to evaluate composite materials manufacturing process to identify components out of specification. For this, it is necessary to understand the influence of design variables on the dynamic behaviour of a specimen, construct a numerical model to represent the specimens and develop criteria to classify the analysed specimens. To achieve these goals, the research methodology should consider the use of methods like the design of experiments, Kriging model update, and vibration-based methods. First, the geometrical characteristics of the composite plates are evaluated by a 3D scanner machine. In addition, the materials properties presented in the literature are listed to define an approximate range where the real values have more probability to be present. Afterward, a Design of Experiments (DoE) is used for screening the variables and evaluate the main effect of each variable on each vibrational mode. The DoE results are used as base information to a model update procedure that results on the estimated materials properties and a refined numerical model. In this work, the model update process is improved using Kriging metamodel aiming to reduce the computational time required. Finally, the updated numerical model is used to obtain the FRFs that composes the envelope representing the composite plate set. This envelope can help engineers to evaluate other composite plates and classify them accordingly to the design specifications. The proposed methodology presented relevant results, by defining the main variables that influence the dynamic behaviour and supporting the model update process resulting in errors in the order of 1 and 2%. Besides the good approximation, the model update process using Kriging was efficient in terms of computational time, requiring half of the time when compared with a methodology without using metamodels. Finally, it is discussed the advantages and limitations of the applicability of this methodology in the presentation of two case studies.

Orientador: Prof. Dr. Ricardo de Medeiros

Joinville, 2018

YEAR 2018 LUIZ FERNANDO DOS SANTOS SOUZA

A METHODOLOGY TO ANALYSE THE DYNAMIC RESPONSE OF COMPOSITE PLATES USING DESIGN OF EXPERIMENTS AND KRIGING MODEL



SANTA CATARINA STATE UNIVERSITY – UDESC
COLLEGE OF TECHNOLOGICAL SCIENCES – CCT
MASTER IN MECHANICAL ENGINEERING - PPGEM

MASTER THESIS

**A METHODOLOGY TO ANALYSE THE DYNAMIC
RESPONSE OF COMPOSITE PLATES USING DESIGN
OF EXPERIMENTS AND KRIGING MODEL**

LUIZ FERNANDO DOS SANTOS SOUZA

JOINVILLE, 2018

LUIZ FERNANDO DOS SANTOS SOUZA

**A METHODOLOGY TO ANALYSE THE DYNAMIC RESPONSE OF
COMPOSITE PLATES USING DESIGN OF EXPERIMENTS AND
KRIGING MODEL**

Master thesis submitted to the Mechanical Engineering Department at the College of Technological Science of Santa Catarina State University in fulfillment of the partial requirement for the Master's degree in Mechanical Engineering.

PhD. Ricardo de Medeiros

JOINVILLE - SC

August 15, 2018

Ficha catalográfica elaborada pelo(a) autor(a), com
auxílio do programa de geração automática da
Biblioteca Setorial do CCT/UDESC

Dos Santos Souza, Luiz Fernando

A methodology to analyse the dynamic response of
composite plates using design of experiments and
kriging model / Luiz Fernando Dos Santos Souza. -
Joinville , 2018.

118 p.

Orientador: Ricardo De Medeiros

Dissertação (Mestrado) - Universidade do Estado de
Santa Catarina, Centro de Ciências Tecnológicas,
Programa de Pós-Graduação em Engenharia Mecânica,
Joinville, 2018.

1. Dynamic response. 2. Composite Materials. 3.
Design of experiments. 4. Kriging. I. De Medeiros,
Ricardo. II. Universidade do Estado de Santa
Catarina. Programa de Pós-Graduação. III. Título.

**A Methodology to Analyse the Dynamic Response of Composites Plates Using
Design of Experiments and Kriging Model**

por

Luiz Fernando dos Santos Souza

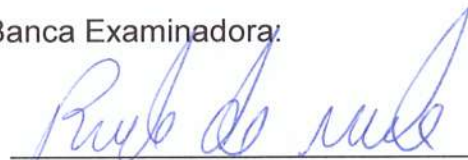
Esta dissertação foi julgada adequada para obtenção do título de

MESTRE EM ENGENHARIA MECÂNICA


Área de concentração em “Modelagem e Simulação Numérica”
e aprovada em sua forma final pelo

CURSO DE MESTRADO ACADÊMICO EM ENGENHARIA MECÂNICA
DO CENTRO DE CIÊNCIAS TECNOLÓGICAS DA
UNIVERSIDADE DO ESTADO DE SANTA CATARINA.

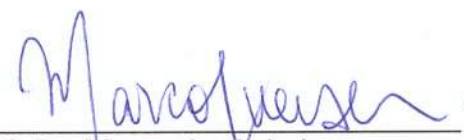
Banca Examinadora:



Prof. Dr. Ricardo de Medeiros
CCT/UDESC (Orientador/Presidente)



Prof. Dr. Eduardo Lenz Cardoso
CCT/UDESC



Prof. Dr. Marco Antonio Luersen
UTFPR

Joinville, SC, 20 de junho de 2018.

ACKNOWLEDGMENTS

Initially, I would like to express my sincere gratitude to my advisor Prof. Ricardo de Medeiros for the continuous support of my study and related research, for his patience, motivation, friendship, and immense knowledge. His guidance helped me in all the time of research and writing of this master thesis. Besides my advisor, I would like to thank Prof. Volnei Tita (São Carlos School of Engineering, University of São Paulo) and Prof. Dirk Vandepitte (Katholieke Universiteit Leuven) for the uncountable useful discussions to improve this research.

I would like to thank the Mechanical Engineering Department of the Santa Catarina State University for the opportunity to carry on this master. In addition, I would like to express my gratitude to Prof. Eduardo Lenz Cardoso, Prof. Pablo Andrés Muñoz Rojas and Prof. Joel Martins Crichigno Filho by the support provided with technical support, bibliography, ABAQUSTM license and great ideas. I also would like to thank my colleagues in our research lab (LAMEC) for their friendship and hours of useful discussions.

I would like to thank my family, especially my dear Vanessa, who supported me throughout my journey and never left to believe in my dreams.

Finally, I gratefully acknowledge the financial support of the Fundação de Amparo a Pesquisa e Inovação do Estado de Santa Catarina - Brazil (FAPESC process number: 2017TR1747 and 2017TR784) and Coordination for the Improvement of the Higher Level Personnel (CAPES).

ABSTRACT

DOS SANTOS SOUZA, Luiz Fernando, A methodology to analyse the dynamic response of composite plates using design of experiments and kriging model. 2018. 118 f. Master Thesis (Master in Mechanical Engineering - Area: Numerical Modeling and Simulation) Santa Catarina State University. Mechanical Engineering Graduate Program Joinville 2018.

In addition to many advantages, composite materials have been increased applications in industries such as aerospace, naval and automobile. However, this technology imposes a new level of difficulties to manufacturers, since small variabilities in the manufacturing of composite components have a high influence on the effective properties of the product. The objective of this work consists of a methodology to evaluate composite materials manufacturing process in order to identify components out of specification. For this, it is necessary to understand the influence of design variables on the dynamic behaviour of a specimen, construct a numerical model to represent the specimens and develop criteria to classify the analysed specimens. To achieve these goals, the research methodology should consider the use of methods like the design of experiments, Kriging model update, and vibration based methods. First, the geometrical characteristics of the composite plates are evaluated by a 3D scanner machine. In addition, the materials properties presented in the literature are listed to define an approximate range where the real values have more probability to be present. Afterward, a Design of Experiments (DoE) is used for screening the variables and evaluate the main effect of each variable on each vibrational mode. The DoE results are used as base information to a model update procedure that results on the estimated materials properties and a refined numerical model. In this work, the model update process is improved by the use of Kriging metamodel aiming to reduce the computational time required. Finally, the updated numerical model is used to obtain the FRFs that composes the envelope representing the composite plate set. This envelope can help engineers to evaluate other composite plates and classify them accordingly to the design specifications. The proposed methodology presented relevant results, by defining the main variables that influence the dynamic behaviour and supporting the model update process resulting in errors in the order of 1 and 2%. Besides the good approximation, the model update process using Kriging was efficient in terms of computational time, requiring half of the time when compared with a methodology without using metamodels. Finally, it is discussed the advantages and limitations of the applicability of this methodology in the presentation of two case studies.

Key-words: Dynamic response, Composite Materials, Design of experiments, Kriging

RESUMO

DOS SANTOS SOUZA, Luiz Fernando, A methodology to analyse the dynamic response of composite plates using design of experiments and kriging model. 2018. 118 f. Dissertação (Mestrado em Engenharia Mecânica - Área: Modelagem e Simulação Numérica) Universidade do Estado de Santa Catarina. Programa de Pós-Graduação em Engenharia Mecânica Joinville 2018.

Dado suas vantagens, os materiais compósitos tem aumentado sua aplicação nas indústrias aeroespacial, naval e automotiva. Porém, esta tecnologia impõe um novo nível de dificuldades aos fabricantes, uma vez que pequenas variações no processo produtivo tem grande influência nas propriedades finais do produto. O objetivo deste trabalho consiste em uma metodologia para avaliar o processo de fabricação de materiais compósitos, identificando componentes fora de especificação. Para isso, é necessário: compreender a influência das variáveis de projeto no comportamento final de uma amostra, construir um modelo numérico e um critério para classificar as estruturas. Assim, é considerado o uso de métodos como, projeto de experimentos (DoE), ajuste de modelo via metamodelos Kriging e métodos baseados em vibração. Inicialmente, as características geométricas das placas de compósito são avaliadas por um scanner 3D. Além disso, as propriedades dos materiais apresentadas na literatura são listadas para definir um intervalo aproximado em que os valores reais têm maior probabilidade de estar presentes. Posteriormente, o DoE é usado para triar e avaliar o efeito principal de cada variável em cada modo. Os resultados do DoE são usados como informações básicas para um procedimento de ajuste de modelo obtendo as propriedades do material e um modelo numérico refinado. Neste trabalho, o processo de ajuste de modelos é aprimorado pelo uso do metamodelo Kriging, com o objetivo de reduzir o tempo computacional demandado durante a otimização. Finalmente, com o modelo numérico atualizado obtém-se as Funções de Resposta em Frequência (FRF) que compõem o envelope representando o conjunto de placas. Esse envelope pode ajudar os engenheiros a avaliar outras placas e classificá-las. A metodologia proposta obteve resultados relevantes, definindo as principais variáveis que influenciam o comportamento dinâmico e apoiando o processo de ajuste de modelo que resultou em erros na ordem de 1 e 2%. Além da boa aproximação, o processo de ajuste do modelo usando Kriging foi eficiente em termos de tempo computacional, exigindo metade do tempo quando comparado com uma metodologia sem uso de metamodelos. Por fim, discutem-se as vantagens e limitações da aplicabilidade dessa metodologia pela apresentação de dois estudos de caso.

Palavras-chave: Resposta dinâmica, Materiais Compósitos, Design de Experimentos, Kriging

List of Figures

2.1	Mobility FRF $M_{11}(\omega)$ of the 4DoF system in linear scale	27
2.2	Receptance FRF of the 4DoF system in dB scale	28
2.3	Real part of a receptance FRF of the 4DoF system	28
2.4	Imaginary part of a receptance FRF of the 4DoF system	29
2.5	Peak picking method	29
2.6	Genetic algorithm general flowchart	39
3.1	Methodology flowchart	42
3.2	Main parameter and flow information for the methodology	43
3.3	Composite material uses in comercial aircrafts	44
3.4	Basic helical horizontal filament winding machine	45
3.5	(a) mandrel schematic and dimensions and, (b) specimen used in experimental tests.	47
3.6	Coordinate machine with the 3D optical scanner.	49
3.7	Specimen and accelerometers (a) schematic representation and (b) experimental analysis.	49
3.8	Experimental set-up	50
3.9	C-Scan test set up used for composite plates	51
3.10	Finite element Model	54
3.11	Numerical mode shape of the plates	55
4.1	Specimen curvatures representation	59
4.2	Thickness distribution for plates with stacking sequence of $[0]_8$. Four squares represent the extensometers attached on the plate.	61
4.3	Thickness distribution for plates with stacking sequence of $[0/15/-15/0/15/-15]_s$. Four squares represent the extensometers attached on the plate . . .	62
4.4	Natural frequencies resulted from the numerical modal analyses $[0]_8$	66
4.5	Natural frequencies resulted from the numerical modal analyses $[0/15/-15/0/15/-15/0]_s$	67
4.6	Main effect mode-by-mode $[0]_8$	69
4.7	Main effect mode-by-mode $[0/15/-15/0/15/-15/0]_s$	70

5.1	Methodology used for the model update strategy adapted from (WANG et al., 2017)	72
5.2	Main effect mode-by-mode with curvature influence highlighted for $[0]_8$ plates	76
6.1	Maximum and minimum limits of natural frequencies and values of natural frequencies of the composite plates.	88
6.2	Limits of the FRF determined by the numerical results.	89
6.3	FRF limits and FRF of Plate 09 and Plate 10	90
6.4	Damage observed by C-scan technique: $[0]_8$. Red box highlights the crack on the plate.	91
6.5	Maximum and minimum limits of the intact composite plates (lines) and damaged frequencies of composite plates (dots) with stack sequence of $[0]_8$.	93
6.6	Damage observed by C-scan technique: $[0/15/-15/0/5/-15]_s$. Red box highlights the crack on the plate.	94
6.7	Maximum and minimum limits of the intact composite plates (lines) and damaged frequencies of composite plates (dots) with stack sequence of $[0/15/-15/0/5/-15]_s$.	96

List of Tables

1.1	An overview of the most commonly used non-destructive testing (NDT) techniques (OOLJEVAAR, 2014).	21
3.1	Plate specimens made of carbon fibre and epoxy resin by filament winding process	46
3.2	Nominal lamina material properties, (TITA et al., 2008)	48
3.3	Resonance modes and damping coefficients	55
4.1	Geometry data collected from composite plates, where C1 and C2 are the curvatures of the plates at $[0]_8$	58
4.2	Geometric data analysis	59
4.3	Factors and its levels from $[0]_8$ plates considered for DoE analyses	64
4.4	Factors and its levels from $[0/15/-15/0/15/-15/0]_s$ plates considered for DoE analyses	64
4.5	Numerical configurations layout of L12 table, Factor's level 1(low), Factor's level 2(high)	65
4.6	Main effect results for stacking sequence $[0]_8$ (units in Hertz)	66
4.7	Main effect results for stacking sequence $[0/15/-15/0/15/-15]_s$ (units in Hertz)	67
5.1	PSO parameter testing results	73
5.2	Comparison between FEA updated results and experimental results for Composite plates $[0]_8$	74
5.3	Updated variables results from FEA model update for Composite plates $[0]_8$	74
5.4	Updated variables results from FEA model update using curvature as design variable	75
5.5	Comparison between FEA updated results (using curvature as design variable) and experimental results	77
5.6	Comparison between FEA updated results and experimental results for Composite plates $[0/15/-15/0/15/-15]_s$	78
5.7	Updated variables results from FEA model update for Composite plates $[0/15/-15/0/15/-15]_s$	78
5.8	Kriging model coefficients after model update for composite plates $[0]_8$	79

5.9	Natural frequencies obtained with the Kriging model compared with the target experimental frequencies for composite plates $[0]_8$.	80
5.10	Comparison between FEA results with experimental data and Kriging values for composite plates $[0]_8$	81
5.11	Kriging model coefficients after model update for composite plates $[0/15/-15/0/15/-15]_s$	82
5.12	Natural frequencies obtained with the Kriging model compared with the target experimental frequencies for composite plates $[0/15/-15/0/15/-15]_s$.	82
5.13	Comparison between FEA results with experimental data and Kriging values $[0/15/-15/0/15/-15]_s$	83
6.1	Experimental natural frequencies compilation and analysis	86
6.2	Minimum and maximum natural frequencies to characterizes the composite plates with stacking sequence $[0/15/-15/0/15/-15]_s$.	86
6.3	Updated frequency results	87
6.4	Updated design variables	87
6.5	Experimental results for intact and damaged plates, stack sequence $[0]_s$.	92
6.6	Experimental results for intact and damaged plates, stack sequence $[0/15/-15/0/5/-15]_s$.	95

Table of Contents

List of Figures	13
List of Tables	15
1 Introduction	19
1.1 Background and Motivation	19
1.2 Objectives and Scope	22
1.3 Outline	22
2 Literature Review	25
2.1 Modal Analyses	25
2.1.1 Structural Dynamics in Frequency Domain	26
2.1.2 Graphic representation of FRF for multiple degree of freedom systems	27
2.1.3 Peak-picking method	29
2.2 Design of Experiments	30
2.3 Model Updating	31
2.3.1 Particle Swarm Optimization	32
2.4 Surrogate Modelling - Kriging	33
2.4.1 Kriging model construction	35
2.4.2 Genetic Algorithm	37
3 Materials and Methods	41
3.1 Methodology	41
3.2 Composite Materials Manufacturing	44
3.3 Composite Materials Tests	48
3.4 Composite Damage Types	51
3.5 Computational Model	52
4 DoE - Design of Experiments	57
4.1 Dimensional analyses	57
4.2 Screening analysis	62

5	Model Updating	71
5.1	Model Update Strategy	71
5.2	Model Update Using FEM	73
5.2.1	Composite plates $[0]_8$	73
5.2.2	Composite plates $[0]_8$ considering curvature as design variable . . .	75
5.2.3	Composite plates $[0/15/-15/0/15/-15]_s$	77
5.2.4	Model Update using Kriging Model	79
5.2.5	Composite plates $[0]_8$	79
5.2.6	Composite plates $[0/15/-15/0/15/-15]_s$	81
6	Case Study	85
6.1	Case Study I: Manufacturing Quality analysis	85
6.2	Case Study II: Damage Identification	90
6.2.1	Results for plates with stacking sequence of $[0]_8$	91
6.2.2	Results for plates with stacking sequence of $[0/15/-15/0/5/-15]_s$. .	93
7	Conclusions and Future Works	97
7.1	Conclusions	97
7.2	Future Works	99
	Bibliography	101
	Apendix	107
A	Scientific Publications	107
B	Kriging Training Script in Python	109

Chapter 1

Introduction

1.1 Background and Motivation

Technology development of complex industries such as automotive, aeronautical and naval always demanded high-performance structural components. During the last decades, composite materials have emerged as the most promising technology to meet the requirements of high specific stiffness and strength, excellent fatigue resistance, longer durability as compared to metallic structures, and their ability to be tailored for specific applications.

Differently, from metallic structures, properties of composites are not easy to control during manufacturing, and as consequence, there is an important level of uncertainty in the properties of these materials. These uncertainties make the design task difficult and increase the probability of errors in predicting the structure life cycle. Therefore, methodologies that take into account the materials properties and geometry uncertainties are very useful to support the engineering design process, and also the quality and control process of the composite industry (JIANG et al., 2008; SRIRAMULA; CHRYSSANTHOPOULOS, 2009; CHANDRASHEKHAR; GANGULI, 2009). Kim and Sin (2001) proposed an algorithm to obtain the optimal design of composite laminated plates, and observed that results for optimal thickness increases, when elastic moduli uncertainties are considered, which indicates that such uncertainties should not be ignored at the design stage. Due to uncertainties, the repeatability of composite components, even in the same manufacturing process, is quite hard. Thus, it is not possible to define reference values to be used in the design phase without experimental tests.

The characterization of materials can be sorted into two main parts, which are destructive technique and non-destructive technique. The destructive technique can be classified as a classical static approach that involves static mechanical tests, such as, tensile test, compression test, bending test, torsion test, etc. in order to acquire the stresses and strains of a specimen. Direct identification of elastic constants of composite materials

can be done based on the fundamental stress-strain theory. For composite materials, the procedures are more cumbersome and time-consuming due to the need of several specimens analyses. Meanwhile, the Non-Destructive Technique (NDT) involves two parts, which are the experimental and numerical part. In experimental part, measurements of significant parameters and data extraction will be conducted for subsequent use in numerical part, while, numerical part involves the use of forward, as well as inverse methods for evaluation of elastic properties of the composite material (WANG; KAM, 2000; BRUNO et al., 2008).

The NDT can be also applied to identify properties of a component during operation, which is known as damage detection methods. Successful damage detection in structures is essential for maintenance. NDE/NDT, which can identify damage, may be used for this purpose. However, most of the non-destructive methods, such as ultrasonic methods, require the location of the damage and that location must be accessible. The methods, which are based on vibration responses (VBM), usually do not show these limitations. The basis of vibration response methods is that damage changes the dynamic behaviour of the structure. Damage in a structure can alter the structural integrity, and therefore, the physical properties like stiffness, mass and/or damping may change, modifying the global structural dynamic response.

Several kinds of NDT have been developed. Table 1.1, presents a resume of the most commonly NDT techniques. Also, every year new researches are developed to show the applicability of new methods and metrics. These damages identification methods can be classified as performance levels (RYTTER, 1993), model and non-model based approach (OOJEVAAR, 2014), local and global methods (FRITZEN; KRAEMER, 2009), baseline and non-baseline (WORDEN et al., 2007).

Dynamic analyses have shown high potential as NDT (SINOUE, 2013; FARRAR et al., 2001). Different methods have been already presented in the literature using natural frequencies and Frequency Response Function (FRF) to detect damages on composite structures (MONTALVAO, 2006; KIM et al., 2003). Several damage detection methods assume that damages cause changes in the mass and stiffness (KESSLER et al., 2002). However, to make this assumption, it is necessary to have a good definition of the undamaged state of the component. A usual methodology is to proceed nondestructive testing on all the components, just before and after the operation to verify its state (MEDEIROS et al., 2015). This is required because it is well known that the characteristics of a composite component are not easy to control. The manufacturing process has several variables that can affect the final properties of the component. Therefore, depending on the manufacturing process and the design tolerances for the structure, it is possible to define a method to provide information about the acceptability of the components based on a set of specimens, reducing the time and cost of the non-destructive evaluations.

Thus, in this work, the dynamic behaviour of composite plates is evaluated in order to propose a methodology to allow a preliminary study of the acceptability of the intact

Table 1.1: An overview of the most commonly used non-destructive testing (NDT) techniques (OOLJEVAAR, 2014).

Technique	Inspection area	Inspection mode	Structure Accessibility
Electric, magnetic and eletromagnetic			
Electrical conductivity testing	Local/global	Off-/on-line	Not required
Magnetic particle testing	Local	Off-line	Required
Eddy current testing	Local	Off-line	Required
Radiography (X-ray)	Local	Off-line	Required
Infrared thermography	Local/global	Off-line	Required
Mechanic, dynamic			
Quasi-Static	Local	Off-/on-line	Not required
Structural vibrations and acoustics	Local/global	Off-/on-line	Not required
Electro-mechanical impedance	Local/global	Off-/on-line	Not required
Acoustic emission	Local/global	on-line	Not required
Acoustic-ultrasonic	Local/global	Off-/on-line	Not required
Ultrasonic testing	Local	Off-line	Required
Optical			
Shearography	Local	Off-line	Required
Visual inspection	Local/ global	Off-line	Required

state to the component. This is made based on the assessment of the structural dynamic behaviour of a set of composite plates. To support this study, an inverse identification of properties is carried out by a numerical model updated using a Kriging based methodology. Therefore, numerical and experimental results are used to compose a range of possibilities for the FRF that can be used to verify the state of other composite plates.

Consequently, evaluate the influence of the manufacturing system on the composite structures is an important step. Several authors have been studied composite materials properties and variability in composite materials. Potter (2009b) presents a review of the sources of variability in the manufacture of composite parts by the resin transfer moulding process, identifying more than 130 defect types and more than 60 sources of variability.

1.2 Objectives and Scope

Based on the scenario pointed above, the present work consists of developing a methodology to helps in the initial verification of a manufactured component. Analyzing the design variables most affected during the manufacturing process and the effects on the dynamic behaviour, aiming to define the tolerance limits of a set of components. Computational simulations are used to expand the number of samples, since physical experiments are expensive and have a limited number of specimens. Thus, the main objective can be divided into specific ones:

- Perform a literature review in order to understand the most relevant scientific papers, as well as the most recent publications, which have been developed in the areas of dynamic analysis used in composite structures;
- Analyse the variability of the manufactured composite plates in terms of geometry and material properties;
- Evaluate the dynamic behaviour of composite plates;
- Identify the most influential variables and reduce the number of design variables for further analysis;
- Obtain updated design variables using the Kriging method;
- Obtain the acceptable set of FRFs for the manufacturing process.

1.3 Outline

This work consists of six chapters organized as follow:

- **Chapter 1 - Introduction:** This chapter presents the main literatures to contextualize the scenario about composite materials, design of experiments and materials property evaluation. Also, the objectives and scope of this work are presented.
- **Chapter 2 - Literature Review:** Fundamentals of the main topics and research objectives behind this work. Giving the mathematical and theoretical basis to understand the implementations and analysis although this work.
- **Chapter 3 - Methodology:** Describes the methodology used in this work, providing the description of the materials and methods used to manufacture and test the composite structures and experimental tests.
- **Chapter 4 - DoE - Design of Experiments:** Provides a literature search about the design of experiments (DoE). Presents analyses of the material and geometrical variabilities of the composite plates. Describes the application of a DoE technique to identify the most influential parameters on the dynamic behaviour of composite plates, and carry out a screening of the design variables.
- **Chapter 5 - Model updating:** Describes the model update methodologies used in this work. Providing an overview and the application of a simple model update using Particle Swarm Optimization and Finite Element Method as a benchmark. In addition, the Kriging model construction is explained and a model update process is carried out using this model. A brief discussion about quality and computational cost of the model updating is given.
- **Chapter 6 - Case Study:** Presents the case study to demonstrate the applicability of the methodologies presented in this work. The case study one shows a methodology to define a frequency range to characterize a composite plate as intact structure. The case study two uses the results of the case study one to identify damage on composite plates.
- **Chapter 7 - Conclusions:** This chapter begins by summarizing the work performed. Final conclusions are then presented along with the recommendations on future's research needs.

Chapter 2

Literature Review

2.1 Modal Analyses

Excessive Structural vibration continues to present a major hazard and design limitation for a very wide range of engineering products today. First, there are a number of structures, from turbine blades to suspension bridges, for which structural integrity is of paramount concern, and for which a thorough and precise knowledge of the dynamic characteristics is essential. Then, there is an even wider set of structural components or assemblies for which vibration is directly related to performance, either by virtue of causing a temporary malfunction during excessive motion or by creating disturbance or discomfort, including noise. For all these examples, it is important that vibration levels encountered in service or operation be anticipated and brought under satisfactory control.

The experimental study of structural dynamics has provided a major contribution to understanding and to controlling many vibration phenomena encountered in practice. Since the beginning of structural vibration study, experimental observations have been necessary for determining the nature and extent of vibration response levels in operation, verifying theoretical models and predictions of various dynamic phenomena and the measurement of the essential material properties under dynamic loadings, such as damping capacity, friction, and fatigue endurance.

Modal analysis is the process of determining the inherent dynamic characteristics of a system in forms of natural frequencies, damping factors, and mode shapes. The formulated mathematical model is referred to as the modal model of the system, and the information for the characteristics are known as its modal data. Furthermore, modal testing is an experimental technique used to derive the modal model of a linear time-invariant vibratory system. The theoretical basis establishes the relationship between the vibration response at one location and excitation at the same or another location as a function of excitation frequency. This relationship, is known as Frequency Response Function (FRF). Combinations of excitation and response at different locations lead to

a complete set of FRFs which can be collectively represented by an FRF matrix of the system. This matrix is usually symmetric, reflecting the structural reciprocity of the system.

The mathematical development presented in this section can be found in more detail on classical references as Fu and He (2001) and Ewins (2000).

2.1.1 Structural Dynamics in Frequency Domain

The governing equation of structural dynamics in the time domain can be developed by applying Newton's 2nd law of motion for the analytical model of a structure undergoing small deformations, by equating the internal resisting forces (inertia, damping, and elasticity) with the external excitation can be written as,

$$\mathbf{M}\ddot{\mathbf{X}}(t) + \mathbf{C}\dot{\mathbf{X}}(t) + \mathbf{K}\mathbf{X}(t) = \mathbf{F}(t), \quad (2.1.1)$$

where \mathbf{M} , \mathbf{C} and \mathbf{K} are the mass, damping and stiffness matrices of the structure, $\mathbf{F}(t)$ is the external excitation, and $\ddot{\mathbf{X}}(t)$, $\dot{\mathbf{X}}(t)$ and $\mathbf{X}(t)$ are the acceleration, velocity and displacement vectors, respectively.

Considering the response to harmonic system, we have the harmonic excitation as,

$$\mathbf{F}(t) = \mathbf{F}_0 e^{i\omega t}, \quad (2.1.2)$$

where F_0 is the static force, X_0 is the amplitude, and ω is the frequency. Considering a solution the displacement with the same form,

$$\mathbf{X}(t) = \mathbf{X}_0 e^{i\omega t}. \quad (2.1.3)$$

Applying the derivatives to displacement we have,

$$\dot{\mathbf{X}}(t) = i\omega \mathbf{X}_0 e^{i\omega t}, \quad (2.1.4)$$

and

$$\ddot{\mathbf{X}}(t) = -\omega^2 \mathbf{X}_0 e^{i\omega t}. \quad (2.1.5)$$

Therefore, substituting into equation of motion we have,

$$(-\mathbf{M}\omega^2 + i\omega\mathbf{C} + \mathbf{K})\mathbf{X}_0 e^{i\omega t} = \mathbf{F}_0 e^{i\omega t}, \quad (2.1.6)$$

resulting on,

$$(\mathbf{K} + i\omega\mathbf{C} - \omega^2\mathbf{M})\mathbf{X}_0 = \mathbf{F}_0. \quad (2.1.7)$$

Rewriting the equation we can obtain the Frequency Response Function of the

system as,

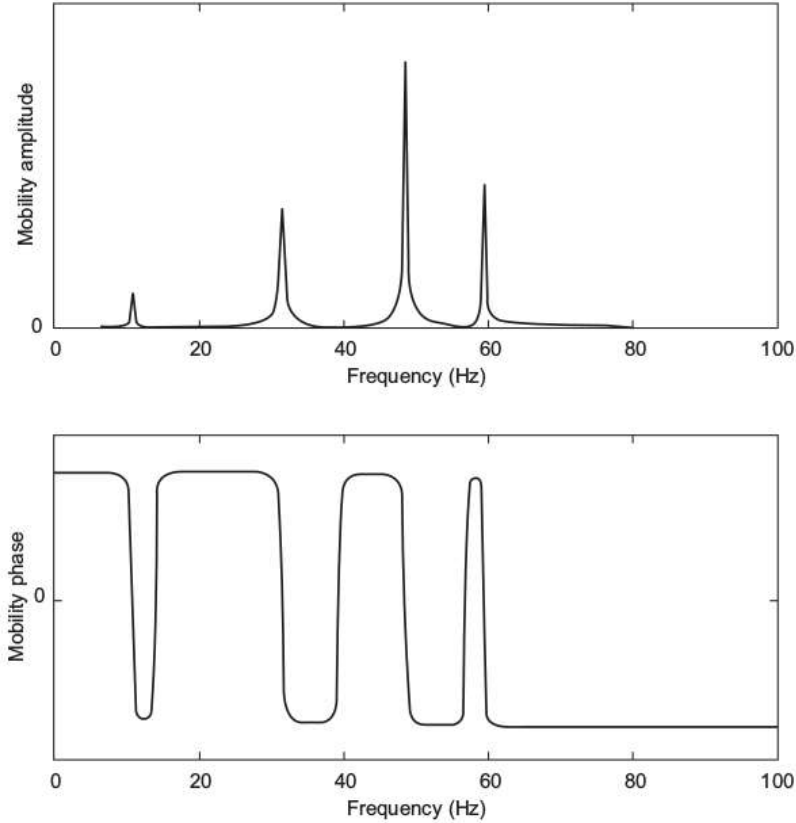
$$\frac{\mathbf{X}_0}{\mathbf{F}_0} = \frac{1}{(\mathbf{K} + i\omega \mathbf{X}_0 \mathbf{C} - \omega^2 \mathbf{M})} \quad (2.1.8)$$

2.1.2 Graphic representation of FRF for multiple degree of freedom systems

The FRF of multiple degree of freedom (MDoF) system has different ways to be graphically presented, such as Amplitude Phase plot, log log plot, Real and Imaginary plots and Nyquist plot.

The amplitude phase plot of the FRF, for a damped MDoF system, consists of the plot of its magnitude versus frequency and that of its phase versus frequency. Figure 2.1 shows the amplitude and phase of the mobility $M_{11}(\omega)$ of the 4DoF system in linear scale. As expected, the amplitude plot is dominated by resonance. The phase plot reflects the existence of a vibration mode from its visible phase change.

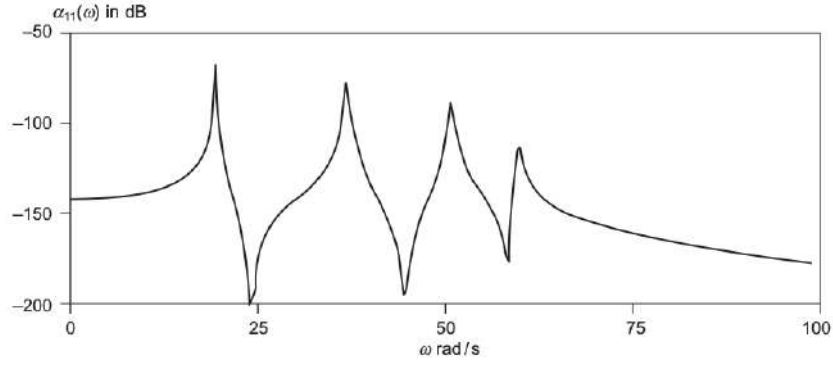
Figure 2.1: Mobility FRF $M_{11}(\omega)$ of the 4DoF system in linear scale



Source: Fu and He (2001).

The log-log plot is useful to better visualize the resonances and anti-resonances of a systems. This plot consists of the receptance plotted in dB scale. Figure 2.2 shows an example of a 4DoF systems in log-log plot.

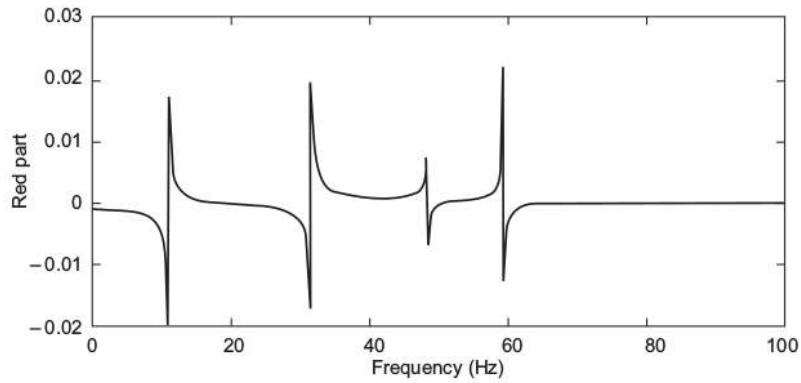
Figure 2.2: Receptance FRF of the 4DoF system in dB scale



Source: Fu and He (2001).

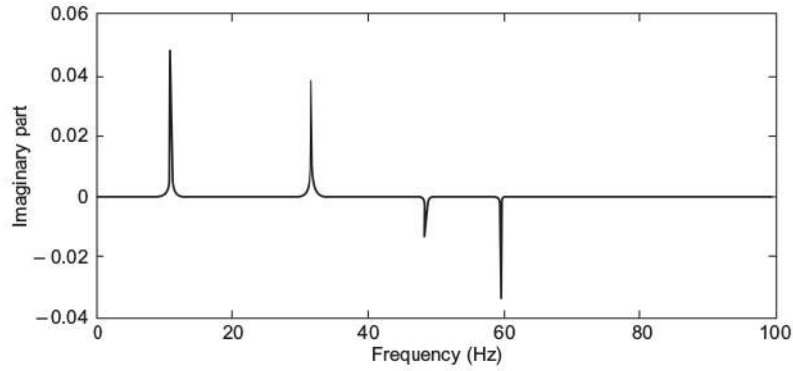
The real and imaginary plots consist of two parts: the real part of the FRF versus frequency (Figure 2.3) and its imaginary part versus frequency (Figure 2.4). Real and imaginary plots are retracted to be its first part without damping.

Figure 2.3: Real part of a receptance FRF of the 4DoF system



Source: Fu and He (2001).

Figure 2.4: Imaginary part of a receptance FRF of the 4DoF system



Source: Fu and He (2001).

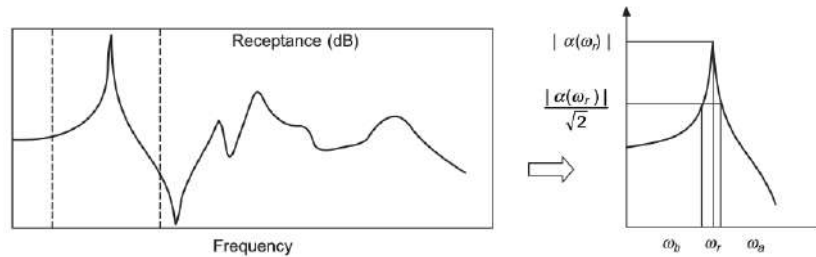
2.1.3 Peak-picking method

The peak picking method is the first part of the so-called modal extraction methods. The objective is to obtain the main modal parameters of the system based on the FRF of the structure. This method is based on an algorithm that searches by a point of maximum amplitude next to the natural frequency. This point is called resonance frequency (ω_r) and it is a good approximation to the natural frequency in a lower damping system. To define damping, two points next to a peak of magnitude in the FRF are selected (ω_1 and ω_2). These points are settled to correspond to a half of the frequency power. Then the critical damping ratio can be defined as,

$$\xi_r = \frac{\omega_{2,r} - \omega_{1,r}}{2\omega_r} \quad (2.1.9)$$

Figure 2.5 graphically represents the points used in the peak-picking method.

Figure 2.5: Peak picking method



Source: Adapted from Fu and He (2001).

2.2 Design of Experiments

Experiments in engineering are essential to understanding the behaviour, the amount of variability, and its impact on a given process. Experiments are often carried out without a solid methodology, depending many times on guesswork, luck, experience, and intuition for its success. Design of experiments (DoE) refers to the process of planning, designing, and analyzing the experiment so that valid and objective conclusions can be drawn effectively and efficiently. To draw statistical conclusions from the experiment, it is necessary to integrate simple and powerful statistical methods into the experimental design methodology.

Design of Experiments was introduced in the 1920s by Sir Ronald A. Fisher in England in the field of agricultural research. Fisher was able to lay out all combinations of factors included in the experimental study and with the help of a table conduct the experiments and after analyze data. Since then many scientists and statisticians have contributed to DoE development and to its application in different fields.

Classic DoE methods focus on planning experiments so that the random error in physical experiments has a minimum influence on the approval or disapproval of a hypothesis. Widely used classic experimental designs include factorial or fractional factorial design, central composite design (CCD), Box-Behnken, Plackett- Burman designs (MYERS et al., 2016) and optimal design (DEY et al., 2016).

In the last decade, the number of numerical experiments has increased considerably to help product development and research activities. A computer experiment is a number of simulations with various inputs. A feature of many computer experiments is that the output is deterministic, there is no difference between simulations with identical inputs (SACKS et al., 1989). Computer experiments are used to obtain information from processes, where the physical tests are complex or too expensive. Computational experiments are different from the physical experiment, on computer experiment, there is no experimental error, no blocking needed, no randomization needed and no external noise. Comprehensive reviews concerning the design of computational experiments were made by Chen et al. (2006), Wang and Shan (2007), Chaloner and Verdinelli (2013).

As computer experiments involve mostly systematic error rather than the random error as in physical experiments, Sacks et al. (1989) stated that in the presence of systematic rather than a random error, a good experimental design tends to fill the design space rather than to concentrate on the boundary. They also stated that classic designs, e.g. CCD and D-optimal designs can be inefficient or even inappropriate for deterministic computer codes. Jin et al. (2001) confirmed that a consensus among researchers was that experimental designs for deterministic computer analyses should be space filling. Four types of space filling sampling methods are relatively often used in the literature. These are orthogonal arrays (SLOANE; NJA, 1999), Latin Hypercube designs (PARK, 1994),

Hammersley sequences (MECKESHEIMER et al., 2002) and uniform designs (FANG et al., 2000).

2.3 Model Updating

Finite Element Methods (FEM) are mathematical tools to solve differential equations. It is very useful to engineers that can represent different kinds of physicals phenomenon by differential equations. In many real-life situations, the deterministic analysis is not sufficient to assess the quality of a design. In a design stage, some physical properties of the model may not be determined yet. But even in a design ready for production, design tolerances and production inaccuracies introduce variability and uncertainty (MUNCK et al., 2008). Also, the results obtained by FEM are strongly dependent on the inputs provided by the user. Thus, to match numerical with experimental results, it is necessary the knowledge of the exact value for several parameters. To overcome these issues, some strategies can be used, like the use of approximate models to represent the FEM and obtain results without solving all the equations or use model update techniques as an alternative to find the right parameters to set a simulation.

Model updating methods simultaneously utilize the structural response obtained by the FEM and the measured structural response to calibrate mathematical modeling. The model update aims to reduce the errors between the results from the numerical simulation compared to the results from the experimental data. In the literature, it is possible to find methodologies to use model update via modal parameters even as Frequency Response Function (FRF), as presented by Imregun and Visser (1991) and Mottershead and Friswell (1993).

Model updating methods can be broadly classified into direct methods, which are essentially non-iterative ones, and the iterative methods. Direct methods are essentially based on changes in the mass and stiffness matrix to obtain the results that better fit on experimental data, even if these changes are not physically meaningful (LIM, 1990). Iterative methods are based on minimizing an objective function that is generally a non-linear function of selected updating parameters. Quite often eigenvalues, eigenvectors or response data are used to construct an objective function (CHEN; GARBA, 1980).

Recently, Zang et al. (2012) investigated a novel method using the Equivalent Element Modal Strain Energy (EEMSE) and Equivalent Element Modal Kinetic Energy (EEMKE) to localize errors in the finite element model, and applied to select parameters in the model updating process. The results demonstrate the effectiveness of the method and show great potential for industrial application. Sipple and Sanayei (2014) presented a frequency response function based finite element model updating method and used to perform parameter estimation. The proposed method is used to calibrate the initial finite element model using measured frequency response functions from the undamaged, intact

structure. Stiffness properties, mass properties, and boundary conditions of the initial model were estimated and updated. The usefulness of the proposed method for finite element model updating is shown by being able to detect, locate, and quantify changes in structural properties. Shadan et al. (2016) validated a finite element model updating method using frequency response functions. They used a sensitivity-based model updating approach, which utilizes a pseudo-linear sensitivity equation. The method is applied to identify the location and amount of the changes in structural parameters. The results indicate that the location and the size of different level of changes in the structure can be properly identified by the method.

Sensitivity based optimization algorithms have the disadvantage that can be computationally expensive and have difficulties to converge, mainly when applied to complex models. However, algorithms as Particle Swarm Optimization (PSO), Genetic Algorithms (GA), Ant Colony (AC), etc., can avoid calculating the sensitivity. However, these algorithms need high numbers of computation of the Finite Element Analysis problem, being time consuming too. To work around this problem, metamodel techniques, which is known as an approximate model or surrogate model, can be used to turn model update a practical tool even for complex models.

2.3.1 Particle Swarm Optimization

Particle Swarm Optimization (PSO) is an evolutionary optimization method, widely used for its easy implementation. The PSO algorithm was introduced by Dr. Kennedy and Dr. Eberhart in 1995 with the basic assumption of reproduce the collective behaviour of groups of birds, fish and insects. Based on the natural communication process to share the knowledge of individuals to the group when searching for something. PSO algorithm is applied to different scientific areas as, traffic routes, image processing, structural optimization, and materials parameter characterization (Vaz Jr et al., 2013).

The PSO algorithm has a simple implementation, the main steps and equations involved in this process are presented. The initial population (P) is defined as a matrix of random numbers where each line represents a particle and each column a design variable. Then, the objective function is calculated for each particle and stored in the vector P_f . Other variables to be initialized are a matrix to store the best position of each particle during the population evolution P_{ib} and the velocity matrix v . The PSO iterative process starts with the actualization of the matrix P_{ib} by storing the new best position of each particle. Therefore, it is possible to identify the best particle P_{gb} . Hence, the particles velocity can be calculated by,

$$v_j(i) = wv_j(i-1) + r(0, \phi_1)(P_{ib}(i) - P_j) + r(0, \phi_2)(P_{gb}(i) - P_j), \quad (2.3.10)$$

where $r(0, \phi_1)$ e $r(0, \phi_2)$ are random values, ϕ_1 and ϕ_2 represents the individual cognitive parameter and the social parameter associated with the collective effect of the population. The variable w is the inertia parameter that is introduced to reduce the particles velocity when close to the convergence (SHI; EBERHART, 1998). High values of w provides a better exploration of the solution space and lower values are better to local search. Hence, it is interesting to define w with a decreasing linear variation during the iterations.

Calculating the particles velocity of each particle, the respective new position is defined as,

$$P(i) = P(i - 1) + v(i). \quad (2.3.11)$$

A verification of the particle's position is done to identify if the particle is within the boundaries defined to the design variables. The strategy used in this algorithm consists on return the particle position to the boundary every time that particles exceed the limits.

The convergence is achieved when all of the particles are concentrated in a point, and the velocities approach to zero. Therefore the convergence criterium is based on the mean velocity of the particles on each iteration. The convergence is done when all individuals are concentrated in a point and the mean velocity of the group is near to zero.

2.4 Surrogate Modelling - Kriging

Nowadays, engineering problems become more and more complex, in the same way, that the time to develop products must to be shorter than ever. In this context, companies need teams with specialists and powerful infrastructure for making important decisions based on the analysis. For example, in modern aerospace design offices, the computational power needed to support advanced decision making can be prodigious and, even with the latest and most powerful computers, designers still wish for greater understanding that can be gained by straightforward use of the familiar analysis tools, such as those coming from the fields of computational fluid dynamics or computational structural mechanics. One way of gaining this desirably increased insight into the problems being studied is via the use of surrogate models (or metamodels). Such models seek to provide answers in the gaps between the necessarily limited analysis runs that can be afforded with the available computing power. They can also be used to bridge between various levels of sophistication afforded by varying fidelity physics-based simulation codes, or between predictions and experiments.

This technique considers the relationship between the input and output as a black-box system, and other system information, such as the internal process of dynamic analysis is not required. It can create, for example, a fast running surrogate model to replace the exact FEA, and then the solving time of optimization will be reduced

significantly. Thus, the potential of metamodel techniques is indisputable in model updating field. A comparison of the most commonly used metamodels is presented by Simpson et al. (2001b). In addition, Simpson et al. (2001a) investigated the use of kriging models as alternatives to traditional second-order polynomial response surfaces for constructing global approximations for use in a real aerospace engineering application, namely, the design of an aerospike nozzle. They find that the kriging models yield global approximations that are slightly more accurate than the response surface models.

Kriging model is constructed based on the correlation function theory. Particularly, it is an exact interpolation of the given data and goes through all the sampling points. Therefore, the Kriging model usually has a higher approximation accuracy than traditional Root Mean Square (RSM). Jeong et al. (2005) applied the kriging-based genetic algorithm to aerodynamic design problems. The kriging model drastically reduces the computational time required for objective function evaluation in the optimization (optimum searching) process. Based on the result of the functional ANOVA, designers can reduce the number of design variables by eliminating those that have a small effect on the objective function. Huang et al. (2006) proposed a new method that extends the Efficient Global Optimization to address stochastic black-box systems. The method is based on a kriging meta-model that provides a global prediction of the objective values and a measure of prediction uncertainty at every point. The results suggest that the proposed method has excellent consistency and efficiency in finding global optimal solutions, and is particularly useful for expensive systems.

Yuan and Guangchen (2009) presented the metamodeling capabilities of two methods, i.e. neural network (NN) and Kriging approximation, in the context of simulation optimization. Preliminary research results reveal that Kriging approximation is in general likely to be preferred. Khodaparast et al. (2011) solved the problem interval model updating by using the Kriging method, and the good accuracy of Kriging method was illustrated by beam experiment. Liu et al. (2014) calibrated the FEM based on the modal parameters of a complex structure, the Kriging model was taken as a surrogate model. Dey et al. (2015) presented the Kriging model approach for stochastic free vibration analysis of composite shallow doubly curved shells. The stochastic natural frequencies are expressed in terms of Kriging surrogate models. The influence of random variation of different input parameters on the output natural frequencies is addressed. Also, it is very important to highlight the difficulty to find in the literature valuable scientific contributions to developing accurate models to represent manufactured components to aid the design of structural health monitoring (SHM) systems.

In this context, this work presents a model updating strategy to obtain the input parameters used in a Finite Element Method (FEM), which represent the experimental dynamic behaviour of a composite plate. For this, a Kriging metamodel is chosen to reduce the computational cost of the optimization process into the model update. A set

of finite element analyses are used to training the metamodel. After that, the kriging model is used every time when the objective function is evaluated. This strategy provides a considerable reduction in the computational time during the optimization process, where a PSO is going to be used. These results are analyzed in order to evaluate the potentialities and limitations of the proposed methodology in the context of SHM systems.

2.4.1 Kriging model construction

The best linear unbiased predictor, also known as Kriging, is a surrogate model, frequently used to represent a physic phenomenon or process, which is difficult to represent by numerical models or to measure experimentally. The name Kriging was introduced by Matheron (1963), in honour of the South African mining engineer Danie Krige, who first developed the method now called Kriging (KRIGE, 1951). Kriging made its way into engineering design following the work of Sacks et al. (1989), who applied the method to the approximation of computer experiments.

For a given set of samples data, $\mathbf{X} = \mathbf{x}_1, \mathbf{x}_2, \dots, \mathbf{x}_n^T$, and the observed responses, $\mathbf{Y} = \mathbf{y}_1, \mathbf{y}_2, \dots, \mathbf{y}_n^T$, the expression of the Kriging model that reflects the relationship between them is,

$$y(\mathbf{x}_i) = \mathbf{f}^T(\mathbf{x}_i)\boldsymbol{\beta} + z(\mathbf{x}_i), \quad (2.4.12)$$

where $\mathbf{f}(\mathbf{x})$ is a polynomial vector of the sample \mathbf{x} , $\boldsymbol{\beta}$ is the vector of the linear regression coefficients to be estimated, and $z(\mathbf{x}_i)$ represents errors and is assumed to be a stochastic process that follows a normal distribution of $N(0, \sigma^2)$, with a zero mean and standard deviation σ .

It should be noted that the basic assumption of the Kriging model is that the same input will lead to an identical output. Therefore, the deviation between the output response and the polynomial regression part is only due to the modelling error itself, regardless of the measurement error and other random factors. This method does not depend on the simulated precision of the polynomial part to the response surface but focuses on constructing the appropriate surrogate model by the effective filling of the stochastic process part, which makes it more suitable for dealing with nonlinearity. Thus, the polynomial part is often taken as a constant in some other references.

To estimate the stochastic process $z(\mathbf{x})$, the Kriging method assumes that the true response surface is continuous, any two points will tend to have the same value as the distance in between approaches zero and it is the same for $z(\mathbf{x})$ of two points. Thus, the correlation between $z(\mathbf{x})$ of any two sample points can be expressed as a function of their spatial distance. The most widely used Gaussian correlation model is adapted as,

$$R(z(\mathbf{x}_i), z(\mathbf{x}_j)) = \exp \left(- \sum_{k=1}^m \theta_k |x_i^k - x_j^k|^2 \right), \quad (2.4.13)$$

where x_i^k and x_j^k are the k^{th} components of the two sample points \mathbf{x}_i and \mathbf{x}_j , m denotes the number of design variables, θ_k controls the decay rate of correlation on different dimensions. And, then the matrix of correlation functions between sample points is obtained as,

$$\mathbf{R} = \begin{Bmatrix} R(\mathbf{x}_1, \mathbf{x}_1) & \cdots & R(\mathbf{x}_1, \mathbf{x}_n) \\ \vdots & \ddots & \vdots \\ R(\mathbf{x}_n, \mathbf{x}_1) & \cdots & R(\mathbf{x}_n, \mathbf{x}_n) \end{Bmatrix}. \quad (2.4.14)$$

The likelihood function of the sample point can then be written as,

$$L = \frac{1}{(2\pi\sigma^2)^{\frac{m}{2}} |\mathbf{R}|^{\frac{1}{2}}} \exp \left[- \frac{(\mathbf{Y} - \mathbf{F}\boldsymbol{\beta})^T \mathbf{R}^{-1} (\mathbf{Y} - \mathbf{F}\boldsymbol{\beta})}{2\sigma^2} \right], \quad (2.4.15)$$

where \mathbf{F} is a matrix of vector $\mathbf{f}(\mathbf{x})$ for each sample point. $|\mathbf{R}|$ is the determinant of \mathbf{R} which is a function of θ_k . According to the maximum likelihood function method, one can get,

$$\hat{\boldsymbol{\beta}} = \left(\frac{\mathbf{F}^T \mathbf{R}^{-1} \mathbf{Y}}{\mathbf{F}^T \mathbf{R}^{-1} \mathbf{F}} \right), \quad (2.4.16)$$

$$\hat{\sigma}^2 = \frac{((\mathbf{Y} - \mathbf{F}\boldsymbol{\beta})^T \mathbf{R}^{-1} (\mathbf{Y} - \mathbf{F}\boldsymbol{\beta}))}{n}. \quad (2.4.17)$$

Based on this, the logarithm form of the maximum likelihood function can be written as,

$$\ln(L) \approx -\frac{m}{2} \ln(\hat{\sigma}^2) - \frac{1}{2} \ln|\mathbf{R}|. \quad (2.4.18)$$

The maximum value of the function above is solved by the genetic algorithm to determine the value of the decay rate θ_k on different dimensions.

At this point, a Kriging model linking the sample point and the response is constructed. The next step is to predict the value of new points. For any point \mathbf{x}_0 , following the principle that the predicted value for the point continue to maximize the augmented likelihood function of both the sample point and the new point, the predicted response value can be obtained by,

$$\hat{y}(\mathbf{x}_0) = \mathbf{f}^T \hat{\boldsymbol{\beta}} + \mathbf{r}^T(\mathbf{x}_0) \mathbf{R}^{-1} (\mathbf{Y} - \mathbf{F} \hat{\boldsymbol{\beta}}). \quad (2.4.19)$$

And the mean squared error (MSE) of the predictor can also be calculated to estimate the accuracy of the predicted value, which is denoted by $\hat{s}^2(\mathbf{x})$,

$$\hat{s}^2(\mathbf{x}) = \sigma^2 \left[1 - \mathbf{f}^T \mathbf{x}, \mathbf{r}^T \mathbf{x} \begin{bmatrix} 0 & \mathbf{F}^T \\ \mathbf{F} & \mathbf{R} \end{bmatrix}^{-1} \begin{Bmatrix} \mathbf{f}(\mathbf{x}) \\ \mathbf{r}(\mathbf{x}) \end{Bmatrix} \right], \quad (2.4.20)$$

where $\mathbf{r}^T(\mathbf{x}_0)$ is a row vector of correlation function between the new point and each sample point,

$$\mathbf{r}^T(\mathbf{x}_0) = [R(\mathbf{x}_0, \mathbf{x}_1), \dots, R(\mathbf{x}_0, \mathbf{x}_n)]. \quad (2.4.21)$$

It is worth noting that when the value of the i^{th} sample point is predicted, since $\mathbf{r}^T(\mathbf{x}_i)\mathbf{R}^{-1}$ equals the i^{th} order unit vector, therefore,

$$\hat{y}(\mathbf{x}_i) = \mathbf{f}^T(\mathbf{x}_i)\hat{\boldsymbol{\beta}} + y_i - \mathbf{f}^T(\mathbf{x}_i)\hat{\boldsymbol{\beta}} = y_i, \quad (2.4.22)$$

which shows that the Kriging model predicts the real response value at the sample point. That is why it can be considered an interpolation technique.

2.4.2 Genetic Algorithm

The Genetic Algorithm (GA) is an adaptive heuristic search method based on population genetics. The Genetic Algorithm was introduced by John Holland in the early 1970s (HOLLAND, 1975). It is a probabilistic search algorithm based on the mechanics of natural selection and natural genetics.

The GA algorithm has as mains steps the initialization, evaluation of objective function, selection, crossover, mutation, actualization, and finalization. Basically, the algorithm creates a population of possible results to the problem and submit the individuals to the evolution process, that can consist of the following steps,

- Initialization: Initializes the population with random values for design variables;
- Evaluation: Evaluates the objective function of each individual;
- Selection: A set of individuals are selected based on its fitness value, then giving bests chances to individuals with higher fitness values;
- Crossover: The selected individuals are combined to generate new ones for the next generation;
- Mutation: Characteristics of the individuals are randomly changed to insert variety in the population and avoiding a quick convergence to the local minimum;
- Actualization: New individuals are inserted in the population;
- Finalization: Verifies the convergence criterion, return to the evaluation step or finalizes the evolution.

The main characteristics of GA are,

- Codified search;
- Generalist algorithm;
- Explicit parallelism;
- Stochastic search .

Figure 2.6 presents the flowchart of the algorithm, where the needed parameters to initialization are,

- Population size;
- Number of bits to represent design variables;
- Number of design variables;
- Upper and lower limits for each design variable;
- Crossover ratio;
- Mutation probability;
- Total number of generations.

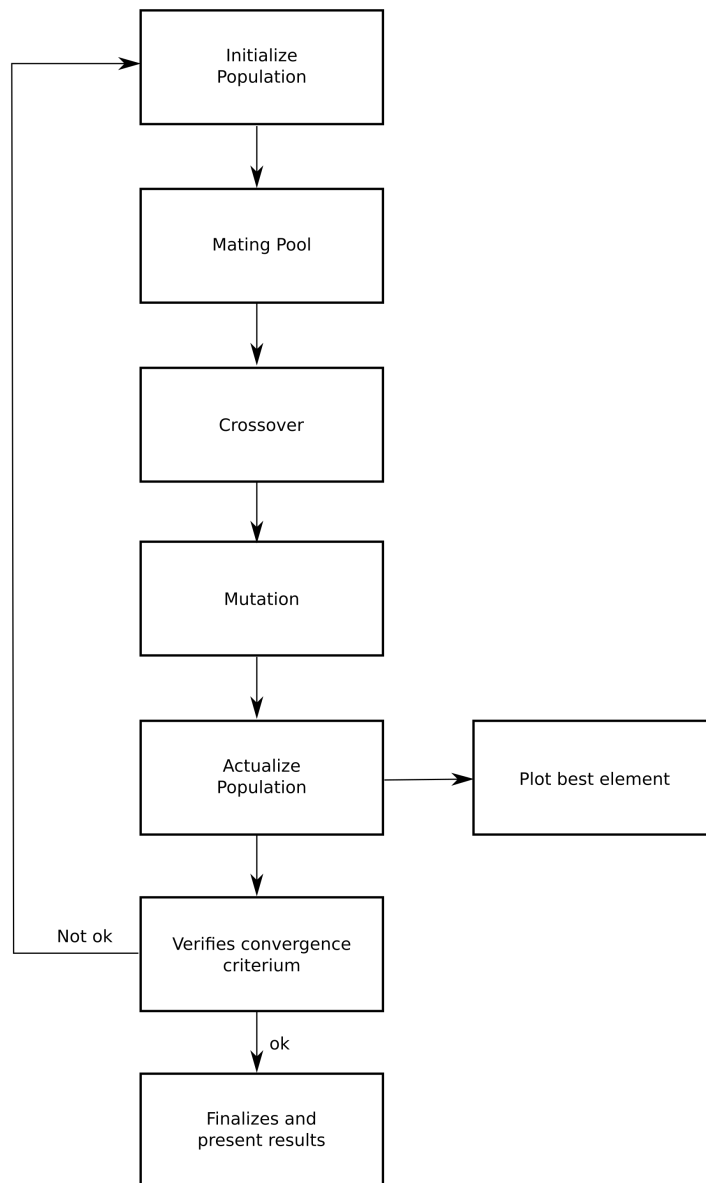


Figure 2.6: Genetic algorithm general flowchart

Chapter 3

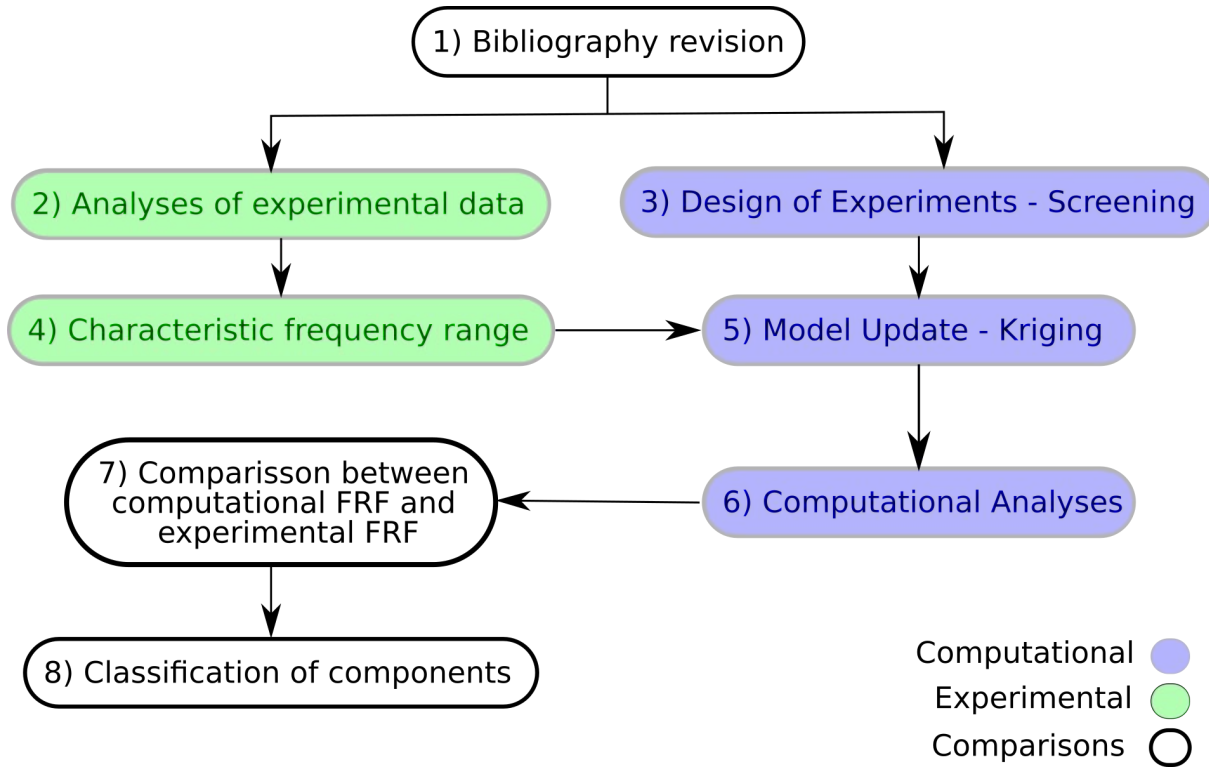
Materials and Methods

3.1 Methodology

The structural dynamic response of composite plates is investigated evaluating the influence of the manufacturing process. Experimental and numerical tests are performed and compared to understand the variabilities of the component properties. To study the variables influence the dynamic response, a Design of Experiments method is applied. Furthermore, analyzing the experimental data, it is possible to infer the frequency range of the composite plate set. Therefore, to obtain the numerical model that represents the frequency range bounds, a model update process is required. This is a very common procedure to adjust numerical with experimental or analytical models presented in the literature.

However, depending on the complexity of the problem, it can become computationally expensive. Some techniques, like metamodels, can be used to approximate the expensive computational model to an analytical solution, and solve the problem quickly. Therefore, the numerical FRFs, to represent the boundaries, can be calculated and used as a reference to evaluate the quality of the manufactured components. Figure 3.1 shows the methodology workflow.

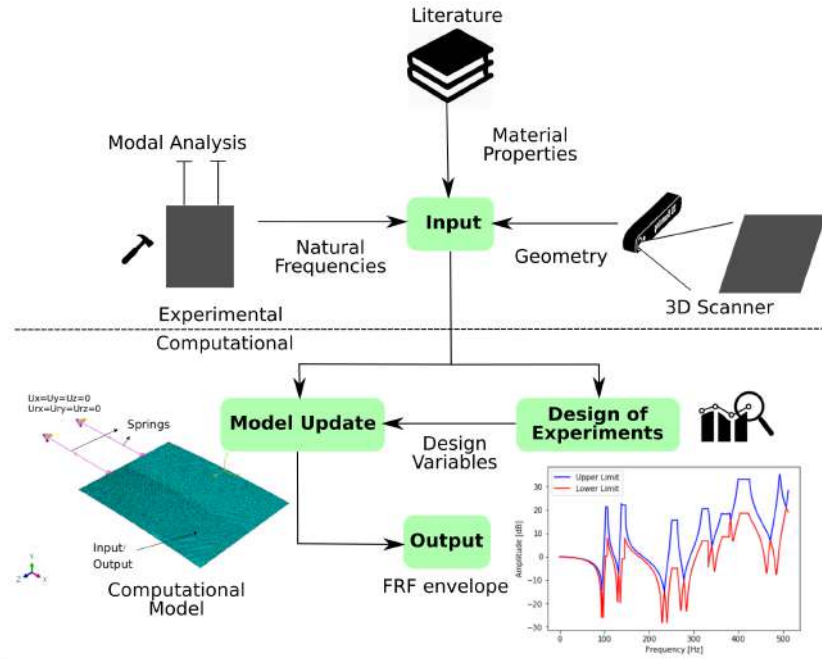
Figure 3.1: Methodology flowchart



Source: Author's production.

1. Consists of an updated review of dynamic modal analysis, model updating, and metamodeling techniques.
2. Covers the analysis of experimental data collected during the modal analysis (natural frequencies and FRF) and also during the geometry evaluation of the manufactured components.
3. Consists of the application of the Design of Experiments to study dynamic behaviour depending on the variabilities of the component geometry and property. In addition, a screening is performed on the variables to reduce the number of design variables during the model update process.
4. The experimental data available is used to define a range of natural frequencies comprises the most part of the specimens evaluated. Allowing to consider that the manufactured set of plates has the dynamic behaviour of this range.
5. Consists of an improved model update process using a Kriging metamodel that returns the set of design variables that allows representing the dynamic behaviour of a component using FEM.

Figure 3.2: Main parameter and flow information for the methodology



Source: Author's production.

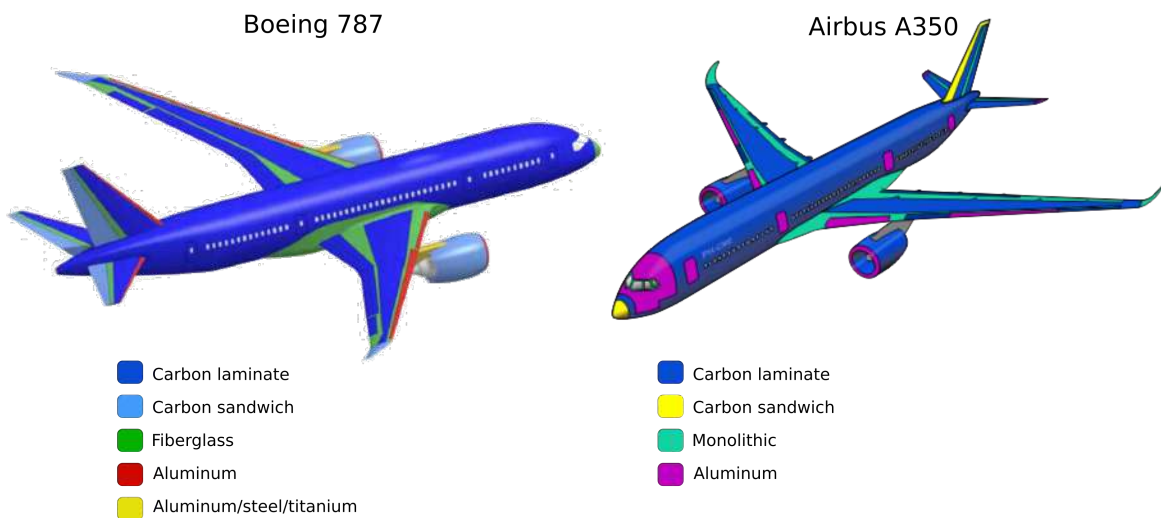
6. Represents the updated computational model that allows performing dynamic modal analyses to obtain the FRF. This model also can be used to carry out virtual tests to study the performance of a specific component.
7. The computational FRF of the frequency range can comprise an envelope. The experimental FRFs can be compared against this envelope to verify if the component is in the specifications.
8. This step classifies the components accordingly the comparisons performed before.

Figure 3.2 shows the information flow of the methodology, presenting the main tests and results obtained during this process. It clearly shows the experimental and numerical approaches used during this work. There, modal analysis and 3D scanner were used to obtain information about natural frequencies and geometry, respectively. Materials properties were obtained based on different pieces of literature that use the same kind of material. Hence, the experimental data is the base of the input data. After that, Design of Experiment process uses the input data to evaluate variables and screening them, to serves the model update process, that returns a computational model representing the experimental set of data. Therefore, analyzing the computational data the FRF envelope to characterizes the undamaged components results as output.

3.2 Composite Materials Manufacturing

Advanced composite materials have been used to fabricate many structural parts in engineering applications. Mainly to their attractive characteristics such as lightweight, high strength, high stiffness, good fatigue resistance and good corrosion resistance (DANIEL, 1993). Also, the ability to manufacture parts with complicated geometry using few components. It enables manufacturers to save cost, as compared with the same parts made of conventional metallic materials. These characteristics are very attractive to the aeronautical industry. Firstly used in military aircraft in the 80's. The F117, F/A18 and Mirage 2000, which around 15% of their structures were made of in composite materials. After that, it has exponentially increased until now, where airplanes as the F35 has around 50% of its structure in composite materials. Furthermore, composite materials in the civil aviation became more evident with the A350 in 2013 and the Boing 787 in 2011. The later, using more than 50% of its structures made of composite materials. The components usually manufactured in composite include the flaps, ailerons, rudder, radome, spars, longerons, etc. Most parts of these components are flat and produced by several processes.

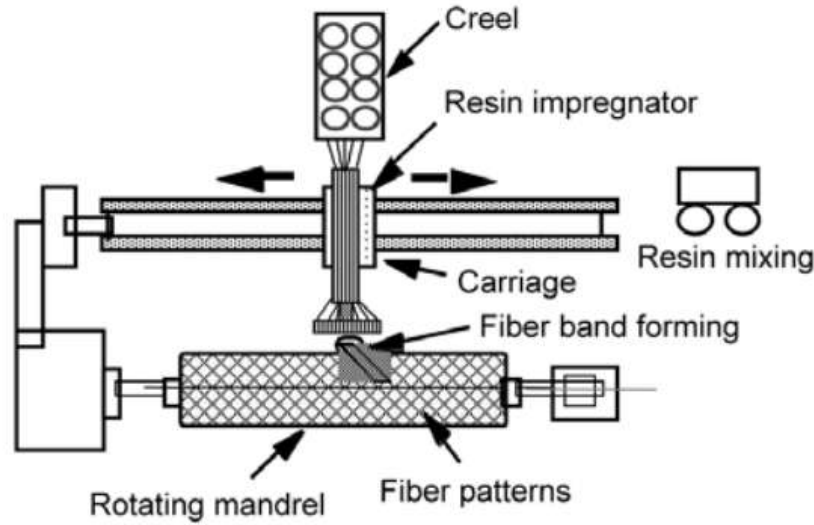
Figure 3.3: Composite material uses in comercial aircrafts



Source: Adapted from Ghobadi (2017), Alarifi et al. (2017).

Several manufacturing techniques have been created to support the industry to produce more, with low cost, and good quality. One of the most common processes is the hand laminating (or wet lay-up), that consists on, to place the composite layers manually and apply the matrix. This process is used to make low-cost components and corrosion-resistant components in the chemical process industry. For more complex geometries

Figure 3.4: Basic helical horizontal filament winding machine



Source: Adapted from (DANIEL, 1993).

and components with higher structural requirements, the hand laminating process can be finalized using an autoclave. Another important process is the filament winding process, which consists of continuous reinforcements in the form of rovings or monofilaments wound over a rotating mandrel.

The basic helical filament winding machine (Figure 3.4) consists of a group of tools, including creel, wind eye, resin impregnator, motors and controls, and heating or other curing devices (ovens, mainly), that cover a form (mandrel), with continuous resin-impregnated fibres. A creel stores continuous fibres in packages that are stationary or rotating. The creel can be stationary or alternately move from one end of the machine to the other. The completed filament-wound item is cured (resin is polymerized) at room temperature, in an oven, or by other heating means, depending on the resin requirements. After cure, the wound product and mandrel are separated.

Specially designed machines, traversing at speeds synchronized with the mandrel rotation, control the winding angles and the placement of the reinforcements. Structures may be plain cylinders or pipes or tubing, varying from a few centimetres to one or two meters in diameter. A survey presented by Minsch et al. (2017) showed different techniques of filament winding, and also experimental analysis aiming to make reliable statements concerning process parameters and properties. As aforementioned, flat structures are found all over an aircraft that requires a consistent manufacturing process and also an automated way to verify the manufactured components.

The methodology proposed in this work is carried out by using data from experimental tests, performed in carbon-epoxy composite plates, as well as numerical simulations. The set of specimens used is composed of fourteen carbon fibre with epoxy

Table 3.1: Plate specimens made of carbon fibre and epoxy resin by filament winding process

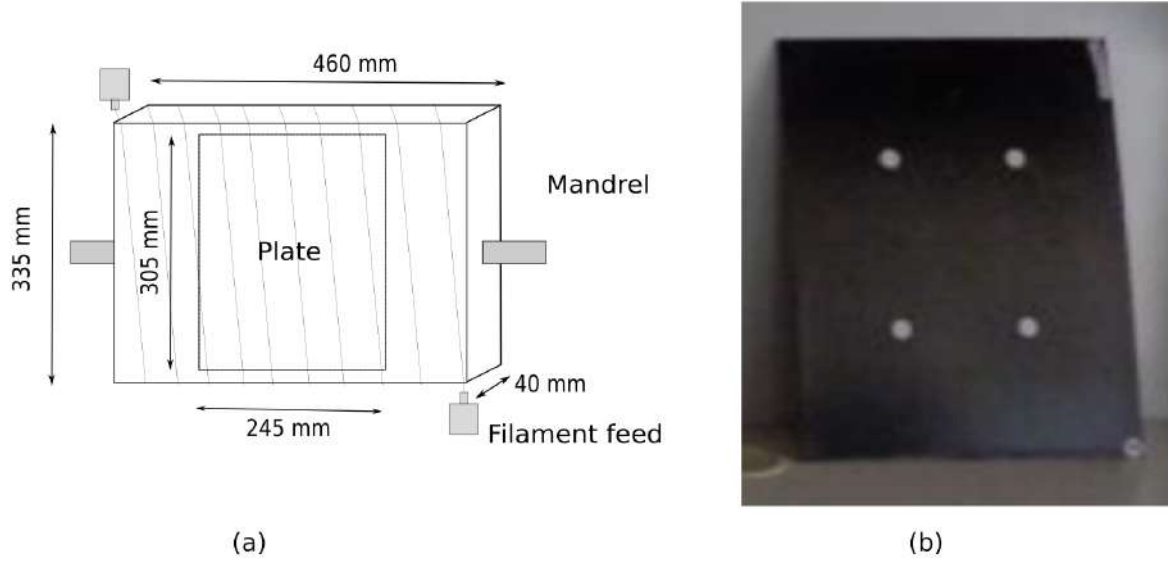
Plate	Length (mm)	Width (mm)	Thickness (mm)	Stacking sequence
P01	305.00	245.00	2.247	$[0]_8$
P02	305.39	244.86	2.245	$[0]_8$
P03	305.39	244.71	2.257	$[0]_8$
P04	305.00	245.00	2.246	$[0]_8$
P05	304.90	245.67	2.207	$[0]_8$
P06	304.94	246.12	2.218	$[0]_8$
P07	305.30	245.79	2.208	$[0]_8$
P08	303.84	245.88	2.212	$[0]_8$
P09	306.64	247.45	3.331	$[0/15/-15/0/15/-15]_s$
P10	305.52	246.19	3.336	$[0/15/-15/0/15/-15]_s$
P11	305.45	245.21	3.493	$[0/15/-15/0/15/-15]_s$
P12	305.82	243.55	3.468	$[0/15/-15/0/15/-15]_s$
P13	306.62	247.13	3.370	$[0/15/-15/0/15/-15]_s$
P14	304.14	245.21	3.333	$[0/15/-15/0/15/-15]_s$

resin (Carbon Fibre Reinforced Polymer - CFRP) composite plates manufactured by filament winding (Figure 3.5), with a nominal length of 305 mm and a nominal width of 245 mm. Two configurations are used: 8 unidirectional plies $[0]_8$ at a total thickness of about 2.2 mm and a 12 ply $[0/-15/15/0/-15/15]_s$ stacking sequence at a total thickness of 3.3 mm. Table 3.1 summarizes the main characteristics of the specimens. The precision of the measurement system is of the order of 10^{-3} mm.

Regarding the stacking orientation, the main reasons for this choice are due to the limitations of the manufacturing process used to obtain carbon fibre reinforced plastic specimens (filament winding), which were produced by CTM-SP (Brazilian Navy Research Centre). It is important to highlight that there is a confidential agreement for scientific cooperation between Aeronautic Structure Group (USP) and CTM-SP. Therefore, it is not possible to provide details about the manufacturing process of the carbon fibre composite specimens.

These two configurations of stack sequence are related to the maximum angle allowed, ± 15 degree, and the minimum angle allowed, 0. In the process, fibres are impregnated with resin before winding (wet winding). A parallelepiped shape mandrel (Figure 3.5) is used, and almost flat plates are cut from the two sides after demolding the wound part. This process produces laminate plates with high quality. The plates are then cured in a controlled oven. Depending on the stacking sequence of the laminate, almost flat plates are obtained with a small single curvature, which is caused by residual internal stress.

Figure 3.5: (a) mandrel schematic and dimensions and, (b) specimen used in experimental tests.



Source: Souza et al. (2019).

Besides the variabilities of the geometric characteristics, the material properties are highly affected by the manufacturing process. Because, conditions as resin cure temperature, fibre fraction and cure pressure are not the same for all specimens due the instabilities of the manufacturing process. Therefore, estimate the bounds of the materials properties is very important to consider the uncertainties in the models.

Experimental data of the plate material properties has been not possible to acquire directly, due to the classified information about the manufacturing process. However, to aid the readers in understanding the mechanical behaviour of the composite material. The values used in this work comes from researches with similar material. Tita et al. (2008) and Ribeiro et al. (2012) investigated similar materials and obtained experimentally material properties, which is assumed as the baseline for this work (Table 3.2). In fact, the specimens manufactured and studied by Tita et al. (2008) are made from prepreg M10 from HexelTM, which are pre-impregnated unidirectional carbon fibres by epoxy resin, with a fibre volume ratio of the laminates of 63%. In addition, Tita et al. (2008) compared the values obtained by other results present in the literature for the same material.

Authors as, Potter (2009b) reviewed the sources of variability and defects in aircraft composite parts and attempts to identify approaches that can be taken to generate more robust design and manufacturing processes. More than 130 defect types and more than 60 sources of variability and unreliability can be identified for the autoclave and resin transfer moulding processes. Many of these sources of variability have their roots in the

Table 3.2: Nominal lamina material properties, (TITA et al., 2008)

Material Properties	Value	Unit
Young's Modulus longitudinal. Direction (E_{11})	127	GPa
Young's Modulus transversally. Direction (E_{22})	10	GPa
Shear Modulus in plane 2-3 (G_{23})	3.05	GPa
Poisson in plane 1-2 (ν_{12})	0.34	-
Shear Modulus in plane 1-2 (G_{12})	5.4	GPa

reinforcements used and in the ways that those reinforcements map to the geometry of components. Also, reviews presented by Ibrahim (1987), Manohar and Ibrahim (1999) and more recently Gupta and Ghosh (2017) showed the structural dynamic problems with parameter uncertainties.

Limited literature is available on composite structures with random material properties. Leissa and Martin (1990) analysed composite material panels with variable fibre spacing using the classical laminate theory. Free vibration and buckling of flat plates have been analyzed, taking them to be macroscopically orthotropic but non-homogeneous because of variable fibre spacing. Results obtained for glass, boron and graphite fibres with the epoxy matrix for simply supported square plates.

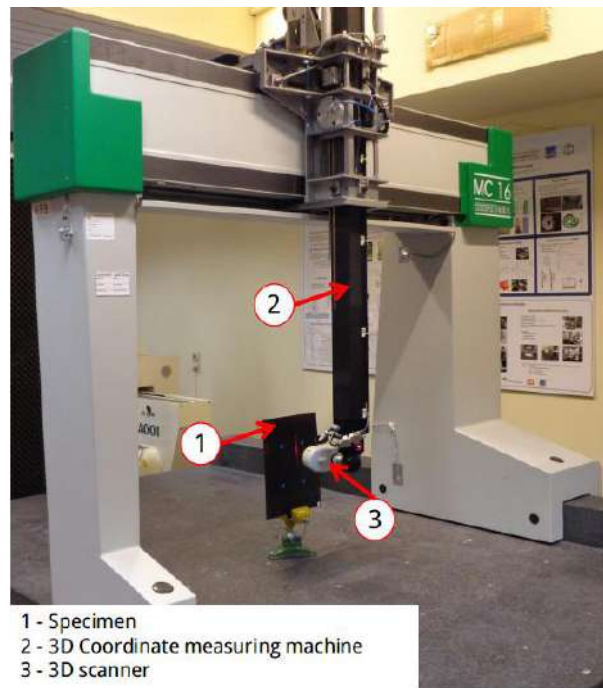
3.3 Composite Materials Tests

Considering the methodology shown in Figure 3.1, a sequence of experimental tests is proposed. Aiming to evaluate the characteristics of the composite plates manufactured, in terms of geometry and dynamic behaviour, 3D scanning technique and dynamic tests have been carried out. The 3D scanning technique (Figure 3.6) allows to have a better comprehension of the variabilities caused by the manufacturing process and helps to improve the quality of the numerical models. On the other hand, dynamic tests have been chosen to be carried out in this work because is a state of the art technology to evaluate the structural state of a component.

An experimental apparatus was prepared to conduct the dynamic analyses of the composite plates. The natural frequencies and FRFs were obtained using accelerometers attached to the plates in the positions as shown in Figure 3.7. The used accelerometer is a model 352A24 (Bruel & Kjaer) lightweight structure with the sensitivity of 102.34 mV/g.

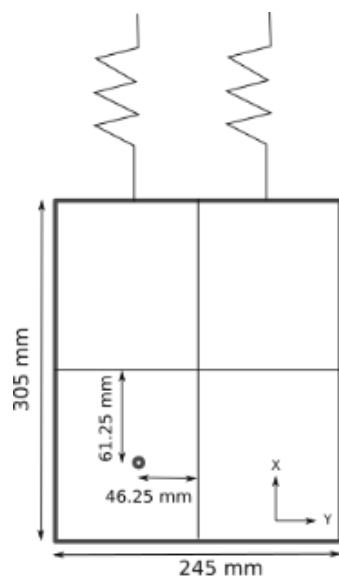
The excitation for both sets of vibration tests is applied using an impulse signal, through an impact hammer PCB Model 0860C3 (Piezotronics). The input is applied to the same position of the accelerometer on the back side of the plate (Figure 3.7). The set-up used in the experiments consists of a plate suspended by elastomer wires to simulate free-free boundary conditions, whereas accelerometer and the impact hammer

Figure 3.6: Coordinate machine with the 3D optical scanner.

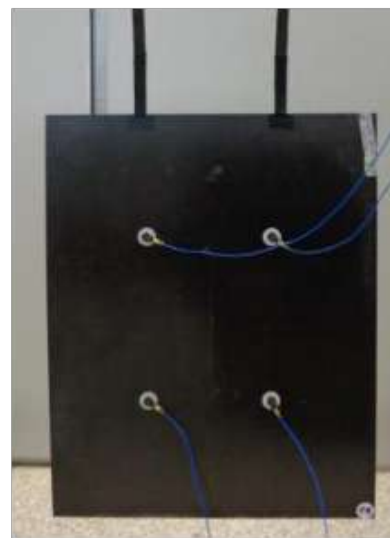


Source: Souza et al. (2019).

Figure 3.7: Specimen and accelerometers (a) schematic representation and (b) experimental analysis.



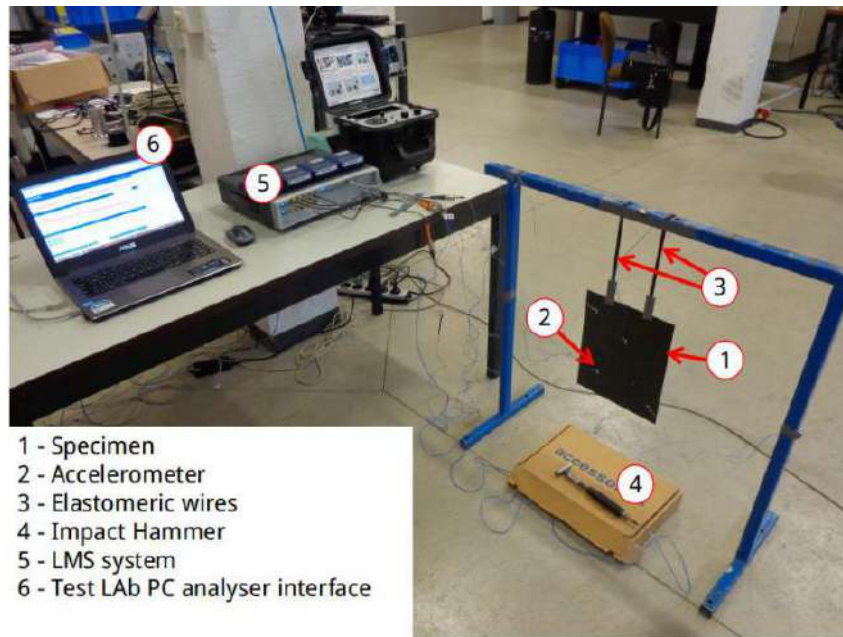
(a)



(b)

Source: Souza et al. (2019).

Figure 3.8: Experimental set-up



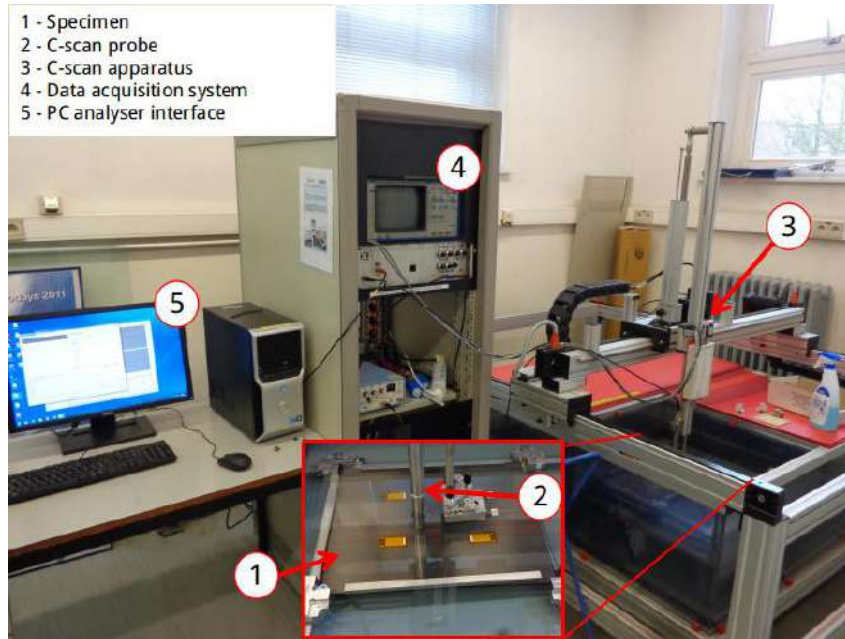
Source: (SOUZA et al., 2019).

are connected to an LMS SCADAS Mobile equipment controlled by the Test.Lab software (LMS Test.Lab) (Figure 3.8).

The impact hammer excites the panel with a wide frequency spectrum. This is important because different types of damage can affect different frequency ranges, and the resonant and anti-resonant characteristics of a structure may be good indicators of damage. In this experiment, the lower eight modal frequencies are investigated. The signal consists of 2048 points over the frequency range from 0 to 512 Hz. The acquisition time is 4 seconds with a resolution of 0.25 Hz.

Defects in composite materials, after manufacturing, can be presented in different ways. Matrix cracks, fibre cracks, and delamination are common forms of damage on composites. These structural degradations can be inserted into the structure after manufacturing by using an impact machine. Thus, analysing this kind of results is interesting to evaluate the methodology behaviour of this work faced in damaged components. Also, impact events are very common during the aircraft lifecycle, such as small debris impact, bird strikes, hail impact, and stone impact. Therefore, impact tests have been chosen to damage the specimens, through a drop mass test. To evaluate the characteristics of the damage caused in the impact test a C-Scan method was employed. The C-Scan method 3.9 allows to visualize the damage phenomena of the damage and helps in the correlations between damage types and changes in dynamic behaviour.

Figure 3.9: C-Scan test set up used for composite plates



Source: Souza et al. (2019).

3.4 Composite Damage Types

Due to their complex nature, fibre reinforced plastics suffer from various damage types unknown to homogeneous materials. These damage types can be examined at different scales, the macro scale related to the laminate structure, mesoscale where is considered only a single lamina and the microscale where analyses are made on a representative finite volume.

One of the first damage mechanisms to occur is known as transverse (matrix) cracking. This type of crack grows parallel to the fibre and in the thickness direction of the laminate (DANIEL, 1993). Transverse cracks can be caused during production by, for example, the difference in thermal expansion coefficient between fibre and matrix or by in-service loading (e.g. impact). The small size makes them generally hard to detect during inspections. The formation of transverse cracks rarely means the total fracture of a laminate, as it does not affect the load carrying capacity of the fibres. Most importantly, this type of cracking forms a trigger for further damage mechanisms.

Delamination is a damage type that generally is preceded by transverse cracking. This damage type is a debonding between individual plies of a laminate. The crack runs again in a parallel plane to the fibres, but at the interface between two layers. Delaminations are hardly visible on the surface since they are embedded within the composite structure. This makes them barely detectable during, for example, visual inspections. Although delaminations do not lead to complete fracture, they can seriously

affect the thermal and mechanical properties of the laminate.

A widely used test to study damages in composite materials is the impact test. This type of test can produce all sort of damage mechanisms in the structure, from cracks to delaminations and fibre rupture. In this work, a low-velocity impact test is carried out using a drop mass machine. This test consist of a known mass dropping from a known height to produce the desired impact energy.

Structural components used in aircraft are usually designed according to the damage tolerance principle. This principle implies that the structure needs to function safely despite the presence of (minor) flaws. The severity of damage in aircraft structures is classified into five categories, according to Composite Materials Handbook CMH-17-3G (2009). This classification is linked to the required residual strength and ranges from allowable damage, category 1, up to very severe damage, category 5. The assessment of damage in aircraft structures has historically relied on visual inspection methods to identify damage. Category 1 is classified as Barely Visible Impact Damage (BVID) and may remain undetected, while repair scenarios are required for the Visible Impact Damage (VID) of category 2 to 5. Structures containing BVID must sustain ultimate load for the life of the aircraft structure. The dent depth is often used as the damage metric to define BVID (BAARAN, 2009). This criterion sets the lower bounds to the identification capabilities of a structural health monitoring approach.

Hassan et al. (2017) presented a recent review about manufacturing defects in laminates applied on aircraft composite structures. The discussion included the effects of the parameters on the defect formation during the sub-processes involved. It was found that the defects occurring were substantially affected by various factors, including mould selection, material characteristics, bagging configuration, etc. Also, the correlation between the processing parameters and the related defects was thoroughly investigated. Different authors have been conducted studies to evaluate the influence of the manufacturing process in the final composite properties (CANTWELL; MORTON, 1992; COHEN, 1997; HUBERT; POURSAITIP, 2001; LI et al., 2009; POTTER, 2009a).

3.5 Computational Model

This work presents a hybrid numerical-experimental approach to evaluate the composite plates. Now, the main definitions and concepts used to formulate the numerical model are presented. Two different analyses were carried out. In the first, modal analysis was used to obtain the natural frequencies and mode shapes of the composite plates. In addition, this analysis was used during the model update as part of the optimization process. In the second one, a steady-state analysis is used to obtain the Frequency Response Function to compare with the experimental data and compose the envelope of the permissible components.

Finite element models of the laminated composite plates are built in ABAQUSTM software complemented by Python subroutines. The element type and size were chosen based on previous analyzes (BORGES, 2012). Quadrilateral 8-node shell elements are used (defined as S8R5). Thin shell elements provide solutions to shell problems that are adequately described by classical (Kirchhoff) shell theory, thick shell elements yield solutions for structures that are best modeled by shear flexible (Mindlin) shell theory, and general-purpose shell elements can provide solutions to both thin and thick shell problems. All shell elements use bending strain measures that are approximations to those of Koiter-Sanders shell theory (Budiansky and Sanders, 1963). Thin shell elements may provide enhanced performance for large problems where reducing the number of degrees of freedom through the use of five degree of freedom shells is desirable. However, they should be used only for the modeling of thin structures that exhibit at most weak nonlinearities in problems where rotation degree of freedom output is not required and for situations where the shell surface and the displacement field are smooth so that higher accuracy can be achieved with the use of second-order shells. The Discrete Kirchhoff (DK) constraint, which refers to the satisfaction of the Kirchhoff constraint at discrete points on the shell surface, is imposed in all thin shell elements in Abaqus. For S8R5 element the discrete Kirchhoff constraint is imposed numerically where the transverse shear stiffness acts as a penalty that enforces the constraint. 5640 elements and 8784 nodes are used to mesh the plate domain, this mesh size (3 mm) is defined after a refinement analysis to obtain the six first modes.

A numerical modal analysis procedure identifies the natural frequencies for each configuration, which is defined by the DoE. Abaqus uses the Lanczos process to extract the eigenvalues and the correspondent eigenvectors of a sparse symmetric generalized eigenproblem. The Lanczos procedure in ABAQUS/Standard consists of a set of Lanczos “runs,” in each of which a set of iterations called steps is performed. For each Lanczos run the following spectral transformation is applied,

$$(\mathbf{K} - \sigma \mathbf{M})^{-1} \phi = \theta \phi, \quad (3.5.1)$$

where σ is the shift, ϕ is the eigenvector and θ is the eigenvalue.

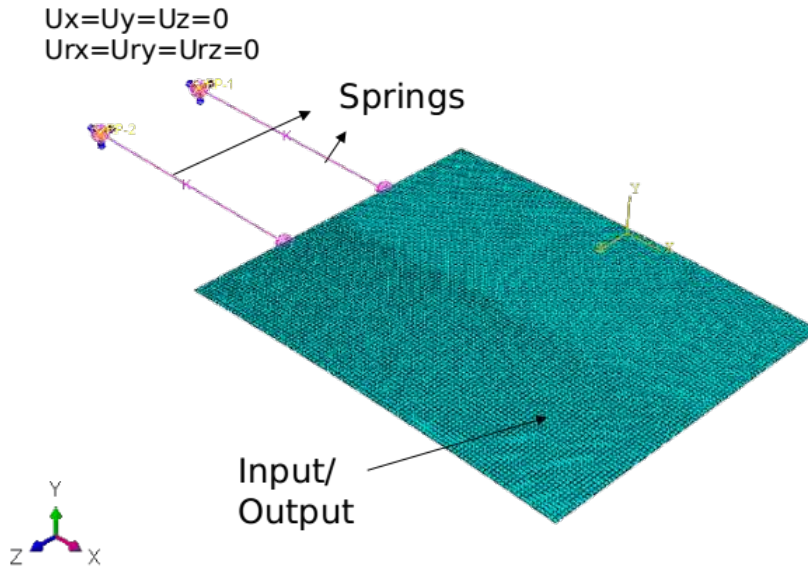
A Lanczos run will be terminated when its continuation is estimated to be inefficient. Within each run a sequence of Krylov subspaces is created, and the best possible approximation of the eigenvectors on each subspace is computed in a series of “steps.” In each Lanczos step the dimension of the subspace grows, allowing better approximation of the desired eigenvectors. This is in contrast to the subspace iteration method, in which the dimension of the subspace used to approximate the eigenvectors is fixed. In theory the basic Lanczos process (in the assumption of “exact” computations without taking into account round-off errors) is able to determine only simple eigenvalues. The shifting

strategy (and the Sturm sequence check as a part of it) detects missing modes and enforces computation of all the modes during the subsequent Lanczos runs.

However, this approach is expensive if the multiplicity of certain eigenvalues is high. Therefore, a “blocked” version of the Lanczos algorithm is implemented in ABAQUS/Standard. The idea is to start with a block of orthogonal vectors and to increase the dimension of the Krylov subspaces by the block size at each Lanczos step. This approach allows automatic computation of all multiple eigenvalues if the largest multiplicity does not exceed the block size. Another important advantage of the blocked Lanczos method is that it allows efficient implementation of expensive computational kernels such as matrix-blocked vector multiplications, blocked back substitutions, and blocked vector products.

The numerical analyses are done in quasi-free-free boundary conditions. Elastic wires, which very low yet non-zero low stiffness (10 N/m), are attached to the composite plate. The elastic wires are fixed on translation (U_x , U_y , U_z) and also on rotations (U_{rx} , U_{ry} , U_{rz}). The excitation is applied in the same position as in the experimental tests (Figure 3.10). The accelerometer has much lower mass than the composite plates, for this reason, no additional mass is included in the numerical analyses.

Figure 3.10: Finite element Model



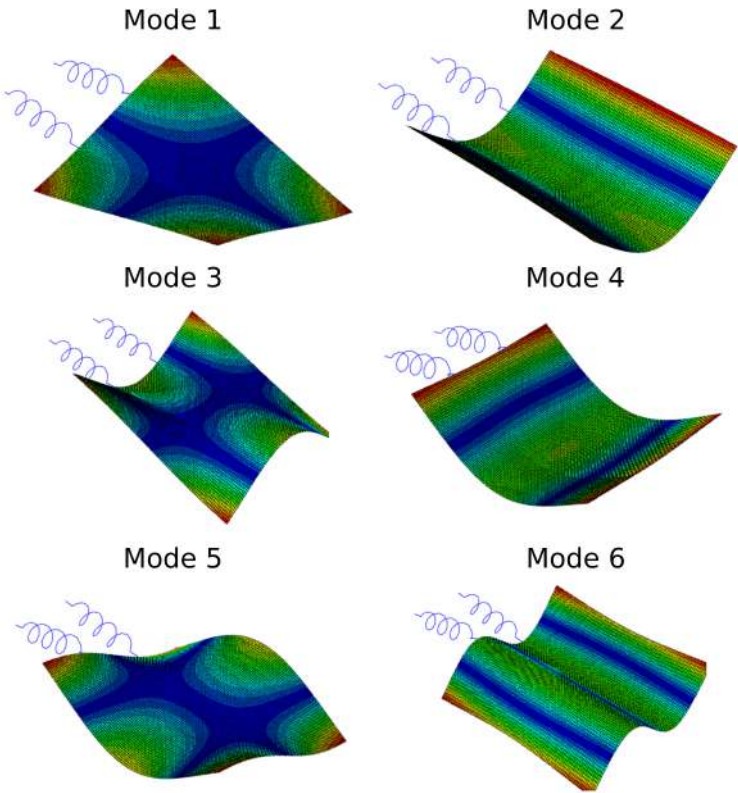
Source: Author’s production.

The damping coefficients have been extracted experimentally from all plates, using the Peak Picking method (REN; ZONG, 2004). Table 3.3 shows the mean and the standard deviation of the damping coefficients between the plates for each mode. Figure 3.11 shows the mode shapes of the plates, where both stacking sequences have the same mode shape.

Table 3.3: Resonance modes and damping coefficients

$ 0\rangle_s$			$ 0\ 15\ -15\ 0\ 15\ -15\rangle_s$		
Mode	Damping		Mode	Damping	
	Mean	Std. dev		Mean	Std. dev
1	0.77%	0.20%	1	0.63%	0.09%
2	0.53%	0.05%	2	0.58%	0.03%
3	0.66%	0.03%	3	0.57%	0.06%
4	0.76%	0.09%	4	0.66%	0.12%
5	0.68%	0.06%	5	1.08%	0.25%
6	1.06%	0.32%	6	0.44%	0.03%

Figure 3.11: Numerical mode shape of the plates



Source: Author's production.

Chapter 4

DoE - Design of Experiments

4.1 Dimensional analyses

Composite materials manufacturing is a complex process. Even, a well-controlled process, as filament winding and autoclave techniques produce components with considerable differences in its properties. The variability between different samples of the same component adds a degree of complexity to the task of predicting the dynamic behaviour of the component.

Directly overcome this problem creating a manufacturing process that results in perfectly equal components is an unfeasible solution. It is necessary, to workaround by identifying the variabilities of the process and propose a strategy to deal with these uncertainties. Therefore, the first step is to know the characteristics of the samples, the uncertainties and the most influential parameters on the process.

One of the first hypothesis, in a composite structure design, is that the thickness is given by the sum of the ply thickness forming the laminate, it means constant thickness (LEE et al., 2008, 2010). The effects of the ply thickness variations have been studied in the literature as localized defects due to manufacturing conditions, in the form of wrinkles and warpings (BARKANOV et al., 2010; LI et al., 2009), and on singular zones such as L-shaped stringers (SUN et al., 2012). Conversely, there are few publications that address the representation of thickness variations spread over a laminated structure (LIGHTFOOT et al., 2013).

It is well-known that the composite structure cannot be dissociated from its manufacturing conditions. The volume fractions of constituent materials (fibre and matrix), as well as porosities, are directly linked to the stratification of the composite, the nature of the raw materials and the curing cycle (OLIVIER; CAVARERO, 2000). These changes in the volume fraction can be a source of uncertainties for thin laminates (global on the scale of the plate and local on the scale of the plies). Hsiao and Daniel (1996) and Chun et al. (2001) studied the effects of the fibre waviness on thick unidirectional stratifications

Table 4.1: Geometry data collected from composite plates, where C1 and C2 are the curvatures of the plates at $[0]_8$

Plate	Length (mm)	Width (mm)	Thickness (mm)	Stacking sequence	C1 (mm)	C2 (mm)
P01	305.00	245.00	2.247	$[0]_8$	3.924	3.219
P02	305.39	244.86	2.245	$[0]_8$	3.959	3.666
P03	305.39	244.71	2.257	$[0]_8$	4.111	4.324
P04	305.00	245.00	2.246	$[0]_8$	3.923	4.319
P05	304.90	245.67	2.207	$[0]_8$	3.337	4.816
P06	304.94	246.12	2.218	$[0]_8$	3.686	4.639
P07	305.30	245.79	2.208	$[0]_8$	3.880	4.639
P08	303.84	245.88	2.212	$[0]_8$	3.923	4.765
P09	306.64	247.45	3.331	$[0/15/-15/0/15/-15]_s$	-	-
P10	305.52	246.19	3.336	$[0/15/-15/0/15/-15]_s$	-	-
P11	305.45	245.21	3.493	$[0/15/-15/0/15/-15]_s$	-	-
P12	305.82	243.55	3.468	$[0/15/-15/0/15/-15]_s$	-	-
P13	306.62	247.13	3.370	$[0/15/-15/0/15/-15]_s$	-	-
P14	304.14	245.21	3.333	$[0/15/-15/0/15/-15]_s$	-	-

(up to 150 plies), generated by local and periodic perturbations in the stratification. Few papers were found that accounts for the local changes spread over the composite structure applied to multidirectional laminates fabricated with UD prepregs. Davila et al. (2017) studied the spatial thickness variation over laminate composites, and its continuous patterns, including the continuous ply thickness variation in a finite element (FE) model, considering actual variations of thickness in the composite laminate.

Regarding the aforementioned literature, it is important to evaluate the thickness distribution of the specimens used. This analysis gives important information to be taken into account during the Finite Element Model, and also on the uncertainties models.

In this work, the fourteen plates have been experimentally analysed in terms of its geometric characteristics. Geometry data are obtained using a 3D optical scanner, and the results for each individual plate are listed in Table 4.1. The thickness values of each plate were obtained using the average of measured points (around 325000 points), from the 3D optical scanning (Figure 3.6). The mean ply thickness obtained matches with some literature results, as the values reported by Collombet et al. (2006), a minimum value of about 0.258mm, a maximum value of about 0.270mm, a general mean thickness of 0.264mm, a standard deviation of 0.002mm and a 3 sigma tolerance of ± 0.007 mm, in a 28-ply M21/T700 carbon/epoxy laminate.

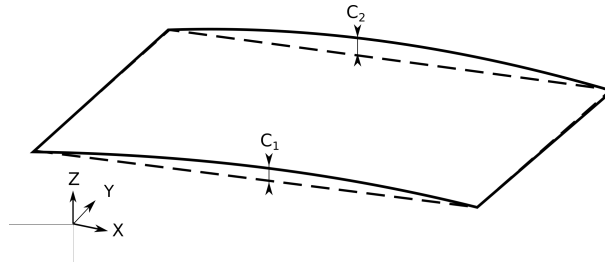
Statistics on plate geometry data are summarised in Table 4.2. It shows the variability of the thickness in the manufacturing process. The maximum and minimum values of width (W), length (L) and central distances (C1, C2) are taken. The curvature has the shape of a circular arc (Figure 4.1), with C1 and C2 the maximum distance from

Table 4.2: Geometric data analysis

Stacking sequence		Length (mm)	Width (mm)	Thickness (mm)	C1 (mm)	C2 (mm)
$[0]_8$	Average	305.00	245.34	2.176	3.923	4.324
	St. Deviation	0.50	0.54	0.018	0.251	0.598
	Upper value	306.50	246.96	2.231	4.677	6.120
	Lower value	303.50	243.71	2.120	3.168	2.527
	Range	2.99	3.25	0.110	1.508	3.592
$[0/15/-15/0/15/-15]_s$	Average	305.67	245.21	3.341	-	-
	St. Deviation	0.93	1.28	0.066	-	-
	Upper value	308.48	249.06	3.538	-	-
	Lower value	302.85	241.36	3.144	-	-
	Range	5.63	7.70	0.394	-	-

the plate to the horizontal reference line. The difference on central distances between the two sides of the plate, C1 and C2, can be explained due to residual stress provided by the curing process and the variation of the total thickness of the plate. The upper and lower values for thickness were obtained evaluating the distribution provided by the 3D scanner. Where a normal distribution has been observed. Therefore, the upper and lower values for the thickness range was defined in a way that, 99.7% of the measured values were within these boundaries.

Figure 4.1: Specimen curvatures representation



Source: Author's production.

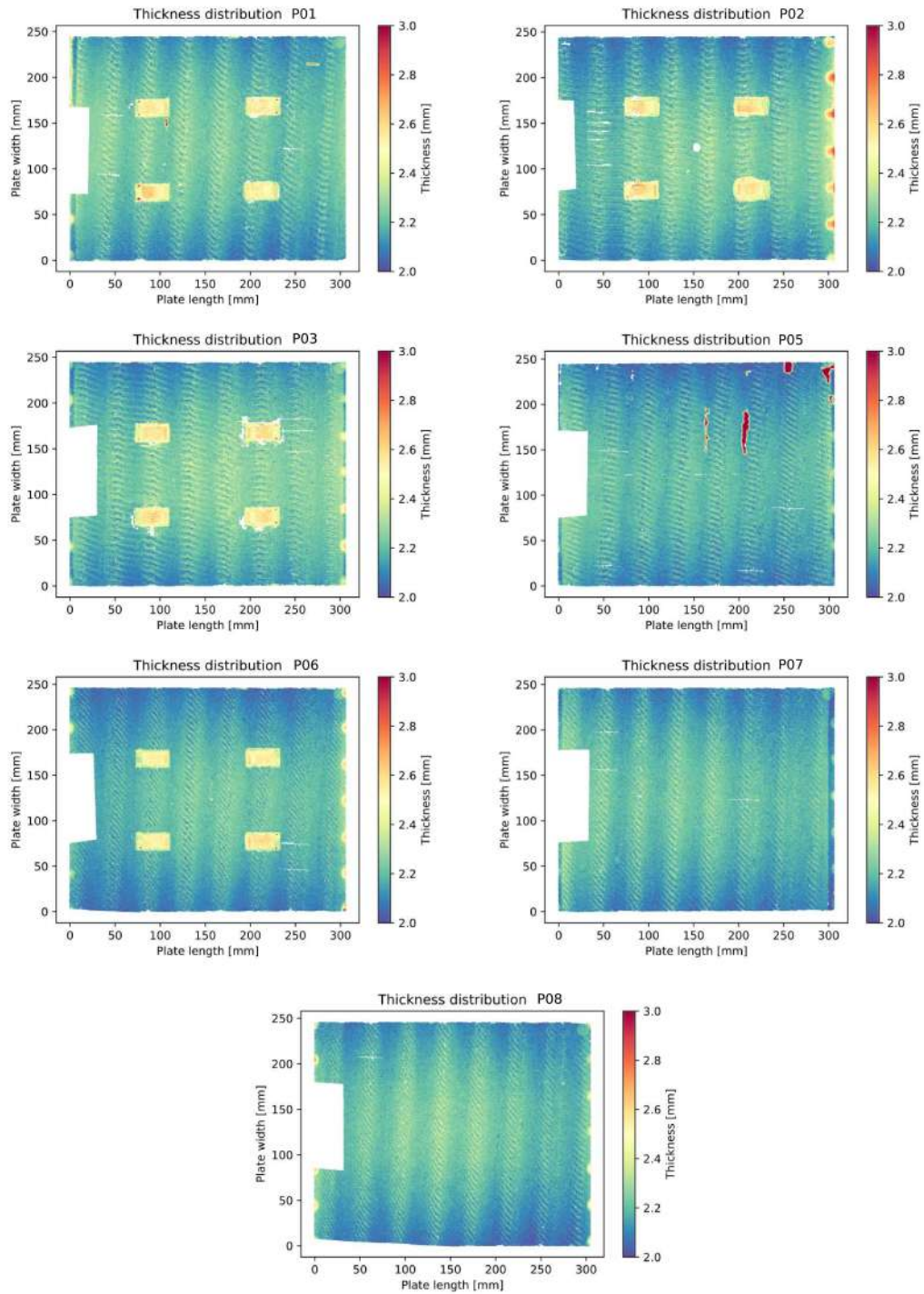
The thickness map can be drawn for each plate, allowing the spatial visualization of the thickness variation. Those colour maps (Figure 4.2, and Figure 4.3) shows that the spatial distribution of the thickness is not uniform in a composite plate, as expected. All plates have a waviness pattern of thickness, that can be due to buckling of the wet hoop-wound filament strands under the pressure exerted by the overwrapped layers during the filament winding process. The set of plates with a stacking sequence of $[0]_8$ have a concentration of high thickness near the centre line. The set of plates with a stacking sequence of $[0/15/-15/0/15/-15]_s$ have some concentration of high thickness at the boundaries, mainly plates P11 and P12, which have a sharp gradient in the width

direction. These manufacture imperfection can result from a resin buildup at the lower boundaries.

The study of those variabilities is very important to define when the hypothesis of constant thickness can be assumed or not. In this case, it is possible to note $[0]_8$ plates have a better uniformity than $[0/15/-15/0/15/-15]_s$. Also, the thickness distribution of $[0/15/-15/0/15/-15]_s$ plates can have an important influence on torsional modes.

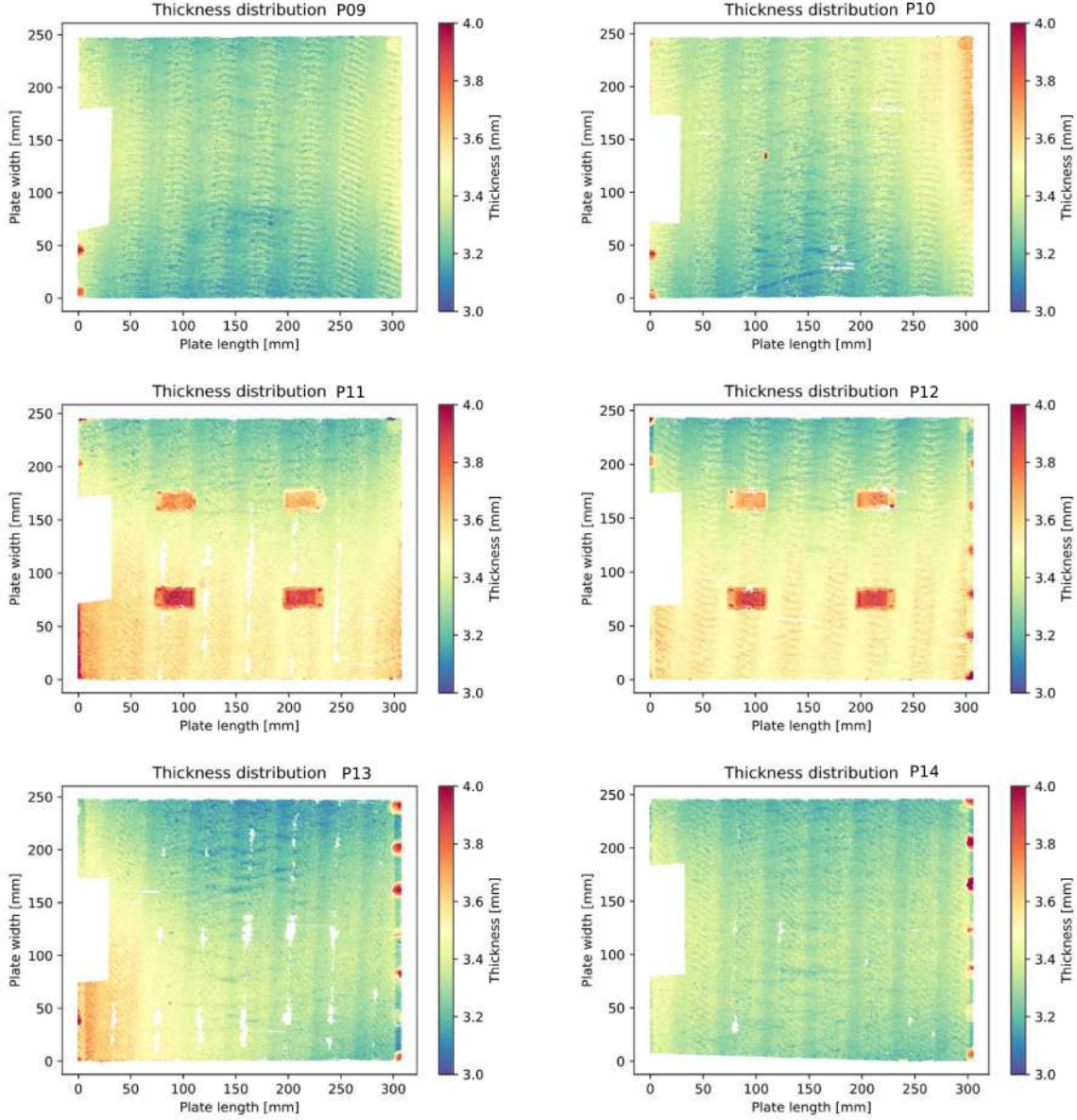
As aforementioned, the thickness is an important parameter for a structure. The data acquired shows the variabilities found on the composite plates manufactured and helps to get a better approximation of the value that can be used as mean thickness. Although, the relevant uncertainties, the constant thickness can be taken into account if the stiffness of the component is adjusted. Therefore, it is essential to use a model update technique to make corrections on the materials properties to have a better fit of experimental behaviour, which takes into account the spatial variability of the thickness, and the numerical model which uses a constant thickness.

Figure 4.2: Thickness distribution for plates with stacking sequence of $[0]_8$. Four squares represent the extensometers attached on the plate.



Source: Author's production.

Figure 4.3: Thickness distribution for plates with stacking sequence of $[0/15/-15/0/15/-15]_s$. Four squares represent the extensometers attached on the plate



Source: Author's production.

4.2 Screening analysis

Main effect plans (MEP) or resolution III designs are commonly used in exploratory studies when a large number of factors need to be considered or screened. The idea is to try to detect factors that exhibit large main effects and discard factors with no noticeable effects from further study. The crucial assumption here is that all interactions are negligible, including 2-factor interactions. This may not always be realistic, but as a

first approximation, this is nevertheless a very valuable method. In some cases, it may be helpful to know with which 2-factor interactions each main effect is aliased. We shall make some remarks about that later.

Plackett Burman designs are experimental designs presented in 1946 by Robin L. Plackett and J. P. Burman (PLACKETT; BURMAN, 1946). Their goal was to find experimental designs for investigating the dependence of some measured quantity on a number of independent variables (factors). In such way, as to minimize the variance of the estimates of these dependencies using a limited number of experiments. Interactions between the factors were considered negligible. The solution to this problem is to find an experimental design, where each combination of levels for any pair of factors appears the same number of times, throughout all the experimental runs.

Plackett-Burman (PB) design is one specific family of fractional factorial designs frequently used for screening. These are used to study $k = n - 1$ factors in $n = 4m$ design points, where m is an integer. PB designs, which n is a power of two, are called geometric designs and are identical to $2^{(k-p)}$ fractional factorials. If n is strictly a multiple of four, the PB designs are referred to as non-geometric designs and have very messy alias structures. Their use in practical problems is problematic, particularly if the design is saturated (i.e., the number of factors is exactly $n-1$). If interactions are negligible, however, these designs allow unbiased estimation of all main effects, and require only one more design point than the number of factors. They also give the smallest possible variance (BOX et al., 1978). Myers et al. (2016) presented a more complete discussion of factorial designs and aliasing of effects.

In this work, PB design is used as a first approach evaluating the most significant parameters on the study of mechanical vibrations on composite plates. A set of 11 variables, which are directly related to the final component and which are taken to be uniform throughout the entire plate, are given as design variables: width, length, thickness, fibre angles, two quantities of curvature (one at each side of the plate), Young's modulus in longitudinal and transverse directions, shear modulus in plane 1-2 and 2-3 and Poisson's coefficient.

The values of the factors have been defined based on the geometry analysis and materials properties analysis as explained previously on materials and methods. Here, the fundamental assumptions of the values chosen to compose the factors levels are going to be clarified.

The range of materials properties as Young's Modulus longitudinal direction (E_{11}), Young's Modulus transversally direction (E_{22}), Shear Modulus in plane 2-3 (G_{23}), Poisson's ratio in plane 1-2 (ν_{11}) and Shear Modulus in plane 1-2 (G_{12}), is defined as a variation of 10% based on the literature values presented in Table 3.2. The 10% value has been chosen after evaluate different results presented in the literature for the same material. The filament winding manufacture process causes a little deviation from the fibre direction

Table 4.3: Factors and its levels from $[0]_8$ plates considered for DoE analyses

Factor	Level 1	Level 2	Unit
Width (W)	243.71	246.96	mm
Length (L)	303.6	306.5	mm
C1	3.17	4.68	mm
C2	2.53	6.12	mm
θ	-0.01	0.01	degrees
Thickness	2.12	2.23	mm
E_{11}	114.3	139.7	GPa
E_{22}	9	11	GPa
G_{23}	2.745	3.355	GPa
ν_{12}	0.306	0.374	
G_{12}	4.86	5.94	GPa

Table 4.4: Factors and its levels from $[0/15/-15/0/15/-15/0]_s$ plates considered for DoE analyses

Factor	Level 1	Level 2	Unit
Width (W)	241.71	249.65	mm
Length (L)	301.34	309.99	mm
θ_{15}	14.0	16.0	mm
θ_{-15}	-14.0	-16.0	mm
θ_0	-2.0	2.0	degrees
Thickness	3.16	3.45	mm
E_{11}	114.3	139.7	GPa
E_{22}	9.0	11.0	GPa
G_{23}	2.745	3.355	GPa
ν_{12}	0.306	0.374	
G_{12}	4.86	5.94	GPa

angle, mainly on $[0]_8$. It is due to the physical impossibility of stacking all fibres at 0 degrees. Therefore, a small deviation based on the fibre diameter was imposed on the DoE process to evaluate the influence of this design variable. All the geometrical factors have been its range defined by the measures obtained with the 3D scanner as previously explained on the dimensional analyses. Parameter ranges are summarized in Table 4.3 for the $[0]_8$ plates, and in Table 4.4 for the $[0/15/-15/0/15/-15/0]_s$ plates.

The study is carried out by two level Plackett-Burman (P-B) design, and considering that there are no iterations between design variables. Allowing to use a saturated design, with only 12 combinations of design variables. To compose the design variables combinations an orthogonal array is constructed (Table 4.5).

Numerical analysis runs are conducted to evaluate each combination of parameters presented in the DoE process. The results of the natural frequencies for each numerical run is presented in Figure 4.4 for stacking sequence of $[0]_8$ and in Figure 4.5 for the

Table 4.5: Numerical configurations layout of L12 table, Factor's level 1(low), Factor's level 2(high)

	W	L	C1	C2	θ	t	E ₁₁	E ₂₂	G ₂₃	ν_{12}	G ₁₂
Run1	low	low	high	high	low	low	low	low	low	low	low
Run2	low	low	high	high	low	high	high	high	high	high	high
Run3	low	low	low	low	high	low	low	low	high	high	high
Run4	low	high	high	low	high	low	high	high	low	low	high
Run5	low	high	low	high	high	high	low	high	low	high	low
Run6	low	high	low	low	low	high	high	low	high	low	low
Run7	high	low	low	low	low	low	high	high	low	high	low
Run8	high	low	low	high	high	high	high	low	low	low	high
Run9	high	low	high	low	high	high	low	high	high	low	low
Run10	high	high	low	high	low	low	low	high	high	low	high
Run11	high	high	high	low	low	high	low	low	low	high	high
Run12	high	high	high	high	high	low	high	low	high	high	low

stacking sequence of $[0/15/-15/0/15/-15/0]_s$, which also shows that, the variability of the resulted frequency increases in high modes. It means that high modes are more sensitive than lower ones. Therefore, in an SHM system, where the objective is to detect small damages, high modes are more strategic to be monitored. On the other hand, all other perturbations can influence the results, interfering in the damage detection.

The main effect of each parameter was obtained from the finite element analysis for each natural frequency and calculated as follow,

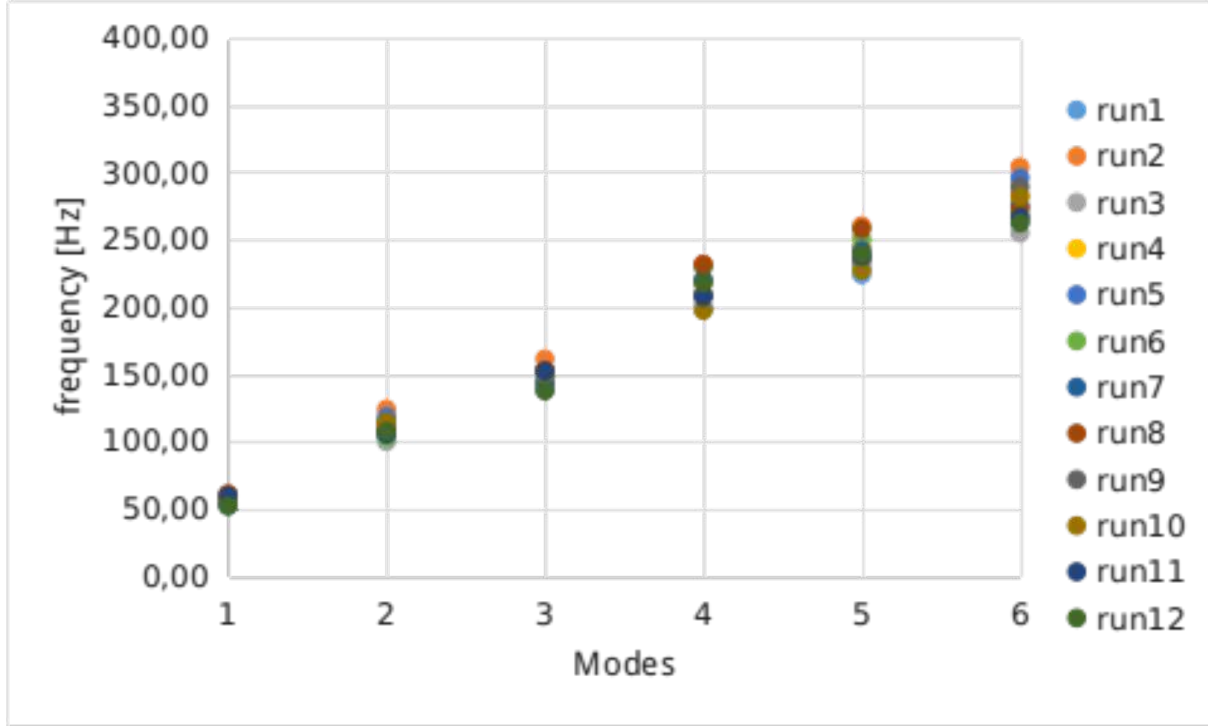
$$\text{Main Effect} = ME1(x) - ME2(x) \quad (4.2.1)$$

where ME1(x) and ME2(x) are the mean of the results influenced by level 1 and level 2 of factor x, respectively. The main effect is calculated for each mode, and after the total main effect is calculated using the sums of the results from each mode. Parameters are ranked in order of decreasing effect. Table 4.6 shows the main effect calculated for the results from plates with stacking sequence $[0]_8$. Similarly, Table 4.7 shows the results from plates with stacking sequence $[0/15/-15/0/15/-15/0]_s$.

Tables 4.6 and 4.7 show that thickness, Young's modulus in longitudinal (E₁₁) and transverse direction (E₂₂) exhibit high influence for both lay-up configurations. This influence is directly related to the mode shape of the plates. For example, mode 2 is a bending mode in the transverse direction, then every change in properties in this direction affect this mode more than others as observed in the numerical results.

Another important remark is related to width and length. Although these parameters are very important in the dynamic response, mainly for the stacking sequence $[0/15/-15/0/15/-15/0]_s$, they are well controlled during the manufacturing process. In addition, manufacturing parameters, as fibre fraction, which affect directly the materials

Figure 4.4: Natural frequencies resulted from the numerical modal analyses $[0]_8$

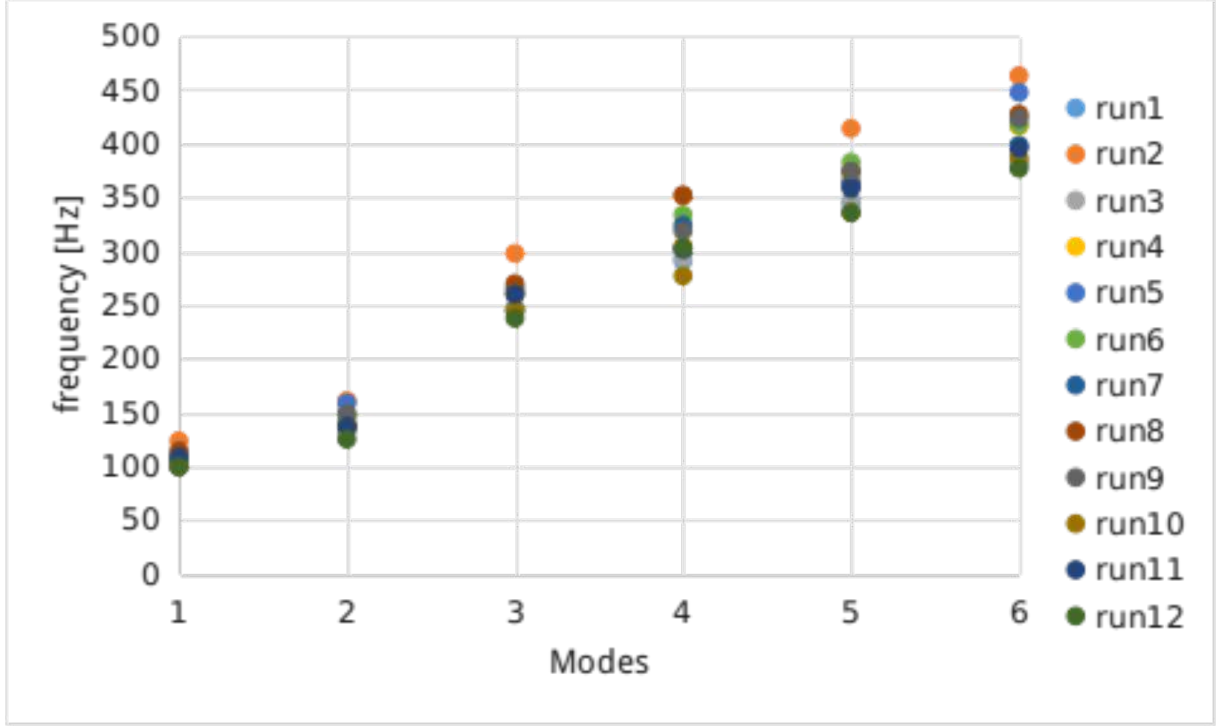


Source: Author's production.

Table 4.6: Main effect results for stacking sequence $[0]_8$ (units in Hertz)

Modes	01	02	03	04	05	06	<i>TotalMain Effect</i>	Rank
Thickness	1.42	2.00	3.72	5.46	5.86	6.37	40.83	1
E ₂₂	0.08	4.72	3.11	0.01	0.57	11.83	33.01	2
E ₁₁	0.06	0.24	0.09	10.66	9.03	0.95	28.22	3
G ₁₂	2.69	0.57	4.18	0.11	2.59	0.81	22.86	4
C2	0.04	3.36	0.38	0.10	0.23	3.80	9.38	5
W	-0.15	-0.66	-0.60	-0.10	-0.20	-1.55	-5.47	6
L	-0.16	-0.11	-0.29	-1.15	-1.18	-0.19	-4.55	7
C1	0.02	1.67	0.18	-0.13	0.15	1.67	4.05	8
ν_{12}	0.02	0.05	0.15	0.05	0.10	0.23	1.35	9
G ₂₃	-0.01	0.14	0.00	0.09	0.02	0.29	0.76	10
θ	-0.02	-0.07	0.01	-0.12	-0.11	0.00	-0.45	11

Figure 4.5: Natural frequencies resulted from the numerical modal analyses $[0/15/-15/0/15/-15/0]_s$



Source: Author's production.

Table 4.7: Main effect results for stacking sequence $[0/15/-15/0/15/-15]_s$ (units in Hertz)

Modes	01	02	03	04	05	06	<i>TotalMain Effect</i>	Rank
Thickness	9.28	12.57	22.84	27.72	29.42	38.62	233.67	1
E_{11}	4.70	0.35	8.19	30.77	18.18	13.52	118.05	2
E_{22}	0.49	13.05	7.99	0.57	12.10	25.54	94.67	3
W	-3.54	-9.20	-10.90	-0.14	-13.06	-16.66	-93.22	4
L	-3.20	0.03	-5.47	-17.97	-12.25	-5.96	-71.19	5
G_{12}	5.81	0.90	10.09	1.28	5.52	4.44	59.28	6
θ_{-15}	-2.22	0.70	-4.55	-0.03	3.64	-8.27	-24.51	7
θ_{15}	2.64	0.72	4.57	-2.16	4.55	-0.56	23.63	8
θ_0	-1.56	0.09	-2.93	-0.55	-5.91	5.11	-12.80	9
ν_{12}	0.27	0.62	1.12	-0.02	0.68	1.99	8.92	10
G_{23}	0.41	0.13	0.63	0.26	3.79	-2.72	4.75	11

properties should be carefully monitored to keep the materials properties under control. Finally, shear modulus (G_{12}) is another important parameter to be investigated.

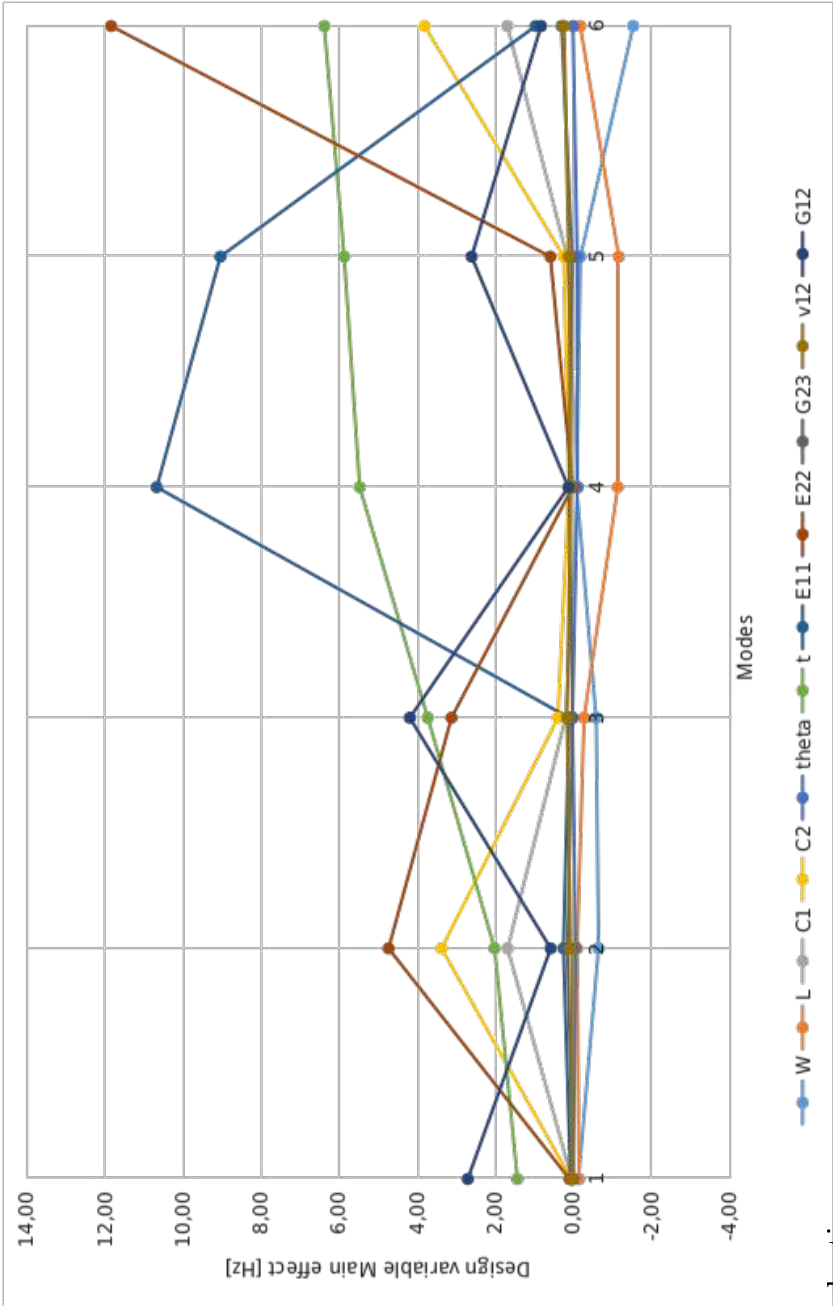
Analysis of the main effect on a mode-by-mode basis for the $[0]_8$ plates shows that some design parameters affect more or less the response at some specific modes. For example, it is possible to note that in the 4th mode, the effect of the changes in the E_{11} (10.66) is twice than the effect of the thickness (5.46). There is a clear relationship between the nature of the mode and the model parameter which affects the modes most strongly. The Figure 4.6 vertical axis represents the magnitude of the variable effect on the systems.

Young's modulus is important when bending phenomena dominate the mode and shear modulus is rather related to torsional modes. It is no surprise that Young's modulus in the longitudinal direction is the dominant factor for 4th and 5th modes. In addition, the Young's modulus in transverse direction shows higher influence for 2nd and 6th modes. This behaviour is explained by the modal shapes of the plate. In addition, it is important to note the influence of the curvatures. Even without a considerable influence in a global point of view, the curvatures have an important contribution on the 2nd mode.

The analysis of the main effect on a mode-by-mode basis for the $[0/15/-15/0/15/-15/0]_s$ plates (Figure 4.7) shows different results. Although the highest influence is provided by the thickness, as expected due to a greater number of layers, the 4th mode remains more sensitive to changes in Young's modulus in the longitudinal direction, and 2nd and 6th modes remain more sensitive to changes in Young's modulus in transverse direction.

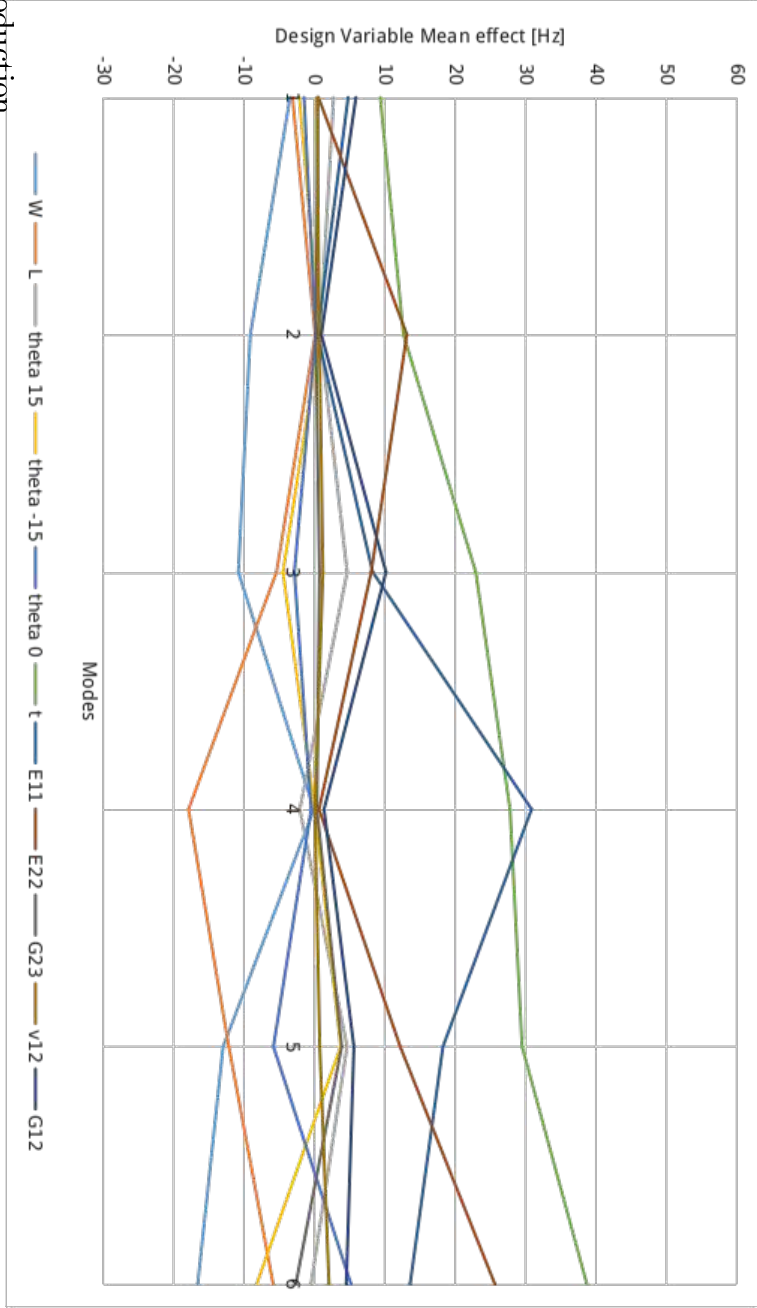
For $[0/15/-15/0/15/-15/0]_s$ plates is observed a more accentuated influence of E_{11} on 4th and 8th modes. Differently from the $[0]_8$ plates, the 5th mode has a lower effect, it is due to the fibre orientations and the mode shape. On 5th mode there are more nodal lines oriented at 15 degrees, reducing the effect of Young's modulus in the longitudinal direction.

Figure 4.6: Main effect mode-by-mode [0]s



Source: Author's production.

Figure 4.7: Main effect mode-by-mode [0/15/-15/0/15/-15/0]_s



Source: Author's production.

Chapter 5

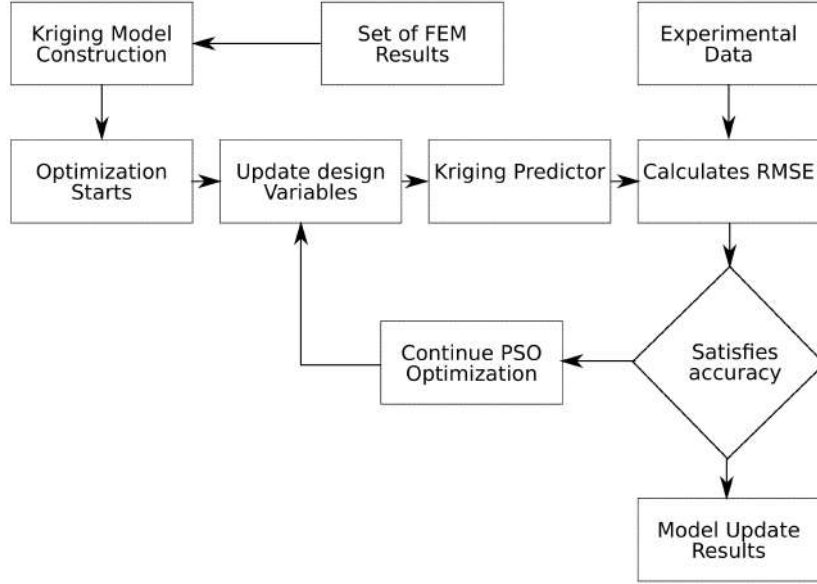
Model Updating

5.1 Model Update Strategy

Regarding the high computational cost involved in dynamic analyses, this work proposes a strategy to use a Kriging model instead of only FEM dynamic analyses during the process of model updating, as is shown in Figure 5.1.

First, the Kriging model construction must be done. For this, the procedure needs a set of initial data from the model, which should be represented by the Kriging approximation. During this step, an optimization problem is solved aiming to define the coefficients for the Kriging estimator. To construct the Kriging model, a set of data composed by values of design variables, and its respective results obtained by the FEM is used. Afterward, the metamodel is ready to represent the FEM during the model updating process. As aforementioned, the model update aims to find the best parameters to set numerical analysis that results in a good representation of the experimental data. Thus, within the model update process, an optimization problem must be done to find these parameters. This work aims to use the model update process to find the best input parameters to use in the FEM and obtain a good approximation to the experimental data. Then, the parameters used as design variables into the optimization of the model update process are Young's modulus at fibre direction (E_{11}), Young's modulus at normal to fibre direction (E_{22}), Shear modulus in ply plane (G_{12}) and the plate thickness. These variables were chosen based on the screening analysis presented in Chapter 4, (SOUZA et al., 2017). Where a screening design is conducted to identify the most significant variables that affect the dynamic behaviour. After that, a Particle Swarm Optimization (PSO) is used to carry out the model update process and find the best combination of the input parameters that result in a minimal difference from the numerical modal frequency and the experimental modal frequency. The limits imposed to the design variables have a range of 20% around the reference values, which are defined in Table 3.2. As an objective function, these differences are evaluated at each frequency using a Root Mean Square

Figure 5.1: Methodology used for the model update strategy adapted from (WANG et al., 2017)



Source: Author's production.

Error, and the optimization problem consists of minimize the sum of this difference. The objective function can be stated as,

$$RMSE = \sum_{i=1}^6 \sqrt{\left(\frac{f_n^i - f_e^i}{f_e^i}\right)^2} \quad (5.1.1)$$

where f_n^i is i^{th} frequency mode from the numerical data, f_e^i is i^{th} frequency mode from the experimental data.

As a reference, a model update procedure has been carried out using FEA and PSO. From this model update, it is possible to obtain the variables updated, and the time consuming to compare with the procedure using the kriging method. In a first step, the model update has applied for the same experimental data, changing the PSO parameters. This procedure allows identifying the better configuration via PSO algorithm. Table 5.1 shows the error, the number of call function and the number of iterations for different configurations of the particle number (N), the inertia parameter (w), the cognitive parameter (ϕ_1) and the social parameter (ϕ_2). The cognitive parameter represents the effect of self-knowledge and the social parameter is associated with the collective effect of the population (Vaz et al., 2013).

The objective of this analysis is to obtain the better PSO configuration, concerning the convergence of the problem, and the lowest number of call functions. Therefore, the configuration with $N = 40$, $w = 0.6$, $\phi_1 = 0.5$ and $\phi_2 = 0.5$ has presented better results,

Table 5.1: PSO parameter testing results

N	w	ϕ_1	ϕ_2	Error	Call function	Iterations	Convergence
16	0.5	0.5	0.5	0.140	512	32	NO
16	0.8	0.5	0.5	0.090	496	31	NO
25	0.8	0.2	0.8	0.066	825	33	NO
40	0.6	0.5	0.5	0.066	920	23	OK
50	0.6	0.5	0.5	0.113	1450	29	OK
60	0.6	0.5	0.5	0.113	1260	21	OK

where small populations do not achieve the convergence and bigger populations, only increase the number of objective function calls. After that, using these PSO parameters and carrying out the model update procedure for another experimental set, it is possible to evaluate the updated values.

Therefore, all of the plates have been submitted to the model update process using FEA model and the results of natural frequencies, compared against the experimental data.

5.2 Model Update Using FEM

Using the finite element analysis provided by Abaqus, the model update process is carried out for the two sets of composite plates studied in this work. The following sections presents the results obtained for each set of plates, including an additional study considering the effect of the curvature for plates at $[0]_8$.

5.2.1 Composite plates $[0]_8$

Table 5.2 presents the natural frequencies obtained in the model update process for composite plates $[0]_8$ compared against the experimental data. Also, an output of the model update process the updated variables are obtained and presented in Table 5.3.

Table 5.2: Comparison between FEA updated results and experimental results for Composite plates $[0]_8$

		f_1 [Hz]	f_2 [Hz]	f_3 [Hz]	f_4 [Hz]	f_5 [Hz]	f_6 [Hz]
P01	Exp	61.350	153.772	163.497	226.081	255.113	333.019
	Num	60.531	99.523	158.159	228.799	256.323	277.201
	Difference	-1.34%	-35.28%	-3.27%	1.20%	0.47%	-16.76%
P02	Exp	61.335	148.846	159.812	222.244	249.581	328.003
	Num	61.116	118.228	171.463	222.189	252.454	328.016
	Difference	-0.36%	-20.57%	7.29%	-0.02%	1.15%	0.00%
P03	Exp	60.206	153.082	158.531	224.791	250.435	324.993
	Num	60.206	117.157	169.392	224.723	253.800	324.996
	Difference	0.00%	-23.47%	6.85%	-0.03%	1.34%	0.00%
P04	Exp	62.519	154.456	161.768	221.158	248.955	328.050
	Num	60.533	118.279	170.655	221.109	250.966	328.163
	Difference	-3.18%	-23.42%	5.49%	-0.02%	0.81%	0.03%
P05	Exp	60.807	158.235	159.514	222.912	251.419	328.349
	Num	60.805	118.356	171.104	222.912	252.794	328.361
	Difference	0.00%	-25.20%	7.27%	0.00%	0.55%	0.00%
P06	Exp	57.726	146.233	154.751	224.814	250.390	316.508
	Num	57.715	114.110	163.664	224.266	251.091	316.512
	Difference	-0.02%	-21.97%	5.76%	-0.24%	0.28%	0.00%
P07	Exp	60.360	154.789	158.399	222.483	250.576	325.658
	Num	60.352	117.385	169.761	221.951	251.518	325.658
	Difference	-0.01%	-24.16%	7.17%	-0.24%	0.38%	0.00%
P08	Exp	59.549	154.414	155.488	224.855	252.458	322.805
	Num	59.013	116.375	167.119	224.758	252.726	322.806
	Difference	-0.90%	-24.63%	7.48%	-0.04%	0.11%	0.00%

Table 5.3: Updated variables results from FEA model update for Composite plates $[0]_8$

	E_{11} [GPa]	E_{22} [GPa]	G_{12} [GPa]	Thickness [mm]
P01	138.0418	11.0000	5.9351	2.2300
P02	122.6882	14.7138	5.6715	2.2917
P03	122.2252	14.0583	5.3505	2.3232
P04	122.3382	14.8313	5.5986	2.2837
P05	125.6290	15.0000	5.7071	2.2722
P06	136.8746	14.9837	5.5119	2.1916
P07	119.7600	14.1844	5.4052	2.3174

On the other hand, plates with stacking sequence of $[0]_8$ presented errors greater than 20% on the second mode. This behaviour results from the curvature of these plates. Examining the graphics resulted from the screening analysis. It is possible to note that the curvature has not a considerable influence when the summation of all modes is analysed. However, when looking only to the second and sixth modes, curvature is one of the most influential variable, as shown in Figure 5.2. Therefore, when using model update techniques on curved plates, it is mandatory to take into account this variable to have a good representation of the second and sixth modes.

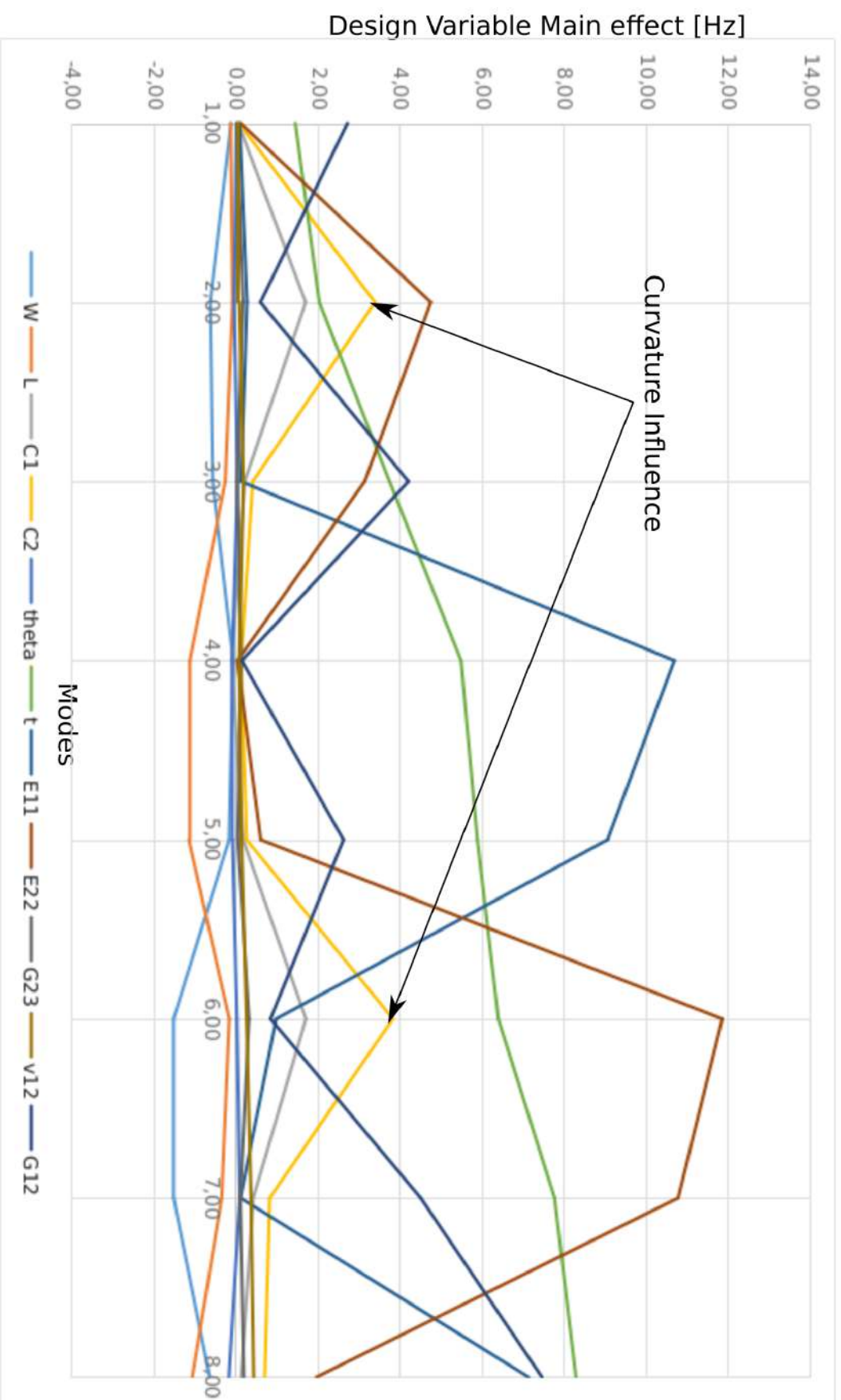
5.2.2 Composite plates $[0]_8$ considering curvature as design variable

Regarding the issue with the curvature, a new model update process including the curvature variables is carried out. The results show that the errors on second and sixth modes become insignificant (Table 5.5). Table 5.4 shows the updated variables obtained by this process. On the updated design variables, it is possible to verify that the mean value of the resulted variables remains into the range specified during the screening analysis phase. It shows that the model update process has converged to a point probably near to the real value of these properties.

Table 5.4: Updated variables results from FEA model update using curvature as design variable

	E_{11} [GPa]	E_{22} [GPa]	G_{12} [GPa]	Thickness [mm]	Curvature [mm]
P01	128.641	9.526	5.809	2.284	3.952692
P02	139.359	11.084	6.105	2.157	3.490802
P03	145.775	10.245	6.497	2.120	3.843471
P04	133.808	10.213	5.942	2.191	3.910242
P05	135.771	9.829	5.991	2.193	4.151295
P06	147.378	11.001	5.738	2.122	3.438376
P07	131.103	9.899	5.943	2.216	3.840755
P08	147.871	10.078	6.355	2.120	3.950333

Figure 5.2: Main effect mode-by-mode with curvature influence highlighted for $[0]_s$ plates



Source: Author's production.

Table 5.5: Comparison between FEA updated results (using curvature as design variable) and experimental results

		f_1 [Hz]	f_2 [Hz]	f_3 [Hz]	f_4 [Hz]	f_5 [Hz]	f_6 [Hz]
P01	Experimental	61.350	153.772	163.497	226.081	255.113	333.019
	FEM	61.350	153.771	162.647	226.000	255.974	333.069
	Difference	0.000%	0.000%	-0.520%	-0.036%	0.338%	0.015%
P02	Experimental	61.335	148.846	159.812	222.244	249.581	328.003
	FEM	59.499	148.796	160.207	222.229	250.985	328.003
	Difference	-2.992%	-0.033%	0.248%	-0.007%	0.563%	0.000%
P03	Experimental	60.206	153.082	158.531	224.791	250.435	324.993
	FEM	60.193	153.081	158.940	223.261	252.476	324.990
	Difference	-0.020%	0.000%	0.258%	-0.681%	0.815%	-0.001%
P04	Experimental	62.519	154.456	161.768	221.158	248.955	328.050
	FEM	59.590	154.456	159.793	221.160	250.126	330.112
	Difference	-4.685%	0.000%	-1.220%	0.001%	0.470%	0.629%
P05	Experimental	60.807	158.235	159.514	222.912	251.419	328.349
	FEM	59.853	158.234	159.785	222.911	251.892	328.347
	Difference	-1.568%	0.000%	0.170%	0.000%	0.188%	0.000%
P06	Experimental	57.726	146.233	154.751	224.814	250.390	316.508
	FEM	56.847	145.366	154.764	224.774	250.816	320.914
	Difference	-1.521%	-0.593%	0.009%	-0.017%	0.171%	1.392%
P07	Experimental	60.360	154.789	158.399	222.483	250.576	325.658
	FEM	60.218	151.830	160.149	221.376	250.876	328.740
	Difference	-0.235%	-1.911%	1.105%	-0.497%	0.120%	0.946%
P08	Experimental	59.549	154.414	155.488	224.855	252.458	322.805
	FEM	59.548	154.413	157.736	224.784	253.217	322.798
	Difference	-0.001%	0.000%	1.446%	-0.031%	0.301%	-0.002%

5.2.3 Composite plates $[0/15/-15/0/15/-15]_s$

Table 5.6 presents the natural frequencies obtained in the model update process for composite plates $[0/15/-15/0/15/-15]_s$ compared against the experimental data. Also, an output of the model update process the updated variables are obtained and presented in Table 5.7.

Table 5.6: Comparison between FEA updated results and experimental results for Composite plates $[0/15/-15/0/15/-15]_s$

P09	Exp	95.379	132.911	250.645	316.229	349.436	405.460
	Num	96.227	132.909	236.400	316.169	351.404	388.611
	Difference	0.889%	-0.001%	-5.6831%	-0.0187%	0.5632%	-4.1553%
P10	Exp	104.152	139.884	261.091	320.690	367.079	411.455
	Num	104.1878	140.03118	253.5284	320.7774	367.0878	404.8923
	Difference	0.0344%	0.1052%	-2.8965%	0.0273%	0.0024%	-1.5950%
P11	Exp	106.412	144.506	265.334	332.630	377.859	424.862
	Num	106.4084	144.5208	259.8236	332.6407	378.7168	418.1251
	Difference	-0.0034%	0.0102%	-2.0768%	0.0032%	0.2270%	-1.5857%
P12	Exp	107.616	146.244	268.219	332.774	381.241	426.971
	Num	107.6175	146.2455	262.7719	332.7749	381.4243	421.5948
	Difference	0.0014%	0.0010%	-2.0308%	0.0003%	0.0481%	-1.2591%
P13	Exp	102.961	139.202	258.850	320.595	365.101	412.746
	Num	102.9642	139.2085	251.0847	320.5707	365.2386	403.0251
	Difference	0.0031%	0.0047%	-2.9999%	-0.0076%	0.0377%	-2.3552%
P14	Exp	99.628	136.840	258.484	324.150	361.405	414.755
	Num	103.829	136.841	251.266	324.173	364.082	401.559
	Difference	4.217%	0.001%	-2.792%	0.007%	0.740%	-3.181%

Table 5.7: Updated variables results from FEA model update for Composite plates $[0/15/-15/0/15/-15]_s$

	E_{11} [GPa]	E_{22} [GPa]	G_{12} [GPa]	Thickness [mm]
P09	149.9990	10.2767	4.0000	3.0653
P10	134.8536	9.8907	4.8220	3.2724
P11	139.3695	10.1438	4.6675	3.3406
P12	133.4922	9.9387	4.6773	3.4137
P13	139.1944	10.1104	4.7407	3.2209
P14	148.5947	10.1416	5.0285	3.1535

Comparing the natural frequencies data, it is possible to note the good approximation for plates with the stacking sequence of $[0/15/-15/0/15/-15]_s$ resulting in errors around 2 and 4%.

These results demonstrate the quality of the model update, showing how good the numerical model fits the experimental data. However, the disadvantage of this method is time-consuming. For the case, the whole model update process takes around 4 hours (desktop computer, memory: 4Gb, processor: Intel i5), to run the 900 finite

element problems needed to converge the optimization process. Depending on the problem complexity, it could become unfeasible due to the time required to simulate each finite element analysis in the optimization algorithm.

5.2.4 Model Update using Kriging Model

The model update process was modified to include the Kriging predictor, i.e., call the Kriging model instead of the FEM. Then, the PSO algorithm searches for the best combination of design variables to fit the experimental results. A reduction in the computational time is expected, since the Kriging model is faster than FEM to make the calculations.

5.2.5 Composite plates $[0]_8$

The design variables resulted from the process for composite plates $[0]_8$ are presented in Table 5.8, and the comparison between the frequencies predicted with the Kriging model and the experimental data is presented in Table 5.9, here is remarkable the approximation obtained with the Kriging predictor, but it is important to remember that the Kriging predictor is an approximation of the FEM behaviour, therefore this results is more an information about the convergence of the model update process than a precision indicative of the method.

Table 5.8: Kriging model coefficients after model update for composite plates $[0]_8$

	E_{11} [GPa]	E_{22} [GPa]	E_{12} [GPa]	Thickness [mm]
P01	138.042	11.000	5.935	2.230
P02	122.688	14.714	5.672	2.292
P03	122.225	14.058	5.351	2.323
P04	122.338	14.831	5.599	2.284
P05	125.629	15.000	5.707	2.272
P06	136.875	14.984	5.512	2.192
P07	119.760	14.184	5.405	2.317
P08	122.922	13.942	5.160	2.317

Table 5.9: Natural frequencies obtained with the Kriging model compared with the target experimental frequencies for composite plates [0]₈.

		f_1 [Hz]	f_2 [Hz]	f_3 [Hz]	f_4 [Hz]	f_5 [Hz]	f_6 [Hz]
P01	Exp	61.350	153.772	163.497	226.081	255.113	333.019
	Kriging	61.350	121.862	173.405	230.151	262.204	333.019
	Difference	0.00%	-20.75%	6.06%	1.80%	2.78%	0.00%
P02	Exp	61.335	148.846	159.812	222.244	249.581	328.003
	Kriging	61.335	118.233	171.795	222.244	253.912	328.003
	Difference	0.00%	-20.57%	7.50%	0.00%	1.74%	0.00%
P03	Exp	60.206	153.082	158.531	224.791	250.435	324.993
	Kriging	60.206	117.221	169.332	224.595	253.204	324.993
	Difference	0.00%	-23.43%	6.81%	-0.09%	1.11%	0.00%
P04	Exp	62.519	154.456	161.768	221.158	248.955	328.050
	Kriging	62.516	120.491	173.002	231.207	260.614	328.050
	Difference	0.00%	-21.99%	6.94%	4.54%	4.68%	0.00%
P05	Exp	60.807	158.235	159.514	222.912	251.419	328.349
	Kriging	60.807	119.808	171.296	229.814	261.109	328.353
	Difference	0.00%	-24.28%	7.39%	3.10%	3.85%	0.00%
P06	Exp	57.726	146.233	154.751	224.814	250.390	316.508
	Kriging	57.726	114.306	162.303	229.696	258.000	316.508
	Difference	0.00%	-21.83%	4.88%	2.17%	3.04%	0.00%
P07	Exp	60.360	154.789	158.399	222.483	250.576	325.658
	Kriging	60.360	117.375	169.756	222.483	252.480	325.658
	Difference	0.00%	-24.17%	7.17%	0.00%	0.76%	0.00%
P08	Exp	59.549	154.414	155.488	224.855	252.458	322.805
	Kriging	59.547	116.370	167.877	224.855	253.276	322.805
	Difference	0.00%	-24.64%	7.97%	0.00%	0.32%	0.00%

Finally, the design variables obtained in the model update using Kriging are used as input in the finite element algorithm. Table 5.10 shows the natural frequencies obtained using FEA, with the inputs defined by the model updating using Kriging, the relative difference presented in this table is in the relation of the FEA results and the experimental data.

Table 5.10: Comparison between FEA results with experimental data and Kriging values for composite plates $[0]_8$

		f_1 [Hz]	f_2 [Hz]	f_3 [Hz]	f_4 [Hz]	f_5 [Hz]	f_6 [Hz]
	Exp	61.350	153.772	163.497	226.081	255.113	333.019
P01	FEA/Kriging	60.609	99.792	158.390	228.642	256.697	277.34
	Difference	-1.207%	-35.103%	-3.124%	1.133%	0.621%	-16.719%
	Exp	61.335	148.846	159.812	222.244	249.581	328.003
P02	FEA/Kriging	61.204	118.572	171.738	221.964	252.539	328.499
	Difference	-0.213%	-20.339%	7.463%	-0.126%	1.185%	0.151%
	Exp	60.206	153.082	158.531	224.791	250.435	324.993
P03	FEA/Kriging	60.282	117.472	169.634	224.467	253.845	325.413
	Difference	0.127%	-23.262%	7.004%	-0.144%	1.362%	0.129%
	Exp	62.519	154.456	161.768	221.158	248.955	328.050
P04	FEA/Kriging	60.621	118.624	170.931	220.887	251.051	328.649
	Difference	-3.035%	-23.199%	5.664%	-0.123%	0.842%	0.183%
	Exp	60.807	158.235	159.514	222.912	251.419	328.349
P05	FEA/Kriging	60.877	118.674	171.339	222.642	252.823	328.775
	Difference	0.116%	-25.001%	7.413%	-0.121%	0.558%	0.130%
	Exp	57.726	146.233	154.751	224.814	250.390	316.508
P06	FEA/Kriging	57.801	114.449	163.948	224.086	251.213	317.016
	Difference	0.131%	-21.735%	5.943%	-0.324%	0.329%	0.161%
	Exp	60.360	154.789	158.399	222.483	250.576	325.658
P07	FEA/Kriging	60.417	117.688	169.978	221.665	251.526	326.036
	Difference	0.096%	-23.969%	7.310%	-0.368%	0.379%	0.116%
	Exp	59.549	154.414	155.488	224.855	252.458	322.805
P08	FEA/Kriging	59.085	116.685	167.356	224.498	252.762	323.218
	Difference	-0.778%	-24.434%	7.633%	-0.159%	0.120%	0.128%

The final design variables configuration obtained with the procedure proposed in this paper, results in a better approximation for almost all modes. The second mode for $[0]_8$ plates has a higher error because this Kriging model is representing the FEA generated without taking into account the curvature.

5.2.6 Composite plates $[0/15/-15/0/15/-15]_s$

The design variables resulted from the process for composite plates $[0/15/-15/0/15/-15]_s$ are presented in Table 5.11, and the comparison between the frequencies predicted with the Kriging model and the experimental data is presented in Table 5.12.

Table 5.11: Kriging model coefficients after model update for composite plates [0/15/-15/0/15/-15]_s

	E ₁₁ [GPa]	E ₂₂ [GPa]	E ₁₂ [GPa]	Thickness [mm]
P09	131.720	10.714	4.484	3.031
P10	139.488	10.015	4.854	3.245
P11	143.986	10.422	4.778	3.306
P12	121.309	9.078	4.066	3.706
P13	140.816	10.021	4.598	3.237
P14	132.190	15.082	2.842	3.338

Table 5.12: Natural frequencies obtained with the Kriging model compared with the target experimental frequencies for composite plates [0/15/-15/0/15/-15]_s.

P09	Exp	95.379	132.911	250.645	316.229	349.436	405.460
	Kriging	95.933	135.119	236.125	316.107	349.436	389.267
	Difference	0.58%	1.66%	-5.79%	-0.03%	0.00%	-3.99%
P10	Exp	104.288	140.612	254.109	320.702	367.074	406.911
	Kriging	104.152	139.884	261.091	320.690	367.079	411.455
	Difference	-0.13%	-0.52%	2.75%	0.00%	0.00%	1.12%
P11	Exp	106.797	144.963	260.675	332.630	377.859	419.966
	Kriging	106.412	144.506	265.334	332.630	377.859	424.862
	Difference	-0.36%	-0.32%	1.79%	0.00%	0.00%	1.17%
P12	Exp	107.641	147.578	268.219	332.774	377.230	426.680
	Kriging	107.616	146.244	268.219	332.774	381.241	426.971
	Difference	-0.02%	-0.90%	0.00%	0.00%	1.06%	0.07%
P13	Exp	102.961	139.202	251.151	320.595	366.074	404.498
	Kriging	102.961	139.202	258.850	320.595	365.101	412.746
	Difference	0.00%	0.00%	3.07%	0.00%	-0.27%	2.04%
P14	Exp	99.628	136.840	258.484	324.150	361.405	414.755
	Kriging	99.628	139.499	254.246	319.215	361.704	403.000
	Difference	0.00%	1.94%	-1.63%	-1.52%	0.08%	-2.83%

The design variables obtained in the model update using Kriging are used as input in the finite element algorithm. Table 5.13 shows the natural frequencies obtained using FEA, with the inputs defined by the model updating using Kriging, the relative difference presented in this table is in the relation of the FEA results and the experimental data.

Table 5.13: Comparison between FEA results with experimental data and Kriging values $[0/15/-15/0/15/-15]_s$

	Exp	95.379	132.911	250.645	316.229	349.436	405.460
P09	FEA/Kriging	94.658	134.225	234.337	293.624	340.787	381.832
	Difference	-0.755%	0.988%	-6.506%	-7.148%	-2.475%	-5.827%
	Exp	104.152	139.884	261.091	320.690	367.079	411.455
P10	FEA/Kriging	104.399	139.722	253.679	323.157	368.584	404.479
	Difference	0.237%	-0.115%	-2.838%	0.769%	0.410%	-1.695%
	Exp	106.412	144.506	265.334	332.630	377.859	424.862
P11	FEA/Kriging	106.866	144.934	260.745	334.393	380.969	418.66
	Difference	0.426%	0.296%	-1.729%	0.530%	0.823%	-1.459%
	Exp	107.616	146.244	268.219	332.774	381.241	426.971
P12	FEA/Kriging	110.252	151.453	269.954	343.970	394.432	434.850
	Difference	2.449%	3.561%	0.646%	3.364%	3.460%	1.845%
	Exp	102.961	139.202	258.850	320.595	365.101	412.746
P13	FEA/Kriging	103.068	139.186	251.179	323.756	367.280	403.395
	Difference	0.103%	-0.011%	-2.963%	0.986%	0.596%	-2.265%
	Exp	99.628	136.84	258.484	324.150	361.405	414.755
P14	FEA/Kriging	95.754	171.951	259.789	323.951	371.801	482.846
	Difference	-3.888%	25.658%	0.504%	-0.061%	2.876%	16.4172%

The model update using the Kriging model shows excellent results in relation to computational time and accuracy. This procedure can help to obtain a good approximation of values for design variables to be used in the computational model instead of to carry out a complete model update using FEA. The final design variables configuration obtained with the procedure proposed in this paper, results in a better approximation for almost all modes.

The Kriging metamodel shows to be very promising to be used in, instead of the FEA, to carry out a quick update of the main design variables, and then, utilize it in the FEM. This procedure demonstrates to be very reliable, since the higher error obtained is around 3.7% (except for the second mode of $[0]_8$ plates that is affected by the curvature, which is not considered during this model update.) and the lower one is about 0.08%. It is important to remark that no kind of pre-processing has been used to choose the best points to train the Kriging model, then future studies could be done to improve the results. This procedure can be used to define the parameters to be monitored in an SHM system, and also how these parameters have an influence on the process, helping engineers to develop better SHM systems.

Chapter 6

Case Study

6.1 Case Study I: Manufacturing Quality analysis

Dynamic analysis is an effective means of damage identification. Due to the manufacturing process, the properties of a component are very hard to control. As many damage detection methods are based on the comparison of intact and damaged plates, the definition of the intact plate must be clearly defined. This case study shows a methodology to define a frequency range to characterize a composite plate as an intact structure. Using the model update process, with Kriging metamodel based on natural frequencies, as presented in previous chapters, the updated variables allowed to obtain the FRF by Finite Element Method. A set of six plates with the stacking sequence of $[0/15/-15/0/15/-15]_s$ were analysed. The applicability of the methodology is presented using one of the known plates. The presented analysis shows that it is possible to make a preliminary study to improve the manufacturing design tolerances.

Intact plates have been submitted to modal analysis and the natural frequencies were obtained. Table 6.1 presents the experimental results for the plates, including the six natural frequencies. In addition, the average and the standard deviation were calculated. Furthermore, Table 6.2 presents the minimum and maximum values for each mode. Those values were obtained using the median and the standard deviation of the experimental analysis.

Table 6.1: Experimental natural frequencies compilation and analysis

	f_1 [Hz]	f_2 [Hz]	f_3 [Hz]	f_4 [Hz]	f_5 [Hz]	f_6 [Hz]
P09	95.379	132.911	250.645	316.229	349.436	405.460
P10	104.152	139.884	261.091	320.690	367.079	411.455
P11	106.412	144.506	265.334	332.630	377.859	424.862
P12	107.616	146.244	268.219	332.774	381.241	426.971
P13	102.961	139.202	258.850	320.595	365.101	412.746
P14	99.628	136.840	258.484	324.150	361.405	414.755
Average	102.691	139.931	260.437	324.511	367.020	416.042
St. Dev	4.542	4.902	6.119	6.824	11.525	8.280

Table 6.2: Minimum and maximum natural frequencies to characterizes the composite plates with stacking sequence [0/15/-15/0/15/-15]s.

	f_1 [Hz]	f_2 [Hz]	f_3 [Hz]	f_4 [Hz]	f_5 [Hz]	f_6 [Hz]
Min	98.149	135.029	254.318	317.687	355.495	407.762
Max	107.233	144.833	266.555	331.336	378.545	424.321

Therefore, using the boundaries found in Table 6.2, it is possible to carry on a modal update process to obtain the design variables that correspond to these results. For this, model update process using Kriging model as explained in the previous chapters is applied. The model update process results on approximate values to the design variables which are going to be used as input in the finite element method to acquire the Frequency Response Functions.

The same process could be done using only FEM, however, the computational time needed to perform this task is almost impracticable. The methodology proposed here also uses the FEM, but the amount of times it is called is much smaller. For a model update process, the FEM should be called at least 800 times. In the methodology proposed, the FEM was called 40 times to training the Kriging model, and after 2 times to build the FRFs. Therefore, in summary, the methodology using FEM has 800 calls against approximately 44 call for the methodology using the Kriging model.

The frequencies updated are shown in Table 6.3, where is presented the experimental column as the reference, Kriging column as the results from the model update and the difference represents the percentage difference between the expected value (Experimental) and the result of the model update (Kriging). The design variables resulted from this model update process are presented in Table 6.4.

Table 6.3: Updated frequency results

	f_1 [Hz]	f_2 [Hz]	f_3 [Hz]	f_4 [Hz]	f_5 [Hz]	f_6 [Hz]
Maximum						
Experimental	107.233	144.833	266.555	331.336	378.545	424.321
Kriging	108.765	145.565	265.019	331.329	376.577	422.484
Difference	1.429%	0.506%	-0.576%	-0.002%	-0.520%	-0.433%
Minimum						
Experimental	98.149	135.029	254.318	317.687	355.495	407.762
Kriging	98.149	139.092	253.457	317.453	361.704	403.000
Difference	0.000%	3.009%	-0.338%	-0.074%	1.747%	-1.168%

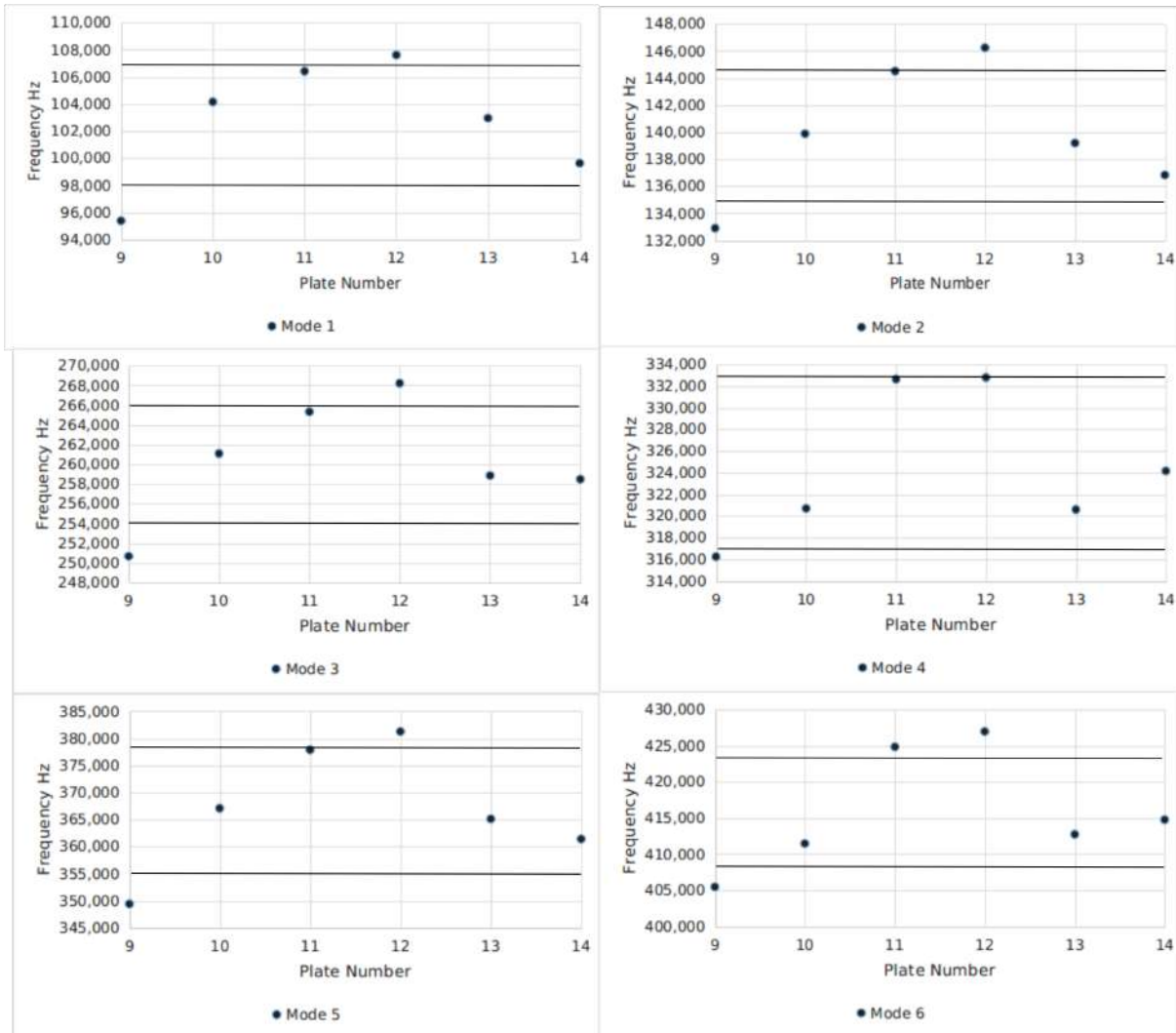
Table 6.4: Updated design variables

	E11 [GPa]	E22 [GPa]	G12 [GPa]	t [mm]
Minimum	130.54	16.00	2.78	3.23
Maximum	137.05	9.47	4.56	3.48

These results allow using the ABAQUS FEM algorithm to calculate the Frequency Response Functions that correspond to the components with the dynamic behaviour predicted before.

Using all the plates available, it is possible to plot in a graphic (Figure 6.1) the maximum and minimum limits, for each natural frequency, and the natural frequency of each plate. This graphic makes it easy to visualize the plates with natural frequencies out of the determined bounds. Analyzing the Figure 6.1 it is possible to note that plates 10, 11, 12, and 13 have more than 60% of its natural frequencies inner the boundaries. Then, according to the hypothesis that a plate with a dynamic behaviour into the limits had a satisfactory manufacturing process, these plates can be considered approved. Otherwise, plates 9 and 14 have strong indications about some manufacturing problem.

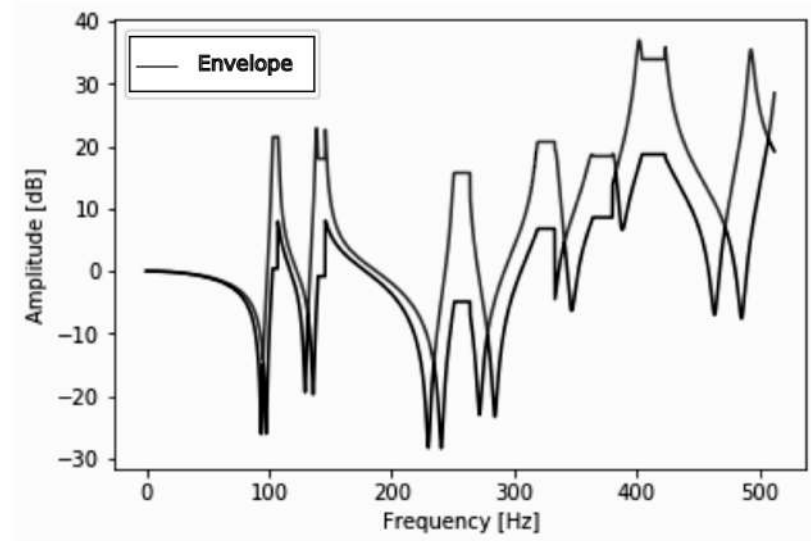
Figure 6.1: Maximum and minimum limits of natural frequencies and values of natural frequencies of the composite plates.



Source: Author's production.

Another way to use the methodology presented is to use the FRFs. With the design variables provided by the model update process, the ABAQUS FEM algorithm can be used to generate the FRFs. In this case, the quality assessment is performed by the percentage of the FRF analysed that is within the limits established by the maximum and minimum FRFs obtained numerically. Figure 6.2 presents the FRF limits obtained by the numerical results.

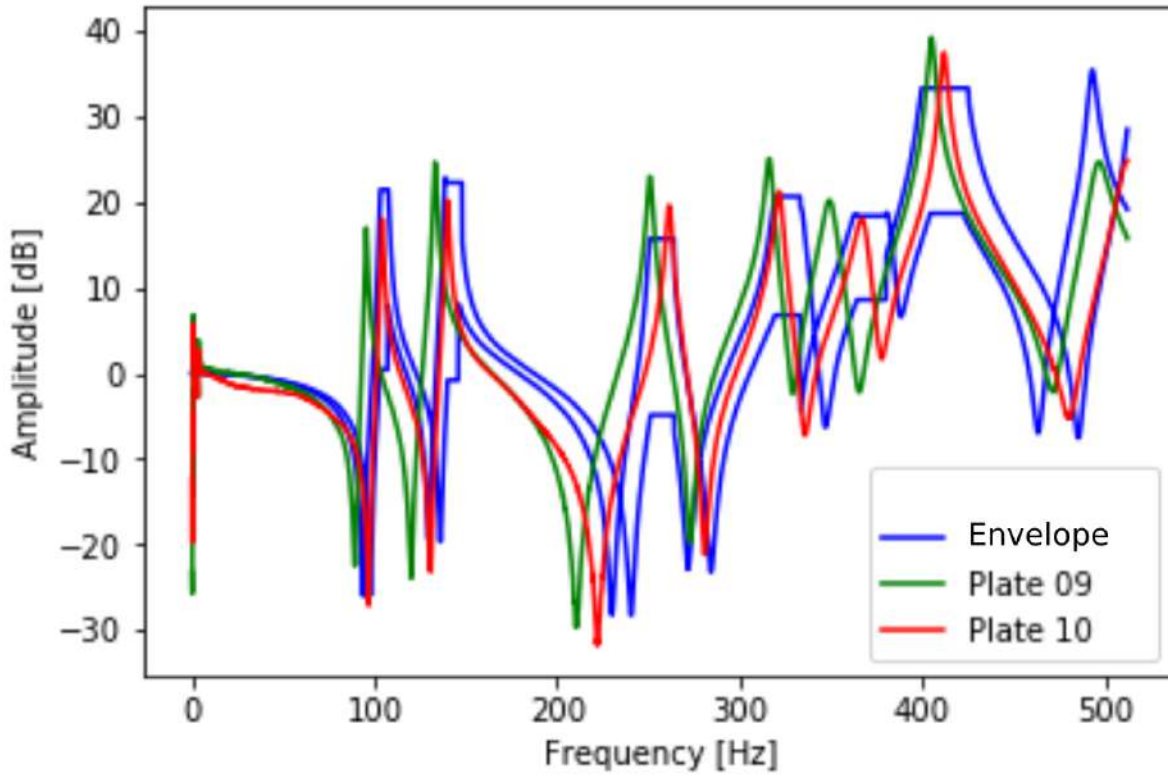
Figure 6.2: Limits of the FRF determined by the numerical results.



Source: Author's production.

Figure 6.3 presents the FRF limits, and also, the experimental FRF of the Plate 09 and Plate 10. As shown in the natural frequency graphics, Plate 09 is out of the range, and Plate 10 has a better fitting into the pre-established range. Calculating the percentage of the points in the limits it is possible to note that Plate 09 has 33.28% of its points inner the limits, and Plate 10 has 48.16%. Despite this, looking only for the positive part of the FRFs, it is possible to note that 48.10% of the FRF from Plate 09 is in the limits, whereas Plate 10 has 74,2% of its points within the limits.

Figure 6.3: FRF limits and FRF of Plate 09 and Plate 10



Source: Author's production.

6.2 Case Study II: Damage Identification

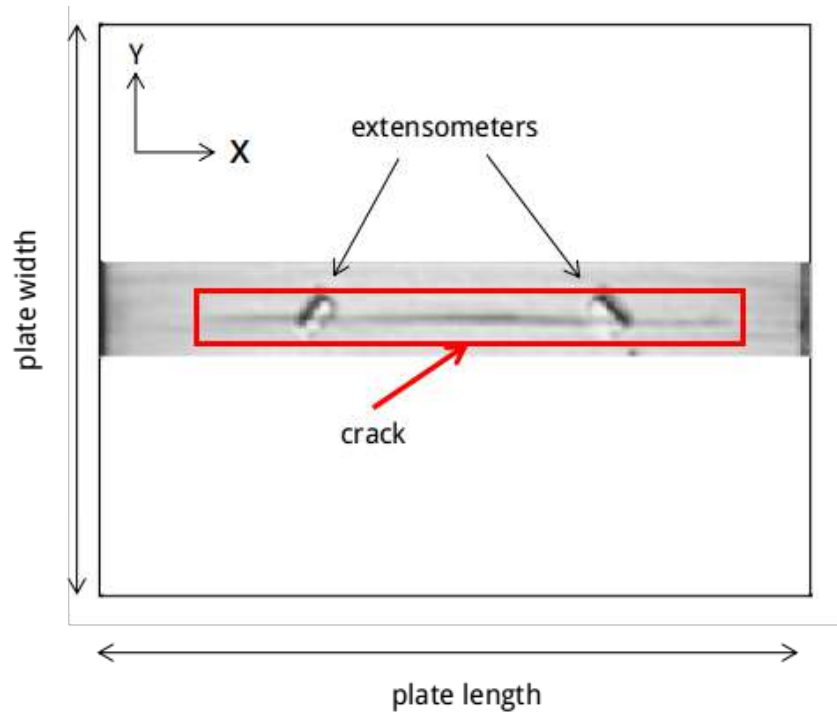
Damage identification by vibration based methods is supported by the hypothesis that damages cause changes in mass and stiffness matrix. However, this results from degradation of material properties or alteration of geometry characteristics. Therefore, using the methodology proposed in this work, two different results can be obtained. First, the indication of damage type can be done based on the correlation of the variation in natural frequencies and the effect of the design variable, presented during screening analysis. Another result is to verify if the damage caused is enough to characterize the plate as out of specification, using the range of FRFs.

The experimental methodology applied here is based on the use of a drop machine to imply impact damage on the composite plates and after analysing the specimens with the C-Scan test to evaluate the damage extension. Cracks are observed on the damaged structures and natural frequencies are obtained to evaluate the changes in the dynamic response.

6.2.1 Results for plates with stacking sequence of $[0]_8$

Cracks are observed on the impacted plates at $[0]_8$ by C-scan technique (Figure 6.4) indicating a long crack on the fibre direction. The natural frequency analysis (Table 6.5) indicates a high difference between intact and damaged frequency in the 2nd mode, which is strongly affected by changes in E_{22} . Changes in E_{22} can characterize matrix cracks in a unidirectional laminate, and this is confirmed by the C-Scan results. It is important to note that the C-Scan was applied only on the damaged region and not on the whole plate.

Figure 6.4: Damage observed by C-scan technique: $[0]_8$. Red box highlights the crack on the plate.



Source: Souza et al. (2019).

The image of the damaged plate shows a crack propagated on the transverse direction, which reduces the E_{22} of the material. This effect is remarked on the experimental results as presented in Table 6.5, where a reduction of 18% is observed. Also, the numerical results have been indicated the same behaviour, which shows that a reduction in the transversal Young's modulus results in a reduction in the natural frequency.

Table 6.5: Experimental results for intact and damaged plates, stack sequence [0]s.

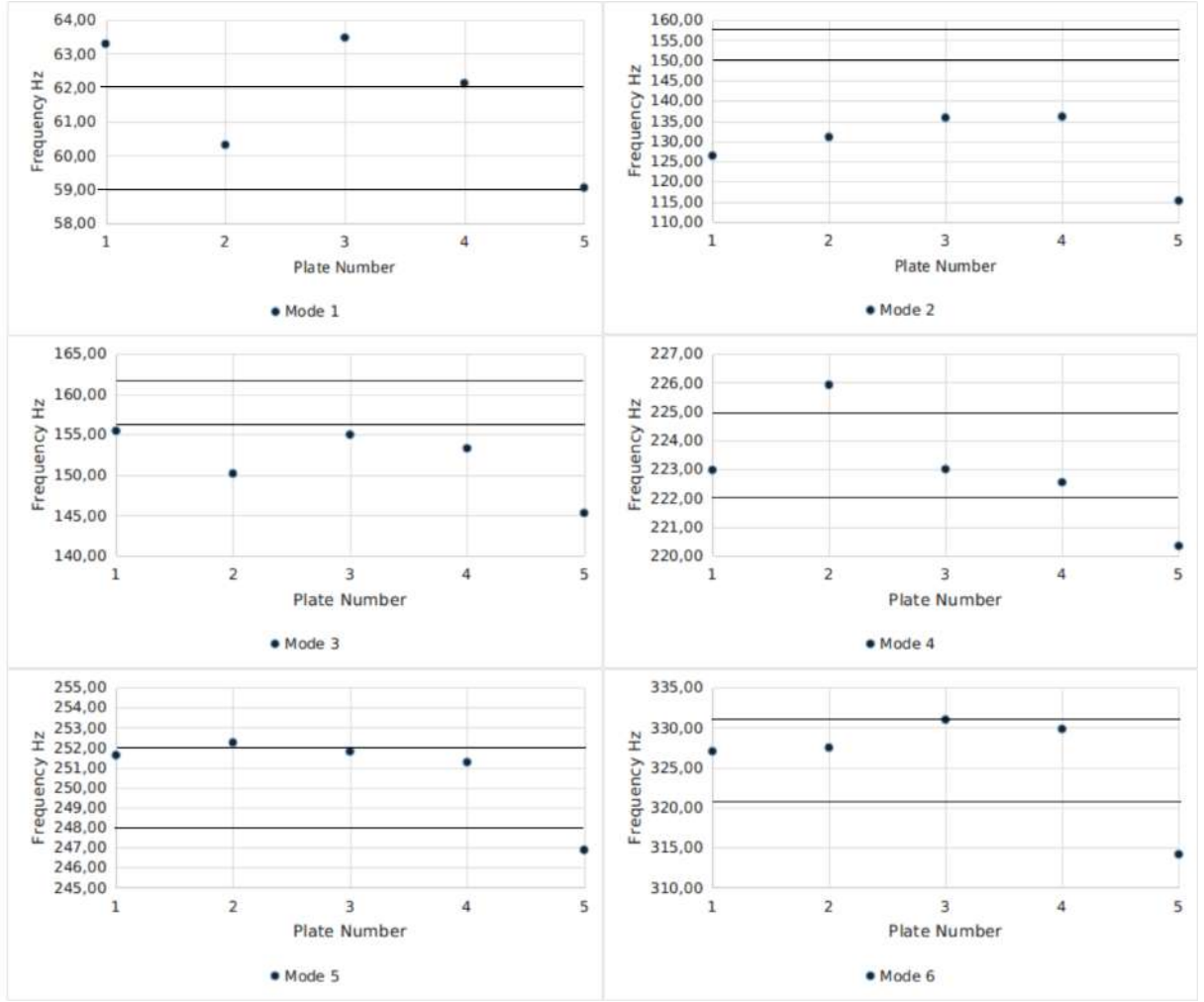
Plate 1			
	Intact	Damaged	Relative difference
f_1 [Hz]	61.89	64.20	3.74%
f_2 [Hz]	155.11	126.35	-18.54%
f_3 [Hz]	164.73	158.38	-3.86%
f_4 [Hz]	226.25	225.53	-0.32%
f_5 [Hz]	255.31	255.82	0.20%
f_6 [Hz]	332.95	336.24	0.99%

Plate 3			
	Intact	Damaged	Relative difference
f_1 [Hz]	60.21	59.42	-1.31%
f_2 [Hz]	153.08	118.92	-22.32%
f_3 [Hz]	158.53	140.65	-11.28%
f_4 [Hz]	224.79	222.72	-0.92%
f_5 [Hz]	250.44	247.92	-1.01%
f_6 [Hz]	324.99	320.26	-1.46%

Plate 4			
	Intact	Damaged	Relative difference
f_1 [Hz]	62.52	63.48	1.53%
f_2 [Hz]	154.46	135.61	-12.20%
f_3 [Hz]	161.77	155.02	-4.17%
f_4 [Hz]	221.16	223.00	0.83%
f_5 [Hz]	248.96	251.81	1.15%
f_6 [Hz]	328.05	331.37	1.01%

Based on the experimental intact data, the maximum and minimum values for the set of plates can be calculated. The Figure 6.5 shows the damaged frequencies (dots) against the maximum and minimum values (lines).

Figure 6.5: Maximum and minimum limits of the intact composite plates (lines) and damaged frequencies of composite plates (dots) with stack sequence of $[0]_8$.



Source: Author's production.

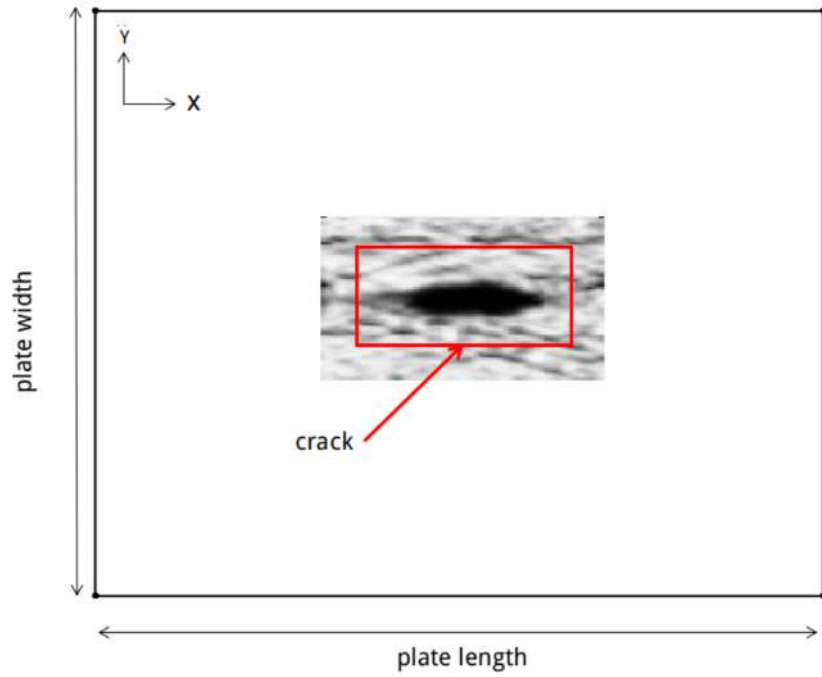
It is clear that modes 2 and 3 are out of the bounds, indicating some difference on dynamic behaviour in relation to the reference set of plates (intact plates). Therefore, it is possible to state that the evaluated plates are not able to continue to be applied on future components.

6.2.2 Results for plates with stacking sequence of $[0/15/-15/0/5/-15]_s$

The $[0/15/-15/0/5/-15]_s$ damaged plates natural frequencies do not differ much from the intact plates, because the extent of damage is much more restricted (Table 6.6). The propagation of a crack in the unidirectional plates is not hindered, whereas the $\pm 15^\circ$ orientation of the fibres creates natural barriers for the extent of damages. The

C-Scan evaluation of the $[0/15/-15/0/5/-15]_s$ plates shows a combination of matrix and fibre cracks (Figure 6.6). Table 6.6 shows the relative difference between the intact and damaged plate for the stacking sequence of $[0/15/-15/0/5/-15]_s$.

Figure 6.6: Damage observed by C-scan technique: $[0/15/-15/0/5/-15]_s$. Red box highlights the crack on the plate.



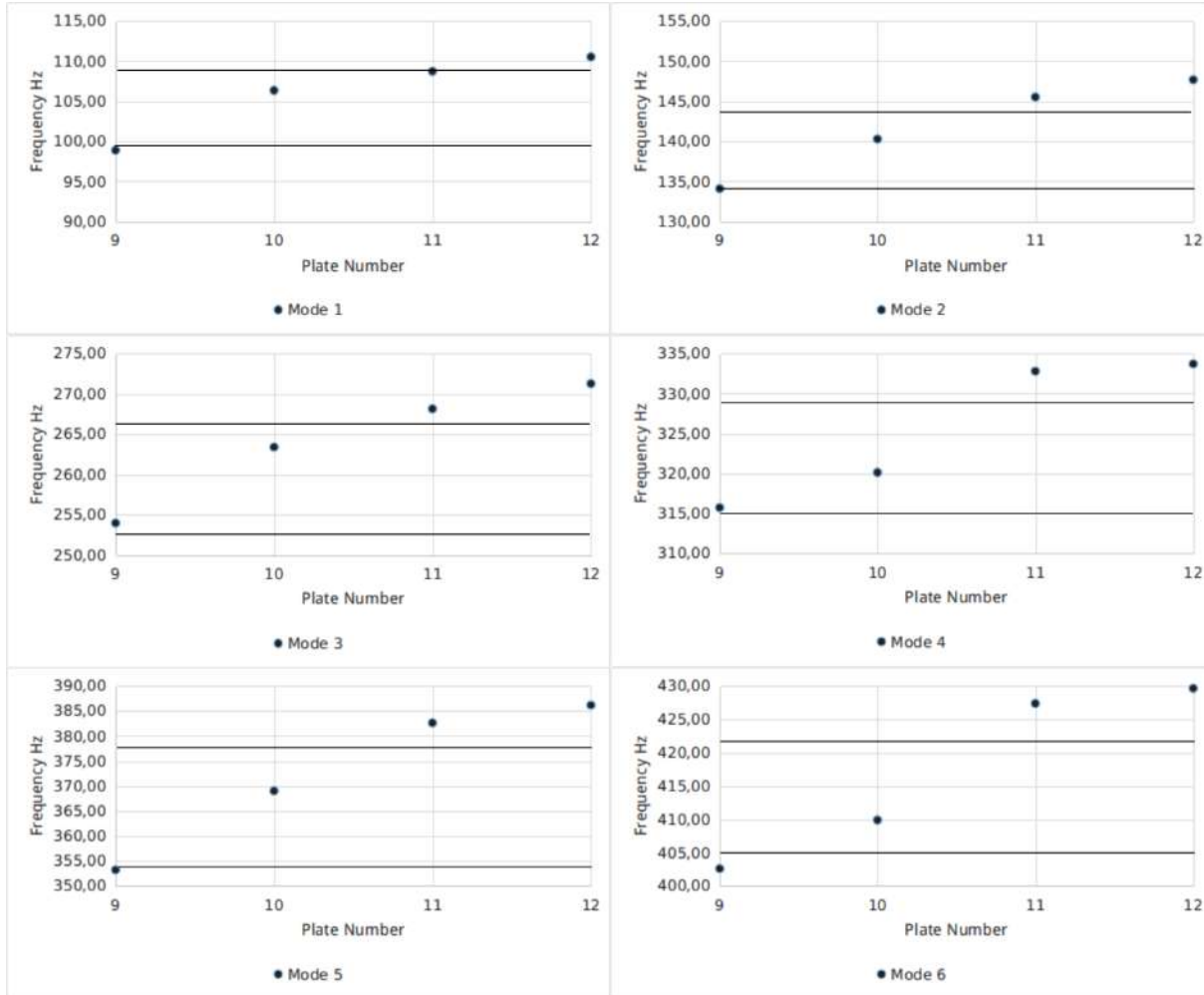
Source: Souza et al. (2019).

Table 6.6: Experimental results for intact and damaged plates, stack sequence $[0/15/-15/0/5/-15]_s$.

Plate 9			
	Intact	Damaged	Relative difference
f_1 [Hz]	95.379	98.904	3.70%
f_2 [Hz]	132.911	134.096	0.89%
f_3 [Hz]	250.645	253.976	1.33%
f_4 [Hz]	316.229	315.735	-0.16%
f_5 [Hz]	349.436	353.229	1.09%
f_6 [Hz]	405.460	402.610	-0.70%
Plate 10			
	Intact	Damaged	Relative difference
f_1 [Hz]	104.152	106.355	2.12%
f_2 [Hz]	139.884	140.295	0.29%
f_3 [Hz]	261.091	263.395	0.88%
f_4 [Hz]	320.690	320.133	-0.17%
f_5 [Hz]	367.079	369.029	0.53%
f_6 [Hz]	411.455	409.900	-0.38%
Plate 11			
	Intact	Damaged	Relative difference
f_1 [Hz]	106.105	108.723	2.47%
f_2 [Hz]	145.625	145.531	-0.06%
f_3 [Hz]	265.984	268.152	0.82%
f_4 [Hz]	332.939	332.784	-0.05%
f_5 [Hz]	379.668	382.615	0.78%
f_6 [Hz]	429.651	427.393	-0.53%

Based on the experimental intact data, the maximum and minimum values for the set of plates can be calculated. The Figure 6.7 shows the damaged frequencies (dots) against the maximum and minimum values (lines).

Figure 6.7: Maximum and minimum limits of the intact composite plates (lines) and damaged frequencies of composite plates (dots) with stack sequence of $[0/15/-15/0/5/-15]_s$.



Source: Author's production.

As aforementioned, the damage caused on plates with stack sequence of $[0/15/-15/0/5/-15]_s$ have less effect on dynamic behaviour when compared with the unidirectional plates. However, it is possible to note that plates 11 and 12 have almost all of its modes out of the bounds. Therefore, following the methodology proposed these plates are not able to perform its functions as structural components.

Chapter 7

Conclusions and Future Works

7.1 Conclusions

The main objective of this research project consists of developing a methodology to help engineers on the verification of composite plates. Evaluating the characteristics of a set of specimens and obtaining reference information to use testing other components manufactured by the same process. Thus, this tool can save time during the inspection process and ensure the integrity of structures on high-quality manufacturers.

This work contributes to the study of dynamics on composite plates by identifying the main parameters of influence, the materials properties using an inverse method, and also this methodology can be used to avoid false damage detection. For this unidirectional laminate and on a laminate with fibre orientations are used. Materials properties and geometry are evaluated and a Design of Experiment procedure based on the Plackart-Burman design is conducted to screening the main parameters on the process. The DoE results are used as base information to a model update procedure that results on the estimated materials properties and a refined numerical model. Finally, the updated numerical model is used to obtain the FRFs that composes the envelope representing the composite plate set. This envelope can help engineers to evaluate other composite plates and classify.

During the first phase of this work, the geometry analysis of the specimens confirmed the high level of uncertainties from the manufacturing process of composite plates. The mean thickness of the plates has a range of uncertainty about 0.11 mm for $[0]_8$ plates and 0.394 for $[0/15/-15/0/15/-15]_s$ plates, which is a bit considerable since the laminate layer thickness is about 0.27 mm for the specimens. Also, the analysis of spatial thickness distribution shows the irregularities on the specimens that can influence the errors in the model update process. However, the assumption of constant thickness for the numerical model can be used and assume the fact that other properties will compensate it, in order to obtain a representative numerical model for the specimens.

Using information about the design variables boundaries, a DoE was carried out to analyze and identify the most important parameters linked to the dynamic response of composite plates. For this, a set of computational analyses was used to obtain the modal frequencies and verify the influence of the parameters under study. The results obtained in the screening design show the most influential parameters such as thickness, Young's modulus in the longitudinal (E_{11}), the transverse direction (E_{22}) and Shear Modulus on plane 1-2 (G_{12}) on a global way considering the first sixth modes. Additionally, for plates $[0]_8$, the curvature has an important influence when considering the 2nd and 6th modes in isolation. Therefore, for composite plates without symmetry, the results obtained in this work shows that the curvature must to be included as a design variable when using model update techniques.

Aiming to obtain values for the most influential parameters reached by screening design, a model update process has been implemented. Using the experimental natural frequencies as a reference, a PSO algorithm is used to find the best combination of design variables to result on the dynamic behaviour near to the experimental specimens. For plates $[0]_8$ two different configurations have been considered. One of the four design variables obtained in the DoE process and another including the curvature as an additional design variable. The first one, resulted in errors at the order of 1% to 6%, except as expected, for the 2nd and 6th modes that reached error at the order of 25% and 16%, respectively. Including curvature effect, the error becomes inferior to 1.5% for almost all of the modes on all the plates, except on the first mode at plates P02 and P04. As observed in the screening analysis, the curvature has an important influence especially on modes two and six. Therefore, when including this variable on the model update process a fine tune is possible on these modes. However, this procedure is computationally expensive since the time duration to accomplish the update of each plate is about 3 to 4 hours (desktop computer, memory: 4Gb, processor: Intel i5).

Regarding this issue, a modification of the model update process has been done to reduce the time cost of the problem. The modification consists of prepare a Kriging metamodel to be used instead of FEM. It means that, FEM is used to training the Kriging model that is used during the PSO algorithm. To construct the Kriging model, 20 FEA is used to generate the training data, after that about 800 calls of the metamodel is needed to reach the convergence of the PSO algorithm resulting on the updated design variables. This process presented promising results, reducing the total time of the model update process from 3 hours to approximately 40 minutes.

In order to exemplify the methodology developed during this work, two case studies were elaborated. The first one, shows that it is possible to define the range of FRFs to characterize the set of composite plates from the model update of natural frequencies. The analysis of the FRF range generated, indicates that one of the composite plates possibly have some manufacture imperfection, because its FRF is out of the specified range. The

second case study, evaluates FRF of the damaged plates to verify its classification in relation with the range established on case study one and also analyses the C-Scan results to confirm the influence of the damage on specific modes. This case study clearly shows the influence of matrix crack damage on 2^{nd} mode which is directly related with E_{22} .

Therefore, the proposed methodology allows not only defines a frequency range to assess the quality of a manufactured composite component, but also, identify the main parameters that influence on dynamic response and approximate elastic properties with an inverse method. In other words, there is a good perspective for the application of this methodology as an engineering tool to in composite components design and analysis.

7.2 Future Works

With respect to the work presented in this master thesis further research is recommended on the following aspects:

- Apply interval field theory aiming to model uncertainties in the geometric and material characteristics of the specimen in order to refine the computer models used. The ability to include non-deterministic properties is of great value for a design engineer. It enables a realistic reliability assessment that incorporates the uncertain aspects of the design. Furthermore, the design can be optimised for robust behaviour under the varying external influence.
- Implement material damage model to composites in order to use the model update process presented in this work to estimate materials properties after damages as impacts or delaminations. One of the main objectives of a model update process is to obtain a numerical model that faithfully represents a physical component. Therefore, with a representative damage model it is possible to carry out destructive tests in the numerical domain to predict the structural behaviour with less cost.
- Improve the model update process based on Kriging metamodel by using Efficient Global Optimization (EGO). Training samples can be determined in an iterative process using EGO, aiming to reduce the number of times that FEM calculating is required. Regarding simple components, like those used in this work, the proposed methodology is efficient enough. However, the improvement that can be achieved with EGO algorithm can help researchers and engineers to apply this methodology to more complex components.
- Apply the proposed methodology to different components, as composite cylinders, glass fibre plates and stiffened panels.
- Apply the proposed methodology to improve Structural Health Monitoring systems. Obtain the dynamic behaviour of each intact component manufactured in an assembly

line can be too onerous. Then, this methodology can be used to determine an envelope for the dynamic response that characterizes the intact components using a set with few specimens.

Bibliography

ALARIFI, I. M. et al. Mitigation of lightning strikes on composite aircraft via micro and nanoscale materials. In: THE ROYAL SOCIETY. *Advances in Nanotechnology*. [S.l.], 2017.

BAARAN, J. Technical report, *Visual inspection of composite structures*. 2009.

BARKANOV, E. et al. Optimal weight design of laminated composite panels with different stiffeners under buckling loads. *27th International Congress of the Aeronautical Sciences*, p. 1 9, 2010.

BORGES, E. N.

Fabricação, Análise Experimental e Computacional de Juntas Híbridas Coladas Monitoradas por Compósitos Inteligentes Escola de Engenharia de São Carlos da Universidade de São Paulo, São Carlos, 2012.

BOX, G. E.; HUNTER, W. G.; HUNTER, J. S. *Statistics for experimenters: an introduction to design, data analysis, and model building*. [S.l.]: JSTOR, 1978. v. 1.

BRUNO, L. et al. Elastic characterization of orthotropic plates of any shape via static testing. *International Journal of Solids and Structures*, Elsevier, v. 45, n. 3-4, p. 908 920, 2008.

CANTWELL, W.; MORTON, J. The significance of damage and defects and their detection in composite materials: a review. *The journal of strain analysis for engineering design*, SAGE Publications, v. 27, n. 1, p. 29 42, 1992.

CHALONER, K.; VERDINELLI, I. Bayesian Experimental Design: A Review. *Statistical Science*, v. 10, n. 3, p. 273 304, 2013.

CHANDRASHEKHAR, M.; GANGULI, R. Uncertainty handling in structural damage detection using fuzzy logic and probabilistic simulation. *Mechanical Systems and Signal Processing*, v. 23, n. 2, p. 384 404, 2009.

CHEN, J. C.; GARBA, J. A. Analytical model improvement using modal test results. *AIAA journal*, v. 18, n. 6, p. 684 690, 1980.

CHEN, V. C. P. et al. A review on design, modeling and applications of computer experiments. *IIE Transactions*, v. 38, n. 4, p. 273 291, 2006.

CHUN, H. J.; SHIN, J. Y.; DANIEL, I. M. Effects of material and geometric nonlinearities on the tensile and compressive behavior of composite materials with fiber waviness. *Composites Science and Technology*, v. 61, n. 1, p. 125 134, 2001.

COHEN, D. Influence of filament winding parameters on composite vessel quality and strength. *Composites Part A: Applied Science and Manufacturing*, Elsevier, v. 28, n. 12, p. 1035–1047, 1997.

COLLOMBET, F. et al. Contribution of embedded optical fiber with bragg grating in composite structures for tests-simulations dialogue. *Mechanics of Advanced Materials and Structures*, v. 13, n. 5, p. 429–439, 2006.

Composite Materials Handbook CMH-17-3G. *Polymer matrix composites: material usage, design and analysis*. [S.l.]: SAE International, 2009.

DANIEL, I. M. *Engineering mechanics of composite materials*. [S.l.: s.n.], 1993. v. 3.

DAVILA, Y. et al. Spatial Evolution of the Thickness Variations over a CFRP Laminated Structure. *Applied Composite Materials*, Applied Composite Materials, v. 24, n. 5, p. 1201–1215, 2017.

DEY, S.; MUKHOPADHYAY, T.; ADHIKARI, S. Stochastic free vibration analyses of composite shallow doubly curved shells a kriging model approach. *Composites Part B: Engineering*, Elsevier, v. 70, p. 99–112, 2015.

DEY, S. et al. A response surface modelling approach for resonance driven reliability based optimization of composite shells. *Periodica Polytechnica. Civil Engineering*, Periodica Polytechnica, Budapest University of Technology and Economics, v. 60, n. 1, p. 103, 2016.

EWINS, D. *Modal testing: theory, practice and application*. [S.l.]: Wiley, 2000.

FANG, K.-T. et al. Uniform design: theory and application. *Technometrics*, Taylor & Francis Group, v. 42, n. 3, p. 237–248, 2000.

FARRAR, C. R.; DOEBLING, S. W.; NIX, D. A. Vibration based structural damage identification. *Philosophical Transactions of the Royal Society of London A: Mathematical, Physical and Engineering Sciences*, The Royal Society, v. 359, n. 1778, p. 131–149, 2001.

FRITZEN, C.-P.; KRAEMER, P. Self-diagnosis of smart structures based on dynamical properties. *Mechanical Systems and Signal Processing*, Elsevier, v. 23, n. 6, p. 1830–1845, 2009.

FU, Z.-F.; HE, J. *Modal analysis*. [S.l.]: Butterworth-Heinemann, 2001.

GHOBADI, A. Common type of damages in composites and their inspections. *World Journal of Mechanics*, Nova Science Publishers, v. 7, n. 02, p. 24, 2017.

GUPTA, S.; GHOSH, D. Uncertainty quantification in structural engineering: Current status and computational challenges. In: *Uncertainty Quantification in Computational Science: Theory and Application in Fluids and Structural Mechanics*. [S.l.]: World Scientific, 2017. p. 119–149.

HASSAN, M.; OTHMAN, A.; KAMARUDDIN, S. A review on the manufacturing defects of complex-shaped laminate in aircraft composite structures. *The International Journal of Advanced Manufacturing Technology*, 2017. ISSN 0268-3768.

- HOLLAND, J. H. *Adaptation in natural and artificial systems: an introductory analysis with applications to biology, control, and artificial intelligence*. [S.l.]: U Michigan Press, 1975.
- HSIAO, H.; DANIEL, I. Effect of fiber waviness on stiffness and strength reduction of unidirectional composites under compressive loading. *Composites Science and Technology*, v. 56, n. 5, p. 581–593, 1996.
- HUANG, D. et al. Global optimization of stochastic black-box systems via sequential kriging meta-models. *Journal of global optimization*, Springer, v. 34, n. 3, p. 441–466, 2006.
- HUBERT, P.; POURSAITIP, A. Aspects of the compaction of composite angle laminates: an experimental investigation. *Journal of Composite Materials*, Sage Publications Sage CA: Thousand Oaks, CA, v. 35, n. 1, p. 2–26, 2001.
- IBRAHIM, R. A. Structural dynamics with parameter uncertainties. *Applied Mechanics Reviews*, American Society of Mechanical Engineers, v. 40, n. 3, p. 309–328, 1987.
- IMREGUN, M.; VISSER, W. A review of model updating techniques. *The Shock and vibration digest*, Sage, v. 23, n. 1, p. 9–20, 1991.
- JEONG, S.; MURAYAMA, M.; YAMAMOTO, K. Efficient optimization design method using kriging model. *Journal of aircraft*, [New York, etc.] American Institute of Aeronautics and Astronautics., v. 42, n. 2, p. 413–420, 2005.
- JIANG, C.; LIU, G. R.; HAN, X. A novel method for uncertainty inverse problems and application to material characterization of composites. *Experimental Mechanics*, v. 48, n. 4, p. 539–548, 2008.
- JIN, R.; CHEN, W.; SIMPSON, T. W. Comparative studies of metamodeling techniques under multiple modeling criteria. *Structural and multidisciplinary optimization*, Springer, v. 23, n. 1, p. 1–13, 2001.
- KESSLER, S. S. et al. Damage detection in composite materials using frequency response methods. *Composites Part B: Engineering*, Elsevier, v. 33, n. 1, p. 87–95, 2002.
- KHODAPARAST, H. H.; MOTTERSHEAD, J. E.; BADCOCK, K. J. Interval model updating with irreducible uncertainty using the kriging predictor. *Mechanical Systems and Signal Processing*, Elsevier, v. 25, n. 4, p. 1204–1226, 2011.
- KIM, J.-T. et al. Damage identification in beam-type structures: frequency-based method vs mode-shape-based method. *Engineering structures*, Elsevier, v. 25, n. 1, p. 57–67, 2003.
- KIM, T.-U.; SIN, H.-C. Optimal design of composite laminated plates with the discreteness in ply angles and uncertainty in material properties considered. *Computers & Structures*, Elsevier, v. 79, n. 29-30, p. 2501–2509, 2001.
- KRIGE, D. G. A statistical approach to some basic mine valuation problems on the Witwatersrand. *Journal of the Southern African Institute of Mining and Metallurgy*, Southern African Institute of Mining and Metallurgy, v. 52, n. 6, p. 119–139, 1951.

- LEE, M. C. et al. Robust design - A concept for imperfection insensitive composite structures. *Composite Structures*, Elsevier Ltd, v. 92, n. 6, p. 1469 1477, 2010.
- LEE, M. C. W. et al. Determination of robustness for a stiffened composite structure using stochastic analysis. *Composite Structures*, v. 86, n. 1-3, p. 78 84, 2008.
- LEISSA, A.; MARTIN, A. Vibration and buckling of rectangular composite plates with variable fiber spacing. *Composite structures*, Elsevier, v. 14, n. 4, p. 339 357, 1990.
- LI, Y. et al. Numerical and experimental study on the effect of lay-up type and structural elements on thickness uniformity of l-shaped laminates. *Applied Composite Materials*, Springer, v. 16, n. 2, p. 101 115, 2009.
- LIGHTFOOT, J. S.; WISNOM, M. R.; POTTER, K. A new mechanism for the formation of ply wrinkles due to shear between plies. *Composites Part A: Applied Science and Manufacturing*, Elsevier Ltd, v. 49, p. 139 147, 2013.
- LIM, T. Submatrix approach to stiffness matrix correction using modal test data. *AIAA journal*, v. 28, n. 6, p. 1123 1130, 1990.
- LIU, Y. et al. Model updating of complex structures using the combination of component mode synthesis and kriging predictor. *The Scientific World Journal*, Hindawi Publishing Corporation, v. 2014, 2014.
- MANOHAR, C.; IBRAHIM, R. Progress in structural dynamics with stochastic parameter variations: 1987-1998. *Applied Mechanics Reviews*, American Society of Mechanical Engineers, v. 52, p. 177 196, 1999.
- MATHERON, G. Principles of geostatistics. *Economic geology*, SecG, v. 58, n. 8, p. 1246 1266, 1963.
- MECKESHEIMER, M. et al. Computationally inexpensive metamodel assessment strategies. *AIAA journal*, AMERICAN INST OF AERONAUTICS AND ASTRONAUTICS, v. 40, n. 10, p. 2053 2060, 2002.
- MEDEIROS, R. et al. A new approach for shm system: Combination of vibration based method and shearography speckle. In: *5th International Symposium on Solid Mechanics (MecSol2015)*, Belo Horizonte, Brazil. [S.l.: s.n.], 2015.
- MINSCH, N. et al. Analysis of Filament Winding Processes and Potential Equipment Technologies. *Procedia CIRP*, v. 66, p. 125 130, 2017.
- MONTALVAO, D. A Review of Vibration-based Structural Health Monitoring with Special Emphasis on Composite Materials. *The Shock and Vibration Digest*, v. 38, p. 295 324, 2006.
- MOTTERSHEAD, J.; FRISWELL, M. Model updating in structural dynamics: a survey. *Journal of sound and vibration*, Elsevier, v. 167, n. 2, p. 347 375, 1993.
- MUNCK, M. D. et al. An adaptive kriging based optimisation algorithm for interval and fuzzy frf analysis. In: KATHOLIEKE UNIVERSITEIT LEUVEN, DEPARTEMENT WERKTUIGKUNDE. *Proceedings of the International Conference on Noise and Vibration Engineering*. [S.l.], 2008. p. 3767 3776.

- MYERS, R. H.; MONTGOMERY, D. C.; ANDERSON-COOK, C. M. *Response surface methodology: process and product optimization using designed experiments*. [S.l.]: John Wiley & Sons, 2016.
- OLIVIER, P.; CAVARERO, M. Comparison between longitudinal tensile characteristics of thin and thick thermoset composite laminates: influence of curing conditions. *Computers and Structures*, v. 76, n. 1, p. 125 137, 2000.
- OOIJEVAAR, T. H. *Vibration based structural health monitoring of composite skin-stiffener structures*. [S.l.: s.n.], 2014. 171 p.
- PARK, J.-S. Optimal latin-hypercube designs for computer experiments. *Journal of statistical planning and inference*, Elsevier, v. 39, n. 1, p. 95 111, 1994.
- PLACKETT, R. L.; BURMAN, J. The design of Optimum Multifactorial Experiments. *Oxford University*, v. 33, n. 4, p. 305 325, 1946.
- POTTER, K. Understanding the origins of defects and variability in composites manufacture. In: *International Conference on Composite Materials (ICCM)-17, Edinburgh, UK*. [S.l.: s.n.], 2009.
- POTTER, K. D. Understanding the origins of defects and variability in composites manufacture. *17 th International Conference on Composite Materials*, p. 27 31, 2009.
- REN, W.-X.; ZONG, Z.-H. Output-only modal parameter identification of civil engineering structures. *Structural Engineering and Mechanics*, Taejon, Korea: Techno-Press, c1993-, v. 17, n. 3-4, p. 429 444, 2004.
- RIBEIRO, M. L.; TITA, V.; VANDEPITTE, D. A new damage model for composite laminates. *Composite Structures*, Elsevier, v. 94, n. 2, p. 635 642, 2012.
- RYTTER, A. Vibrational based inspection of civil engineering structures. Dept. of Building Technology and Structural Engineering, Aalborg University, 1993.
- SACKS, J. et al. Design and Analysis of Computer Experiments. v. 4, n. 4, p. 409 423, 1989.
- SHADAN, F. et al. Experimental validation of a frf-based model updating method. *Journal of Vibration and Control*, SAGE Publications Sage UK: London, England, p. 1077546316664675, 2016.
- SHI, Y.; EBERHART, R. C. Parameter selection in particle swarm optimization. Springer-Verlag, 1998.
- SIMPSON, T. W. et al. Kriging models for global approximation in simulation-based multidisciplinary design optimization. *AIAA journal*, AMERICAN INST OF AERONAUTICS AND ASTRONAUTICS, v. 39, n. 12, p. 2233 2241, 2001.
- SIMPSON, T. W. et al. Metamodels for computer-based engineering design: survey and recommendations. *Engineering with computers*, Springer, v. 17, n. 2, p. 129 150, 2001.
- SINOUE, J.-j. A review of damage detection and health monitoring of mechanical systems from changes in the measurement of linear and non-linear vibrations. *Mechanical Vibrations: Measurement, Effects and Controlical Vibrations*, p. 643 702, 2013.

- SIPPLE, J. D.; SANAYEI, M. Finite element model updating of the ucf grid benchmark using measured frequency response functions. *Mechanical Systems and Signal Processing*, Elsevier, v. 46, n. 1, p. 179 190, 2014.
- SLOANE, H. A.; NJA, S. J. Orthogonal arrays: theory and applications. NY: *Springer-Verlag New York*, 1999.
- SOUZA, L. F. D. S.; TITA, V.; MEDEIROS, R. D. Sensitivity analysis on composite plates by using design of experiments. In: SANTA CATARINA STATE UNIVERSITY. *Proceedings of the 6 th International Symposium on Solid Mechanics (MECSOL)*. [S.l.], 2017.
- SOUZA, L. F. D. S. et al. Dynamic response of laminated composites using design of experiments: An experimental and numerical study. *Mechanical Systems and Signal Processing*, Elsevier Ltd, v. 115, p. 82 101, 2019. ISSN 0888-3270.
- SRIRAMULA, S.; CHRYSSANTHOPOULOS, M. K. Quantification of uncertainty modelling in stochastic analysis of FRP composites. *Composites Part A: Applied Science and Manufacturing*, Elsevier Ltd, v. 40, n. 11, p. 1673 1684, 2009.
- SUN, J. et al. Role of tool-part interaction in consolidation of L-shaped laminates during autoclave process. *Applied Composite Materials*, v. 19, n. 3-4, p. 583 597, 2012.
- TITA, V.; CARVALHO, J. D.; VANDEPITTE, D. Failure analysis of low velocity impact on thin composite laminates: Experimental and numerical approaches. *Composite Structures*, Elsevier, v. 83, n. 4, p. 413 428, 2008.
- Vaz Jr, M.; CARDOSO, E. L.; STAHLSCHMIDT, J. Particle swarm optimization and identification of inelastic material parameters. *Engineering Computations*, v. 30, n. 7, p. 936 960, 2013. ISSN 0264-4401.
- WANG, G. G.; SHAN, S. Review of Metamodeling Techniques in Support of Engineering Design Optimization. *Journal of Mechanical Design*, v. 129, n. 4, p. 370, 2007.
- WANG, J.; WANG, C.; ZHAO, J. Frequency response function-based model updating using Kriging model. *Mechanical Systems and Signal Processing*, v. 87, n. October 2016, p. 1 12, 2017.
- WANG, W.; KAM, T. Material characterization of laminated composite plates via static testing. *Composite Structures*, Elsevier, v. 50, n. 4, p. 347 352, 2000.
- WORDEN, K. et al. The fundamental axioms of structural health monitoring. In: THE ROYAL SOCIETY. *Proceedings of the Royal Society of London A: Mathematical, Physical and Engineering Sciences*. [S.l.], 2007. v. 463, n. 2082, p. 1639 1664.
- YUAN, R.; GUANGCHEN, B. Comparison of neural network and kriging method for creating simulation-optimization metamodels. In: IEEE. *Dependable, Autonomic and Secure Computing, 2009. DASC'09. Eighth IEEE International Conference on*. [S.l.], 2009. p. 815 821.
- ZANG, C.; MA, S.; FRISWELL, M. Structural model updating with an improved parameter selection method. In: KATHOLIEKE UNIVERSITEIT LEUVEN, DEPARTEMENT WERKTUIGKUNDE. *Proceedings of the International Conference on Noise and Vibration Engineering*. [S.l.], 2012. p. 2227 2236.

Appendix A

Scientific Publications

This appendix presented the scientific contributions related directly or indirectly to this Master thesis.

1. SOUZA, L. F. S. ; VANDEPITTE, D. ; TITA, V. ; DE MEDEIROS, R. . Dynamic response of laminated composites using design of experiments: An experimental and numerical study. *Mechanical System and Signal Processing*, Elsevier, v.115, p82-101, 2019. ISSN 0888-3270.
2. SOUZA, L. F. S. ; TITA, V. ; DE MEDEIROS, R. . Dynamic analysis of composite structures using Kriging model applied to manufacturing desing tolerances. In: 4th Brazilian Conference on Composite Materials (BCCM4), 2018, Rio de Janeiro. Proceedings of the BCCM4, 2018.
3. SOUZA, L. F. S. ; TITA, V. ; DE MEDEIROS, R. . Composite plates model updating using Kriging method. In: 24rd ABCM International Congress of Mechanical Engineering (COBEM2017), 2017, Curitiba. Proceedings of the COBEM 2017, 2017.
4. SOUZA, L. F. S. ; TITA, V. ; DE MEDEIROS, R. . Sensitivity analysis on composite plates by using design of experiments. In: 6th International Symposium on Solid Mechanics (MECSOL2017), 2017, Joinville. Proceedings of MecSol. Joinville, 2017. p. 111-123.
5. CHRISTOFF, B. G. ; SOUZA, L. F. S. ; CARDOSO, E. L. ; DE MEDEIROS, R. . Optimal distribution of a hollow sphere material applied to the design of three dimensional structure with minimum volume considering stress constraints. In: 6th International Symposium on Solid Mechanics (MECSOL2017), 2017, Joinville. Proceedings of MecSol. Joinville, 2017. p. 639-654.
6. SOUZA, L. F. S. ; TITA, V. ; DE MEDEIROS, R. . Analise dinâmica de sensibilidade aplicada a placas de material compósito laminado. In: I Simpósio de Métodos

Numéricos em Engenharia, 2016, Curitiba. Anais do 1º Simpósio de Métodos Numéricos em Engenharia, 2016. p. 29-35.

Appendix B

Kriging Training Script in Python

```
1
2 #Script to obtain the Kriging constant to the metamodel.
3 import Model
4 import pandas as pd
5 import numpy as np
6
7 ## Model File
8 class UserVariables(object):
9     def __init__(self):
10         self.output_matrix = []
11         self.input_matrix = []
12         self.ref_freq = []
13         self.low_b = []
14         self.upper_b = []
15
16     def read_data_training(self,path,number_inputs):
17         data = pd.read_csv(path, header=None)
18         number_inputs = int(number_inputs)
19         data = data.as_matrix()
20         self.input_matrix = np.zeros((len(data),number_inputs))
21         self.output_matrix = np.asmatrix(np.zeros((len(data),np.size(data,1)-
22                                                     number_inputs)))
23         for i in range(1,len(data)):
24             for j in range(0,number_inputs):
25                 self.input_matrix[i][j] = int(data[i][j])
26             for k in range(number_inputs,np.size(data,1) - number_inputs + 1):
27                 self.output_matrix[i][k-1] = int(data[i][k])
```

```

28         self.input_matrix = np.asmatrix(self.input_matrix)
29         self.output_matrix = np.asmatrix(self.output_matrix)
30
31
32     class GA(object):
33         def __init__(self, n_bits, n_genes, lb, ub, taxa_crossover, p_mutacao, ite,
34                     input_matrix, output_matrix):
35             self.n_bits = n_bits # Numero de bits para representar um numero
36             self.n_genes = n_genes # Numero de genes na populacao
37             self.lb = lb # Limite inferior das variaveis theta
38             self.ub = ub # Limite superior das variaveis theta
39             self.taxa_crossover = taxa_crossover # Taxa de crossover
40             self.p_mutacao = p_mutacao # Probabilidade de mutacao em um gene
41             self.ite = ite # Numero de geracoes
42             self.input_matrix = input_matrix #Matriz de entrada do problema
43             self.output_matrix = output_matrix #Matriz de saida do problema
44
45         def obj(self, x):
46             [Nlikelihood, Psi, U] = self.likelihood(x, self.input_matrix,
47             self.output_matrix) #Y precisa entrar como um vetor coluna
48             return Nlikelihood
49
50         def start_population(self):
51             np.random.seed()
52             n_variables = len(self.lb)
53             a = np.zeros(n_variables)
54             population = []
55             for i in range(0, self.n_genes):
56                 for j in range(0, n_variables):
57                     a[j] = (self.ub[j] - self.lb[j]) * np.random.rand() * self.lb[j]
58                 population.append(self.create_gene(a))
59             return population #array de genes
60
61
62         def create_gene(self, variables):
63             gene = ""
64             for i in range(0, len(variables)):
65                 a = self.encoding(variables[i], self.lb[i], self.ub[i])
66                 gene = gene + a

```

```

67         return gene #String
68
69     def encoding(self,variavel,lb,ub):
70         n_div = (np.power(2,self.n_bits)-1)
71         div = (ub-lb)/n_div
72         a = lb
73         binario = 0
74         for i in range(0,n_div):
75             a = a+div
76             if (a>variavel):
77                 binario = bin(i)
78                 binario = str(binario)
79                 binario = binario.split("b") #binario = binario[1]
80                 break
81         binario_str = binario[1]
82         while (len(binario_str)<self.n_bits):
83             binario_str = "0"+binario_str
84         return binario_str #String
85
86     def decoding(self,binario,lb,ub):
87         n_div = (np.power(2,self.n_bits)-1)
88         div = (ub-lb)/n_div
89         a = int(binario,2)
90         real = lb+div*a
91         return real #int
92
93     def gene2var(self,gene):
94         n_var = len(self.lb)
95         for i in range(0,n_var-1):
96             lb=self.lb[i]
97             ub=self.ub[i]
98             x = np.zeros(n_var)
99             inicio=0
100            divide = self.n_bits
101            for i in range(0,n_var):
102                var = gene[inicio:divide]
103                dec = self.decoding(var,lb,ub)
104                inicio=inicio+self.n_bits
105                divide=divide+self.n_bits

```

```

106         x[i] = dec
107     return x #list of variables
108
109
110 def rank(self,population):
111     #Rank da populacao
112     #Avaliacao dos genes
113     np.random.seed()
114     N = len(population)
115     x = []
116     mating_pool = []
117     fitness = np.zeros(len(population))
118     for i in range(0,N):
119         x = self.gene2var(population[i])
120         fitness[i] = self.obj(x)
121     ///Mating_pool organiza os genes do melhor para o pior
122     rank_fitness = sorted(fitness)
123         #rank_fitness.sort(reverse=True)
124     for i in range(0,N):
125         for j in range(0,N):
126             if (rank_fitness[i] == fitness[j]):
127                 mating_pool.append(population[j])
128     return mating_pool
129
130 def crossover(self,mating_pool):
131     np.random.seed()
132     N = len(mating_pool)
133     sum_indices=0
134     for i in range(0,N):
135         sum_indices = sum_indices+i
136
137     ///cria vetor de probabilidades para os genes ranquiados
138     P = np.zeros(N)
139     for i in range(0,N):
140         P[i] = (i*100)/sum_indices
141     P.sort()
142     ///Numero de genes a serem selecionados para crossover
143     n_crossover = int(round((self.taxa_crossover*N)/2))
144     ///Realiza o numero de crossovers definido

```

```

145     ###Para cada crossover dois genes sao utilizaddos como base para gerar dois novos
146     ###os novos genes gerados sao colocados na nova geracao
147
148     pop = []
149     for i in range(0,n_crossover):
150         cut = int(np.ceil(self.n_bits*np.random.rand()))
151         gene_A = self.select_gene(P,N,mating_pool)
152         gene_B = self.select_gene(P,N,mating_pool)
153         split_A1 = gene_A[0:cut]
154         split_B1 = gene_B[0:cut]
155         split_A2 = gene_A[cut:len(gene_A)]
156         split_B2 = gene_B[cut:len(gene_B)]
157         gene_a = split_A1+split_B2
158         gene_b = split_B1+split_A2
159         pop.append(gene_a)
160         pop.append(gene_b)
161
162     if (len(pop)<N):
163         k=1
164         for i in range(len(pop),N):
165             pop.append(mating_pool[k])
166             k=k+1
167     return pop
168
169     def select_gene(P,N,mating_pool):
170         np.random.seed()
171         prob = abs(np.random.rand()*100-1)
172         prob_acumulada = P[0]
173         gene_cross = ""
174         if (prob>prob_acumulada):
175             for j in range(1,N):
176                 if (prob>prob_acumulada):
177                     prob_acumulada = prob_acumulada+P[j]
178                 else:
179                     gene_cross = mating_pool[j-1]
180                     break
181             else:
182                 gene_cross = mating_pool[0]
183         if (prob_acumulada == 100):

```



```

184         gene_cross = mating_pool[N-1]
185
186     return gene_cross
187
188
189
190 def mutation(self,pop):
191     n_var = len(self.lb)
192     np.random.seed()
193     N = len(pop)
194     pop_mutado = pop
195     ###Para cada gene verifica se sofre mutacao
196     for i in range(1,N):
197         gene = pop[i]
198         roll = np.random.rand() #roleta da mutacao
199         n_mutacoes = 0
200         gene_m = []
201         intensidade = 0
202         if (roll<self.p_mutacao):
203             n_mutacoes = n_mutacoes+1
204             for j in range(0,(self.n_bits*n_var)):
205                 gene_m.append(gene[j:j+1])
206             intensidade = int(round(np.random.rand()*(self.n_bits*n_var)))
207             for k in range(0,intensidade):
208                 bit = int(np.ceil(np.random.rand()*self.n_bits*n_var))
209                 if (bit == self.n_bits*n_var):
210                     bit = bit - int(np.ceil(np.random.rand()*
211                                     self.n_bits*n_var))
212                 if (gene_m[bit] == "1"):
213                     gene_m[bit] = "0"
214                 else:
215                     gene_m[bit] = "1"
216             gene_mutado = ""
217             if (n_mutacoes>0):
218                 for l in range(0,self.n_bits*n_var):
219                     gene_mutado = gene_mutado+gene_m[l]
220             else:
221                 gene_mutado = gene
222             pop_mutado[i] = gene_mutado

```

```

223     return pop_mutado
224
225 def likelihood(x, sample_location, observed_data):
226     #Calculates the negative of the concentrated ln-likelihood
227     #
228     #Inputs
229     # x - vetor of log(theta) parameters (array)
230     # X - n x k matrix of the sample locations (matrix)
231     # Y - n x 1 vector of observed data (matrix)
232     #
233     #Outputs
234     # NegLnLike - concentrated ln-likelihood
235     # Psi - correlation matrix
236     # U - Cholesky factorization of correlation matrix
237     X = np.asmatrix(sample_location)
238     Y = np.asmatrix(observed_data)
239     #theta = np.asmatrix(np.power(10,x))
240     theta = np.asmatrix(x)
241     theta = theta.T
242     [n,k] = X.shape
243     one = np.asmatrix(np.ones(n))
244     one = one.T
245     Psi = np.zeros((n,n))
246     Psi = np.asmatrix(Psi)
247     for i in range(0,n):
248         for l in range(i+1,n):
249             soma = 0
250             for m in range(0,k):
251                 soma = soma+(theta[m]*(np.power(X[i,m]-X[l,m],2)))
252             Psi[i,l] = np.exp(-soma)
253
254     Psi = Psi+Psi.T+np.eye(n)+np.eye(n)*1e-7
255     detPsi = np.linalg.det(Psi)
256     lndetPsi = np.log(detPsi)
257     invPsi = np.linalg.inv(Psi)
258     mu = (one.T*invPsi*Y)/(one.T*invPsi*one)
259     SigmaSqr = ((Y-one*mu).T*invPsi*(Y-one*mu))/n
260     NgLnLike = -1*((-n/2)*np.log(SigmaSqr)-0.5*lndetPsi)
261     U=0

```

```

262         return[NgLnLike,Psi,U]
263
264
265
266     def GA_run(self):
267         np.random.seed()
268         #Inicializacao de variaveis
269         x = np.zeros(len(self.lb)) # vetor com variaveis de projeto
270         best_fitness = [] #vetor com os melhores individuo em cada geracao
271         ###cria populacao inicial
272         #populacao inicial aleatoria
273         pop = self.start_population()
274         #Inicia loop das geracoes
275         for i in range(0,self.ite):
276             ###Cria mating pool atraves do ranqueamento da populacao
277             #Mating pool com numero de genes igual a metade da populacao
278             pop_rank = self.rank(pop)
279             mating_pool = []
280             for k in range(0,int(self.n_genes/2)):
281                 mating_pool.append(pop_rank[k])
282
283             ###Executa operacao de crossover
284             #dois genes geram dois novos genes, escolha dos individuos
285             #aleatoria mas com pesos diferentes para os melhores
286             pop_cross = self.crossover(mating_pool)
287             pop_new = []
288             for k in range(0,int(self.n_genes/2)):
289                 pop_new.append(pop_rank[k])
290             for k in range(int(self.n_genes/2),self.n_genes):
291                 pop_new.append(pop_cross[k-int(self.n_genes/2)])
292
293
294             #rankeia a populacao antes da mutacao. Na mutacao o melhor
295             #elemento nunca sofre mutacao
296             #pop_new = rank(pop_new,n_bits,len(lb),lb,ub)
297
298             ###Executa operacao de mutacao
299             #intensidade de mutacao aleatoria
300             pop_mutado = self.mutation(pop_new)

```

```

301         ###Melhor elemento da geracao
302         rank_pop = self.rank(pop_mutado)
303         x = self.gene2var(rank_pop[0])
304
305         best_fitness.append(self.obj(x))
306
307         #atualiza a populacao
308         pop = pop_mutado
309         print ("geracao:",i,"melhor valor:", best_fitness[i],
310             "melhor variavel:", x)
311
312         best_variable = x
313         return [best_fitness, best_variable] #Vetor com os melhores de cada
314         #geracao / vetor com variaveis para o melhor da ultima geracao
315
316
317     ## Main File
318     def kriging_training():
319         #Training data file
320         path = "/home/luiz/Documents/Mestrado/Kriging/ProjetoKriging/dados.txt"
321
322         #Create object UserVariables
323         user_data = Model.UserVariables()
324         user_data.read_data_training(path, 1)
325         #Defines Genetic algorithm parameters
326         n_bits = 16 # Numero de bits para representar um numero
327         n_genes = 20 # Numero de genes na populacao
328         lb = [2,2] # Limite inferior das variaveis theta
329         ub = [0,0] # Limite superior das variaveis theta
330         taxa_crossover = 0.8 #Taxa de crossover influencia no numero de crossovers
331         p_mutacao = 0.3 # Probabilidade de ocorrer mutacao em um gene
332         ite = 200 # Numero de geracoes
333         #Run Genetic algorithm
334         GA = Model.GA(n_bits, n_genes, lb, ub, taxa_crossover, p_mutacao, ite,
335             user_data.input_matrix, user_data.output_matrix)
336         [best_fitness, kriging_coeff] = GA.GA_run()
337
338
339     if __name__ == "__main__":

```

